UCLA Samueli School of Engineering

Research Journal

SURP 2021

UCLA SAMUELI SUMMER UNDERGRADUATE RESEARCH PROGRAM

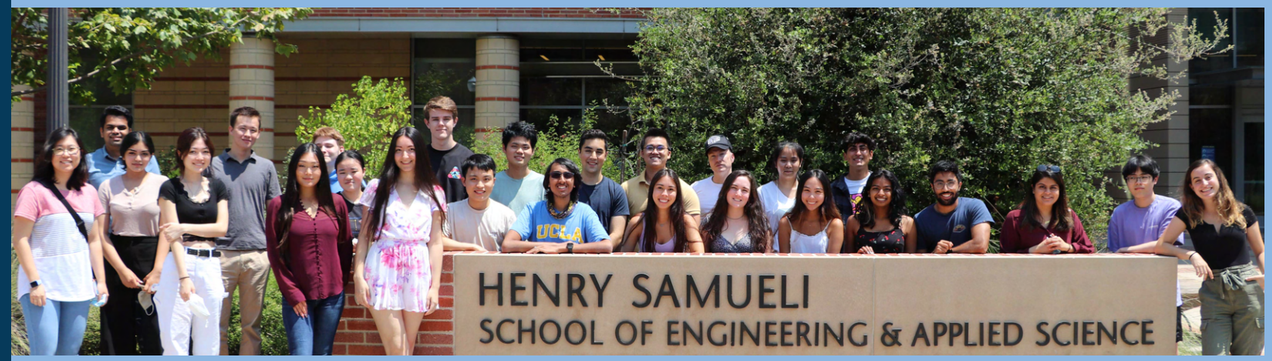

CONTENTS

6 Julia Bi • Ken Yang
8 Gianna Brown • Achuta Kadambi
10 Arlene Constantino • Chi Wei Wong
12 Micah Crook • Carlos Morales Guio
14 Sophia Du • Rob Candler
16 Marisa Duran • Ankur Mehta
18 Virginia Garcia • Junyoung Park
20 Sahiti Gavva • Dante Simonetti
22 Nicholas Hamakami • Christina Fragouli
24 Vanessa Huaco • Samanvaya Srivastava
26 Tricia Jain • Henry Burton
28 Bhavik Joshi • Ankur Mehta
30 Kim Kha • Sam Emaminejad
Enoch Huang
Amanda Hacker
32 Sarah Kimak • Abeer Alwan
34 Ash Kuhlmann • Bruce Dunn
36 Grace Kwak • Ankur Mehta
38 Sung Gyung Lee • Junyoung Park
40 Ella Levine • Carissa Eisler
42 Sandra Li • Benjamin Williams
44 Dehao Lin • Lihua Jin
Scott Cao
46 Angela Liu • Aaron Meyer
48 Matthew Lopez II • Timu Gallien
50 Arthur Lovekin • Mohammad Khalid Jawed
52 Quinlan Mcknight • Sanjay Mohanty
54 Damian Meza • Lihua Jin
56 Krisha Minocha • Achuta Kadambi
58 Zofia Orlowski • CJ Kim
60 Jillian Pantig • Ankur Mehta
62 Mateen Rabbani • Lihua Jin
64 Samantha Rafter • Benjamin Williams
66 Aadhidhya Ravikumar • Danijela Cabric
Jenna Kim
68 Dolores Rodriguez • Carlos Morales-Guio
70 Nicholas Schmidt • Benjamin Williams
72 Sudarshan Seshadri • Ankur Mehta
74 Krish Shah • Anthony Xiang Chen
Waree Protprommart
William Clark
76 Joonwoo Shin • Rick Wesel
78 Jaehoon Song • Ankur Mehta
80 Alethea Sung-Miller • Rick Wesel
Shakeh Kalantarmoradian
82 Andrew Tang • Suhas Diggavi
84 Esha Thota • Rick Wesel
Sraavya Pradeep
86 Brendan Towell • Rick Wesel
Ava Asmani
88 Lizeth Vera • Mitchell Spearrin
90 Kathleen Villasenor • Samanvaya Srivastava
92 Sophie Wells • Jennifer Jay
94 Tyler Xu • Suhas Diggavi
96 Lime Yao • Clarice Aiello
Courtney Gibbons
98 Justin Yao • Kang Wang
Isabella Jordan
100 Ivy Zhang • Lieven Vandenberghe
Tiffany Tsou
102 Jolin Zhang • Greg Pottie
Trung Vong
Rudy Orre
104 David Zheng • Rob Candler
Serina Mummert

DEAN'S MESSAGE

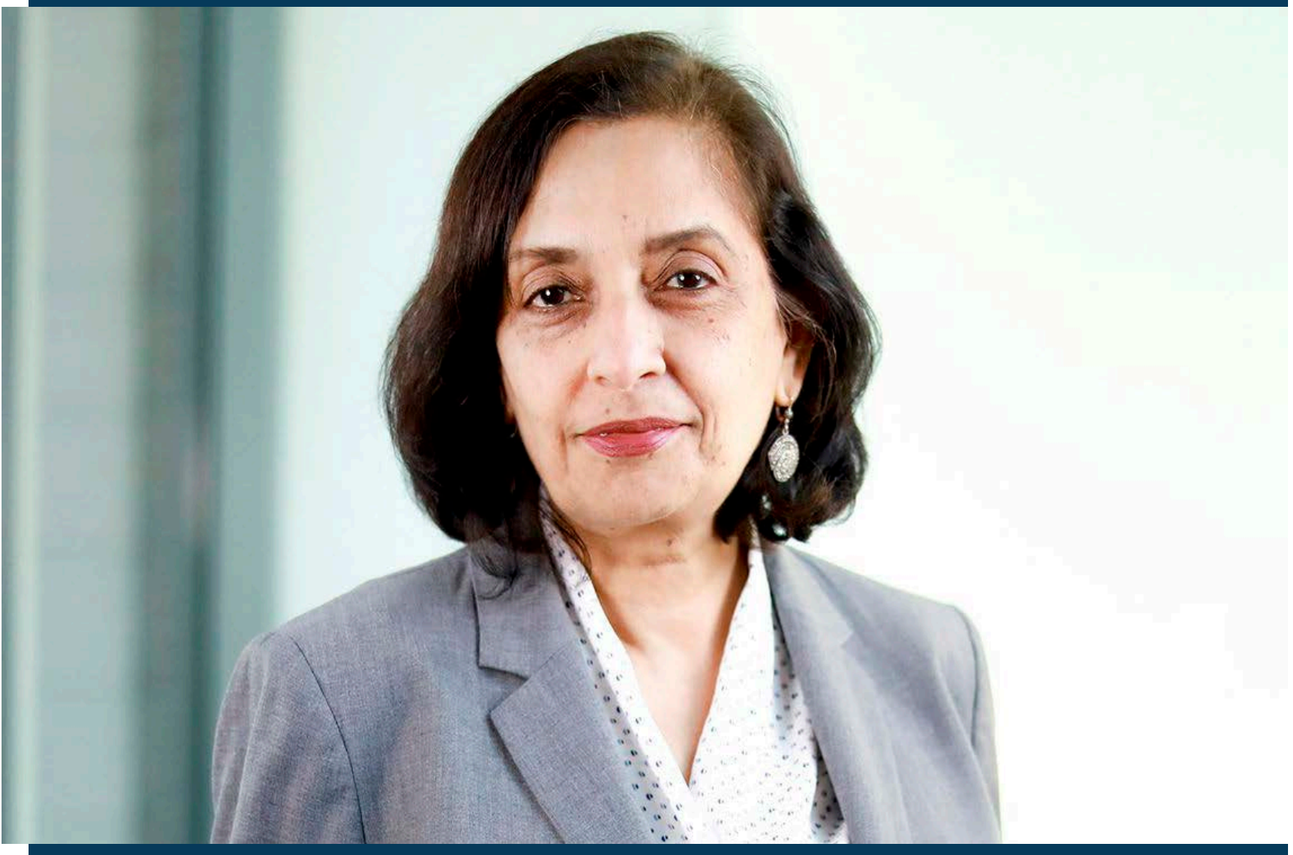

Ronald and Valerie Sugar Dean

The Summer Undergraduate Research Program (SURP) provides an intensive summer research experience in a wide range of engineering and physical science fields. Undergraduate students from all walks of life participate in research with UCLA Samueli School of Engineering faculty to gain real-world lab experience.

Due to the COVID-19 pandemic that is still affecting us this summer, SURP has had to transition the program into a remote learning environment for many of its scholars. Despite this challenge, SURP's many scaffolding resources and social events have still been able to occur and students were able to:

- Conduct research in a cutting-edge field at a world-renowned research institution.
- Meet and network with a community of peers who have similar goals and interests.
- Create a professional scientific poster and publish a research abstract.
- Learn to communicate research outcomes and present a detailed Summary of Project.
- Gain a competitive advantage for engineering graduate schools.
- Learn how you can impact your community as an engineer.

This year, a record 66 undergraduate students were selected to join the 2021 SURP cohort, spread out across 31 faculty in 6 engineering departments. We are happy to announce 64% of these are women, 20% are underrepresented minorities, and many are first generation and low income students. SURP is involved with ongoing efforts in fostering a more diverse, equitable and inclusive community at UCLA Samueli Engineering.

Creating new knowledge is a very difficult yet important task, and these high-performing students have done an outstanding job working through the rigors of academic research. These students should be very proud of all that they have accomplished in a short time this summer. I encourage you to explore our publication and learn about all the cutting-edge knowledge that is being created here.

Sincerely,

Dr. Jayathi Murthy
Ronald and Valerie Sugar Dean

Julia Bi

Electrical Engineering
Freshman, UCLA

Autonomous Vehicle with Offloaded Server Control using Mobile Edge Computing

FACULTY ADVISOR
C.K. Ken Yang

DAILY LAB SUPERVISOR
Jack Irish

DEPARTMENT
Electrical and Computer Engineering

ABSTRACT

Modern day mobile applications not only require a low latency, but but also incur a high energy cost. However, mobile devices are limited in their battery life and computational capabilities. Mobile Edge Computing (MEC) reduces latency and energy consumption by offloading some or all of the computing tasks to MEC servers. The Mobile Edge Compute Applications (MECA) lab establishes a 5G development environment that allows for experiments and testing with the 5G network and MEC. This particular project is an autonomous car controller which offloads control decisions to a central server, using a camera as input. Using gRPC, the camera sends images to the central server, which processes them and returns a control signal to guide the car. The goal is to compare the latency of this setup with traditional autonomous car controllers and achieve similar or better performance. At the moment, since it is difficult to gain access to physical materials, a simulation that imitates the complexity of video processing was used to gather data on the effectiveness of this strategy. As expected, sending the processing to a server is more time consuming with simple tasks, due to the initial time cost associated with the server-client communication. With more complex tasks, the server processing time is faster than processing at the client, since the server has better computational capabilities. The next step is applying these concepts to a physical setup with proper video processing and a car which takes the control signal.

UCLA Samueli School of Engineering

Autonomous Vehicle with Offloaded Server Control Using Mobile Edge Computing

Julia Bi, Jack Irish, Professor C.K. Ken Yang
Department of Electrical and Computer Engineering, University of California – Los Angeles

UCLA Samueli School of Engineering
SUMMER UNDERGRADUATE RESEARCH PROGRAM

Samueli Research Scholars
UCLA Samueli School of Engineering

FAST TRACK TO SUCCESS
UCLA Electrical and Computer Engineering

Introduction

The project aims to test concepts of Mobile Edge Computing (MEC), a technology that reduces latency and energy consumption of mobile devices through offloading computing tasks to external servers. Specifically, this concept was applied to an autonomous car that offloads decisions to a central server.

The goal is to measure the performance and latency of this setup, and compare it to traditional autonomous car controllers. We hypothesize that using MEC will allow the offloaded controller to have similar or better performance.

Background

Modern day mobile applications not only require a low latency, but also incur a high energy cost. However, mobile devices are limited in their battery life and computational capabilities.

Figure 1: Mobile Edge Computing (MEC) solves this issue by offloading some or all of the computing tasks to MEC servers at the edges of mobile networks, therefore improving efficiency and reducing latency.

This project is an autonomous car controller which, instead of making decisions on the car itself like traditional controllers, offloads control decisions to a central server, which becomes more efficient as the computations become more complex. The car uses a camera as input. It streams video to the central server, which processes the video and returns a control signal.

Materials and Methods

Client-Server Communication:

To communicate between the camera, server, and car, the project uses gRPC. gRPC is Google's open source RPC (Remote Procedure Call) system that allows for bidirectional messages as well as streaming.

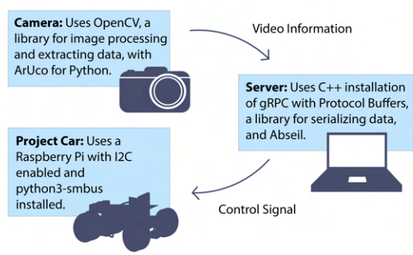

"Standard" Setup: The camera does the image processing and sends its results to the server, which then sends the results to the car. The image processing time is included in the camera-server latency.
"Streaming" Setup: The camera streams video directly to the server, which processes it and sends the result to the car. The image processing time is included in the server-car latency.

Results and Discussion

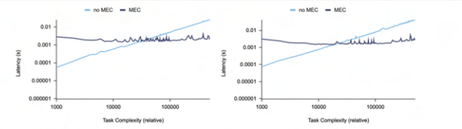

Figure 2: Task Complexity v. Latency Plots. Two simulations that imitate the complexity of video processing were used to gather data. As expected, server processing is more time consuming with simple tasks, due to the initial time cost of communication. With more complex tasks, the server processing time is faster because it has better computational capabilities.

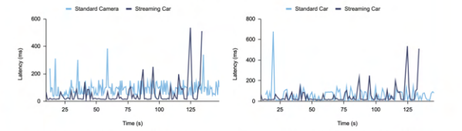

Figure 3: Time v. Latency Plots. *Left Plot:* The camera-server latency for the Standard setup and the server-car latency for the Streaming setup, both of which include the video processing, are plotted. The Streaming latency is on average lower than the Standard Latency by 39.2 ms, since the server has better computational capabilities. *Right Plot:* The server-car latencies for both the Standard and Streaming setup are plotted. The average latencies are roughly equal (Standard: 55.8 ms, Streaming: 49.3 ms), which is unexpected, since while their baseline latencies should be similar, the Streaming setup should be slightly slower on average because of the time taken by the server to do the image processing.

Conclusion

The relative efficiency of MEC vs Non-MEC in the simulation trials is as expected and confirms theory. The relative efficiency in the camera-car trials is somewhat unexpected and unclear, and should be investigated further.

Future Steps:

1. Further refine camera-car systems to stabilize latency measurements.
2. Gather and analyze data to explain unexpected results and confirm trends.

References

Gu, Xiaohui et al. "Energy-Optimal Latency-Constrained Application Offloading in Mobile-Edge Computing." Sensors (Basel, Switzerland) vol. 20,11 3064. 28 May. 2020, doi:10.3390/s20113064 https://pubmed.ncbi.nlm.nih.gov/32481742/

Mobile Edge Compute Applications Laboratory. https://mecalab.seas.ucla.edu

gRPC. https://grpc.io

Acknowledgements

I would like to thank Professor Yang and the MECA Lab, as well as the Samueli Engineering Summer Undergraduate Research Program and the Fast Track Program, for the support and resources. Many thanks to Jack Irish for his guidance and framework for this project. Many thanks to the Samueli Research Scholars Program for funding this research.

Gianna Brown

Bioengineering
Sophomore UCLA

How Implementing a Diverse Training Set Affects Skin Tone Bias in Deep Learning Algorithms

FACULTY ADVISOR

Achuta Kadambi

DAILY LAB SUPERVISOR

Pradyumna Chari

DEPARTMENT

Electrical and Computer Engineering

ABSTRACT

The COVID-19 pandemic has highlighted the growing need for avenues that will allow doctors to assess and treat their patients virtually rather than in person. One important component needed to implement telemedicine visits is the ability to take a person's heart rate virtually. Currently, there are algorithms that are able to do this by extracting ppg, which is the measure of blood flow under the skin. However, previous research has shown that their accuracy varies based on skin tone, with a much higher accuracy for lighter skin tones than darker ones. These inaccuracies need to be corrected before this technology is allowed to be used in the medical field in order to ensure equitable performance among all patients. Our lab attempts to minimize this bias by incorporating diverse training sets to train deep learning algorithms DeepPhys and PhysNet in order to determine the optimal proportion of lighter to darker skin tones in our training set needed to achieve an accurate ppg reading for all skin tones. Participants were asked to connect to a pulse oximeter and placed in front of a white background, while five one-minute videos were taken in sync with the pulse oximeter ppg readings. These videos were then used to train and test DeepPhys and PhysNet with different proportions of lighter skin tones to darker skin tones. Although the experiment is not yet complete, initial results show that having more darker skin participants in the training set decreases the accuracy of the networks in the testing set, but we believe that this is due to not having enough darker skin toned participants needed to truly test our hypothesis.

UCLA Samueli School of Engineering

SUMMER UNDERGRADUATE RESEARCH PROGRAM

How Implementing a Diverse Training Set Affects Skin Tone Bias in Deep Learning Algorithms

Gianna Brown, Pradyumna Chari, Oyku Deniz Bozkurt, Dr. Achuta Kadambi
Department of Electrical and Computer Engineering, University of California Los Angeles

INTRODUCTION

Heart rate can be virtually measured through various algorithms, but previous research has shown that they are less accurate for darker skin tones. Our lab attempted to correct this bias by adjusting the training set of existing algorithms and finding the proportion of dark, medium, and light skin tones that need to be represented in the algorithm's training set in order to get accurate and unbiased results.

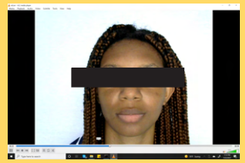

Figure 1 Screenshot from a video These videos are used to train deep learning algorithms DeepPhys and PhysNet before testing them on other videos within our database.

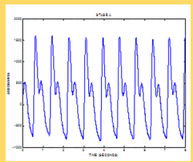

Figure 2 A ppg signal Deep Leaning algorithms can analyze the videos in order to find the ppg, which is the amount of blood flowing under the skin at a certain point in time. From there, it is easy to find the heart rate.

CONCLUSION

Although the experiment is incomplete, the initial results can give insight on how the study is going so far and if there is anything that should be changed to improve the study.

THINGS TO CONCLUDE

- So far, adjusting training set does not do well with addressing current disparities
- This may be due to underrepresentation of darker skin tone participants in data set

NEXT STEPS

- Work to ensure there are enough darker skin tone participants to successfully test the lab's hypothesis
- If this trend continues, look into other factors such as the construction of the algorithm or the background as possible sources of bias

MATERIALS AND METHODS

Figure 3 A picture of the experimental setup as described in Materials and Methods

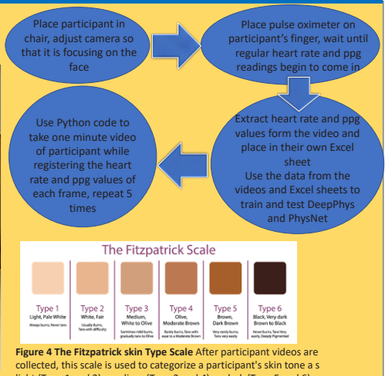

Figure 4 The Fitzpatrick skin Type Scale After participant videos are collected, this scale is used to categorize a participant's skin tone a s light (Type 1 and 2), medium (Type 3 and 4) or dark (Type 5 and 6). The lab them selects an appropriate amount of each skin tone to be included in the training and testing sets.

RESULTS AND DISCUSSION

Although the experiment is not yet complete, the lab has enough data to begin training and testing to gather initial findings.

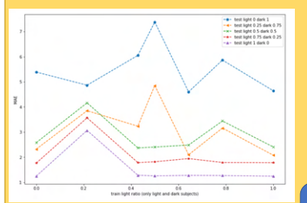

Figure 5 Results Graph This graph describes the mean absolute error of PhysNet based on the proportion of light to darker skin tone participants included in the training set

The graph to the left (Figure 5) shows the mean absolute error (MAE) of videos run through PhysNet trained with different training sets containing different proportions of light skin toned and dark skin toned participants.

IMPORTANT OBSERVATIONS

Tests with more light skin participants fared better

For tests with more dark skin participants, .2 light to .8 dark seems promising

More representation of darker skin tones is needed before we can present conclusive results

ACKNOWLEDGEMENTS

I would like to thank Dr. Achuta Kadambi for allowing me into his lab and thank grad students Pradyumna and Deniz for mentoring me and helping me understand the project.

I would also like to thank the SURP program for mentoring me and providing me with workshops to allow me to learn how to format and share the research done over the summer.

REFERENCES

1 Taken from lab
2 https://www.researchgate.net/figure/PPG-signals-from-commercial-heart-rate-monitor-1_fig10_264622988
3 Taken from lab
4 https://www.skinrenewal.co.za/fitzpatrick-skin-type-iii
5 Taken from lab

Arlene Constantino

Electrical Engineering
Sophomore, El Camino College

LiDAR Data Classification Using Convolutional Neural Network Based on Pointnet Architecture

FACULTY ADVISOR
Chee Wei Wong

DAILY LAB SUPERVISOR
Jaime Flor Flores

DEPARTMENT
Electrical and Computer Engineering

ABSTRACT

Convolutional neural networks are the state-of-the-art algorithm for object classification. Due to the various types of objects that are processed and to facilitate training, typical convolutional neural networks (CNNs) require data preprocessing like zero padding or 3D to 2D space projections and do not work with point cloud data. Light Detection and Ranging (LiDAR) is one of the main technologies used in self-driving cars and terrain mapping. Since LiDAR uses time of flight from laser beams to create a 3D map of the area, the generated data is a point cloud. In order to solve these problems, here we present an implementation of CNNs using a modified PointNet architecture. PointNet architecture is directly capable of taking a point cloud and running it on the classification algorithm, which is much more efficient than transforming the data before being fed to the network. In this study, we optimize the said convolutional neural network based on PointNet architecture. We train the model using LiDAR data taken in Westwood and tune its parameters accordingly to achieve close to state-of-the-art performance. As of now, in preliminary testing, the model achieves an 89.82% training accuracy. The goal is to further achieve a model that can be able to map external environments to aid driver-safety and autonomous navigation.

UCLA Samueli School of Engineering

LiDAR DATA CLASSIFICATION USING CONVOLUTIONAL NEURAL NETWORK BASED ON POINTNET ARCHITECTURE

Arlene Constantino, Jaime Flor Flores, Dr. Chee Wei Wong
Fang Lu, Mesoscopic Optics and Quantum Electronics Laboratory
Department of Electrical and Computer Engineering, University of California – Los Angeles

UCLA Samueli School of Engineering
SUMMER UNDERGRADUATE RESEARCH PROGRAM
MESA

Introduction

Convolutional neural networks (CNNs) are state-of-the-art algorithms for object classification. However, typical CNNs do not directly process data in irregular formats, like point clouds, as an input.

A **point cloud** is a set of 3D points which represent arbitrary objects. It is the data generated by using **Light Detection and Ranging (LiDAR)** since it uses the time of flight to create a 3D map of the area. Working with point clouds requires dimensionality data transformations before being fed to the network because of its irregular size and shape.

This data preprocessing can make LiDAR data classification memory and time expensive. To accomplish the task efficiently, we implemented **PointNet based architecture**, which directly consumes point cloud data.

Objective

To optimize a convolutional neural network based on PointNet architecture to achieve a similar state-of-the-art performance.

Significance

The network will be used to accurately classify objects seen in LiDAR data taken in Westwood. And eventually, be used to map our external environments to aid driver-safety and autonomous navigation.

Materials

- Codes are written in Python
- Source code and the labeled LiDAR data are accessed through Git
- Programs are executed in Google Colaboratory

colab

Methods

Access source code and labeled LiDAR data through Git → Implement PointNet architecture to the model → Train the model by executing the programs in Google Colaboratory → Analyze the training and validation results → Fine-tune the model by adjusting hyperparameters

PointNet Architecture

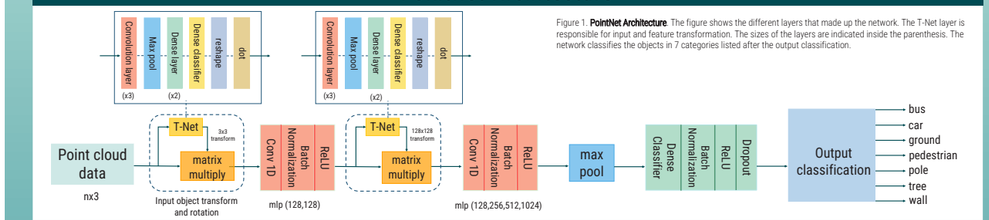

Figure 1. **PointNet Architecture**. The figure shows the different layers that made up the network. The T-Net layer is responsible for input and feature transformation. The sizes of the layers are indicated inside the parenthesis. The network classifies the objects in 7 categories listed after the output classification.

Results and Discussion

Figure 2. **Training and Validation Accuracy.** The figure on the left shows the training and validation accuracy of model in 15 epochs.

Figure 3. **Training and Validation Accuracy.** The figure on the right shows the training and validation accuracy of model in 20 epochs.

We implemented a PointNet based architecture using CNN for classifying LiDAR data. We ran multiple models with different hyperparameters such as learning rate, number of epochs, and dropout rate. Initially, the network was trained in 11,047 clusters with 6 categories. As a result, the model achieved an 89.82% training accuracy and a 59.38% validation accuracy, seen in Figure 2. Afterward, car clusters were retrieved, and the data increased to 11,770 clusters with 7 categories. In Figure 3, the training accuracy went up to 91.25%.

As seen in the figures above, there is a distinct gap between the training accuracy and validation accuracy. Presented above are preliminary results as further work needs to be done to achieve state-of-the-art performance.

Conclusion

In this project, we developed a model based on PointNet architecture that performs LiDAR data classification. The network classifies the objects seen in LiDAR data in 7 categories: bus, car, ground, pedestrian, pole, tree, and wall. In preliminary testing, the model achieves a training accuracy of 89.82% in 6 categories and 91.25% in 7 categories. In conclusion, further work is needed for the model to map our external environments to aid driver-safety and autonomous navigation. Labeling more clusters for some categories, especially cars and buses, would be beneficial for the model.

References

[1] C. Qi, H. Su, et al. *PointNet: Deep Learning on Point Sets for 3D Classification and Segmentation,* arXiv preprint arXiv:1612.00593v2 (2017).
[2] F. Chollet. *Deep Learning with Python.* Manning Publications Co. (2018).

Acknowledgement

I would like to thank Dr. Chee Wei Wong, Arturo Hernandez, and the Summer Undergraduate Research Program for this research opportunity. I would also like to thank the National Science Foundation (NSF) for funding the project. Additionally, I would like to acknowledge Jaime Flor Flores and Noah Himed for their help and guidance throughout the program.

Micah Crook

Chemical Engineering
Freshman, El Camino College

Optimizing the Electrochemical Oxidation of Methane

FACULTY ADVISOR
Carlos Morales-Guio

DAILY LAB SUPERVISOR
Kangze Shen

DEPARTMENT
Chemical Engineering

ABSTRACT

The electrochemical oxidation of methane is a promising reaction that can provide an alternative to methane flaring for gas drilling sites. However, there is still little known about the ideal conditions for this reaction, making it unrealistic for industrial use. This study aims to further the understanding of the methane oxidation reaction (MOR) by analyzing the products under different potentials. A titanium cylinder was plated with a cobalt catalyst and then rotated in a potassium carbonate solution while methane flowed into the solution. Samples were taken from the cell every 20 minutes for 2 hours and analyzed using NMR. It was found that methanol and acetate were predominantly formed at low potentials. Methanol averaged over 1.6 μM at potentials of 0.6 to 1.0 V and acetate averaged 25 μM at potentials of 0.6 and 0.8 V. To add further support, methanol and formate only had a substantial faradaic efficiency at 0.7 V of 7.9% and 7.6% respectively. Formate, a compound not detected in previous MOR studies, was observed when acetate persisted at high concentrations above 40 μM, suggesting that there is a reaction occurring that relates the two. With this knowledge, a baseline for comparison can be set for experiments with other catalysts. The discovery of formate will encourage further studies of the mechanism when acetate is at high concentrations. In future work, additional catalysts will be analyzed using this setup to determine what conditions are the best for producing useful products.

UCLA Samueli School of Engineering

Optimizing the Electrochemical Oxidation of Methane

Micah Crook, Kangze Shen, Professor Carlos Morales-Guio
Department of Chemical Engineering, University of California – Los Angeles

UCLA Samueli School of Engineering
SUMMER UNDERGRADUATE RESEARCH PROGRAM
MESA

Introduction

Problem: Climate Change
- Methane flaring at drill sites accounts for 1% of CO_2 emissions.
- Need a chemical process for an alternative to reduce emissions.

Current Process: Methane Reforming
- Methane transformed into methanol.
- Only profitable at large scales.
- Not economically realistic for drill sites.

Solution: Electrochemical Oxidation
- Methane oxidized with electricity.
- Modular and mobile reactions.
- Profitable at small scales.
- Renewable source of liquid fuels.
- Currently too inefficient to be viable.

Research
- Little is known about optimal conditions.
- Different metal catalysts and potentials will be tested.
- Focusing on cobalt on titanium specifically.

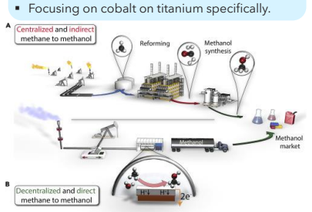

Figure 1. Centralized and decentralized Methane-to-Methanol Technologies [1].
(A) Schematic of methane reforming, the current method for processing methane. Too centralized and indirect to be used by gas drilling sites.
(B) Schematic of electrochemical oxidation of methane, the proposed decentralized method for processing methane. Will be able to be used by gas drilling sites.

Materials

Rotation Cell Components STEP 3
- Working electrode
  - Cobalt catalyst plated on titanium cylinder.
  - Rotated at 800 rpm.
- Counter electrode
  - Platinum foil
- Reference electrode
  - Ag/AgCl
- Selemion membrane
  - Membrane that only allows for anions to pass through.

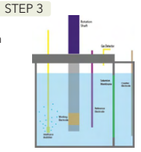

Figure 2. Schematic of rotation cell

Nuclear Magnetic Resonance (NMR) STEP 4
- Measures how molecules interact with a strong magnetic field.
  - Each peak corresponds to a unique molecule.
  - Area under each peak corresponds to concentration.

Potentiostat
- Controls the potential during an electrical process.
- Chronoamperometry STEP 3
  - Constant potential.
  - Main process for experiment.
- Linear Sweep Voltammetry (LSV) STEP 1
  - Potential scanned forward over time.
  - Used to plate cobalt catalyst onto titanium.
- Cyclic Voltammetry (CV) STEP 2
  - Potential scanned forward and reversed over time
  - Used to verify quality of catalyst.

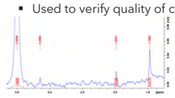

Figure 3. NMR of sample

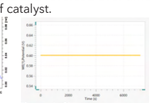

Figure 4. Chronoamperometry

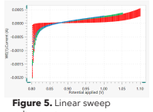

Figure 5. Linear sweep voltammetry

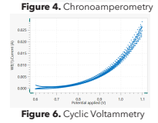

Figure 6. Cyclic Voltammetry

Results

Figure 7. Average concentration of products over tested potentials. Methanol averaged over 1.6 μM at potentials of 0.6 to 1.0 V. Acetate averaged 25 μM at potentials of 0.6 and 0.8 V. Formate was only found at 0.6 and 0.8 V with 1.9 and 2.2 μM, respectively.

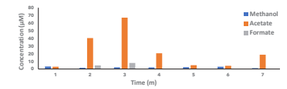

Figure 8. Concentration of products over time at 0.6 V. Formate and acetate were shown to fluctuate over time. Formate only appeared at minute 20 and 40 where acetate was at its highest. Methanol concentration remained constant over time.

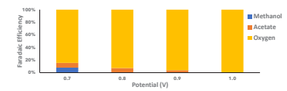

Figure 9. Faradaic efficiency of products over tested potentials. Acetate efficiency found to decrease as potential increases. Methanol efficiency was significant at only 0.7 V at 14%. Formate efficiency was at 0% for all potentials.

Conclusions
- It was found that cobalt catalysts produce useful products at lower potentials.
- First time formate was discovered from this reaction.
- Faradaic efficiency has been shown to be a useful benchmark for reaction efficiency.

Future Work
- Explore the correlation between acetate and formate to figure out a possible reaction mechanism.
- Test different variables:

Methods

Form Catalyst Layer
A titanium cylinder is polished mechanically and then cleaned in an acid bath. The cylinder is placed in a cobalt acetate solution and then plated using linear sweep voltammetry run by a potentiostat.

STEP 1

Confirm Quality of Catalyst
In potassium carbonate solution, cyclic voltammetry is run and current over potential is graphed. The graph is compared from previous runs to ensure the quality is consistent.

STEP 2

Run Reaction at Set Potential
The rotation cell is assembled and filled with potassium carbonate solution. Methane is flowed into the cell and electricity is allowed to flow at a constant potential.

STEP 3

Analyze Products via NMR
Liquid samples are taken every 20 minutes for 2 hours. Concentrations are then quantified using NMR for every time and then compared with other potentials

STEP 4

References

[1] Jang, Joonbaek, et al. "Electrochemical Direct Partial Oxidation of Methane to Methanol." *Joule*, vol. 3, no. 11, 2019, pp. 2589–2593.
[2] Prajapati, Aditya, et al. "Fundamental Insight into Electrochemical Oxidation of Methane towards Methanol on Transition Metal Oxides." *Proceedings of the National Academy of Sciences*, vol. 118, no. 8, 2021.
[3] Infographic elements from FreePix.com and TheNounProject.com

Acknowledgements

I would like to thank El Camino MESA for funding my research through the UCLA Summer Undergraduate Research Program. I would also like to thank Professor Carlos Morales-Guio and Kangze Shen for their resources and support on my project and William Herrera for his guidance throughout the program.

Sophia Du

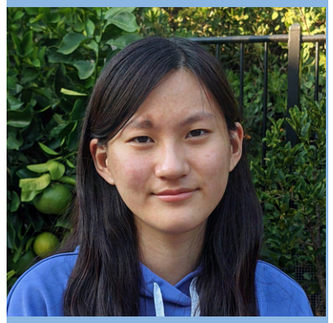

Electrical Engineering
Freshman, UCLA

Thermal Limitations of Miniature Printed Circuit Board (PCB) Photon Sources

FACULTY ADVISOR
Rob Candler

DAILY LAB SUPERVISOR
Benjamin Pound

DEPARTMENT
Electrical and Computer Engineering

ABSTRACT

Modern-day x-ray light sources use relativistic electron beams to produce photons. Quadrupoles and undulators are magnetic devices that form an integral part of these light sources. Current quadrupole and undulator technology at the micro to millimeter scale use electromagnets and are fabricated on silicon wafers. The objective of this research project is to explore the usage of printed circuit boards (PCBs) in quadrupoles and undulators and to test their limitations. PCBs could potentially make the current fabrication process of these devices easier and cheaper. However, PCB-based devices cannot reach the same current densities as silicon-based ones due to heating; the thermal conductivity of FR4, the PCB material, is significantly lower than that of silicon. Four designs (1 quadrupole, 3 undulators) with 1 to 2 trace layers were created in DipTrace and manufactured. COMSOL simulations showed that the four designs could run at current densities from 2.1×10 8 to 2.7×10 8 A/m2 before the FR4 reaches its glass transition temperature (130°C). Experimental data obtained with a thermal camera agreed reasonably well with the simulated data. The simulations and experiments both demonstrated that wider copper traces and more trace layers reduce temperature rise for the same total current but increase temperature rise for the same current density. Initial magnetic simulations of the quadrupole show that the quadrupole design can produce a magnetic gradient up to 34 T/m at the maximum experimental current density and 100 µm gap size. Future works include using active cooling systems to increase thermal performance and conducting real-world magnetic tests with the PCB designs.

UCLA Samueli School of Engineering

Thermal Limitations of Miniature Printed Circuit Board (PCB) Photon Sources

Sophia Du, Benjamin Pound, Rob Candler
Sensors and Technology Laboratory (STL), Department of Electrical and Computer Engineering, University of California - Los Angeles

FAST TRACK TO SUCCESS
UCLA Electrical and Computer Engineering

UCLA Samueli School of Engineering
SUMMER UNDERGRADUATE RESEARCH PROGRAM
STL

Introduction

Modern x-ray light sources, like x-ray free electron lasers and synchrotrons, use relativistic electron beams to produce photons. Quadrupoles and undulators are magnetic devices that form an integral part of these light sources.

Quadrupole — a magnet that focuses the electron beam on one axis and defocuses it on the other. Multiple quadrupoles can be placed in succession with a 90° rotational offset for focusing in both dimensions.

Undulator — alternating dipole magnets that accelerate electrons transverse to their direction of travel in a periodic manner; this causes the electrons to generate photons. The wavelength of the photons depends on the spacing of the dipole magnets, or the undulator period, and the electron velocity.

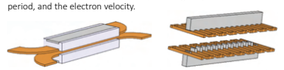

Figure 1: Miniature Panofsky Quadrupole (left) and Serpentine Design Undulator (right) [1]

Current quadrupole and undulator technology at the micrometer to millimeter scale use electromagnets produced on silicon wafers. Electric currents that produce magnetic fields flow through copper traces (orange). Magnetic yokes (dark gray), material with high magnetic permeability, increase the magnetic field strength.

Objectives

1. Design printed circuit boards (PCBs) for quadrupoles and undulators used in miniature photon sources.
2. Test the current and thermal limitations of the PCBs.

Advantages

✓ Fabrication of copper traces on a PCB is easier and cheaper than fabrication with silicon substrates; this can reduce costs significantly, increasing the accessibility of compact light sources.
✓ Multiple quadrupoles and undulators can be placed on one PCB and aligned before manufacturing.

Disadvantages

✗ FR4, the material of the PCB, has a low thermal conductivity compared to silicon. Heat generated by the high currents flowing through the copper traces will dissipate slowly, which can lead to the PCB overheating.
✗ Due to lower currents, PCB-based devices produce weaker magnetic fields compared to silicon-based devices.

Methods

1. Design PCBs for multiple quadrupoles and undulators — DipTrace
2. Find current limits of copper traces for each design using industry standards — IPC
3. Perform thermal simulations of designs — COMSOL
4. Test manufactured PCBs and measure temperature with thermal camera

PCB Designs

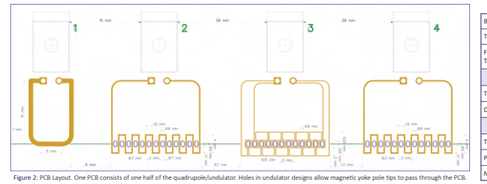

Figure 2: PCB Layout. One PCB consists of one half of the quadrupole/undulator. Holes in undulator designs allow magnetic yoke pole tips to pass through the PCB.

Table 1: Design Specifications

Board Dimensions	37 × 102 × 0.8 mm
Trace Thickness	2 oz (70 µm)
FR4 Transition Temperature	130 - 140 °C
Quadrupole	
Trace Width	1 mm
Device Length	5 mm
Undulator (serpentine, coil)	
Trace Width	0.3 mm, 0.15 mm
Period	3 mm, 3 mm
Number of Periods	6.5, 6

Table 2: Design Descriptions

#	Device	Design	Layers
1	Quadrupole	Miniature Panofsky	1
2	Undulator	Serpentine	1
3	Undulator	Coil	2
4	Undulator	Serpentine	2

- serpentine design undulator — the copper traces wind around the holes.
- coil design undulator — the copper traces closely wrap around each hole.
- two layers — copper traces are on the top and bottom of the PCB, increasing current capacity.

Figure 3: PCB Front and Back

Figure 4: PCB Size Comparison

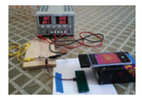

Figure 5: Experiment Setup

Results

Table 3: Maximum current capacity based on the IPC-2152 industry standard [2]

IPC-2152 Standard Maximum Current Capacity	
ambient temperature = 25°C temperature increase = 25°C external trace layer	
Design	Current Per Trace (A)
1	4.68
2	2.34
3	1.57
4	2.34

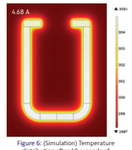

Figure 6: (Simulation) Temperature distribution after 10 seconds of continuous current, Design 1.

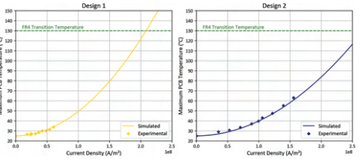

Figure 9: Maximum temperature after 10 seconds of continuous current vs. current density for each design. Lines denote simulated data and diamonds denote experimental data.

Figure 7: (Thermal Camera) Temperature distribution after 10 seconds of continuous current, Design 1. Hottest point is marked.

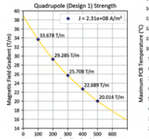

Figure 8: Quadrupole (Design 1) magnetic field gradient vs. gap size.

Conclusion & Future Works

- Simulated data agreed reasonably well with experimental data.
- Wider copper traces and more trace layers reduce temperature rise for the same total current but increase temperature rise for the same current density.

- Perform magnetic simulations and real-world tests with the designs.
- Test the PCB's thermal performance with pulsed current and with active cooling systems.
- Design PCBs with more than 2 trace layers to utilize internal layers.

References

[1] Pound, B. A. (2021). Micro and Milliscale Magnetic Systems for Particle Beam Manipulation [Prospectus].
[2] Sierra Circuits. (2021). PCB trace width, Current capacity and Temperature rise calculator. twcalculator.app.protoexpress.com.

Acknowledgements

I would like to thank Professor Rob Candler for giving me the opportunity to work in his lab and Ben Pound for his guidance throughout my research project. I also would like to thank the National Science Foundation, the UCLA Summer Undergraduate Research Program, and the UCLA ECE Fast Track to Success Program.

Marisa Duran

Computer Science
Freshman, UCLA

Visual Processing for Autonomous Robot Swarms

FACULTY ADVISOR
Ankur Mehta

DAILY LAB SUPERVISOR
Ankur Mehta

DEPARTMENT
Electrical and Computer Engineering

ABSTRACT

Visual processing is an integral piece of robotic autonomy, as cameras attached to the robot collect and process pictures, allowing robots to sense the world around them. Robots collect information from the processed image and use it to make decisions. The goal of this project is to use colored blob detection and AprilTag detection to control low-cost robotic swarms, or cohesive groups of robots. I used an openMV camera, which is a small microprocessor with a camera attached, to accomplish this. To recognize colored blobs, I used thresholds to group pixels by color, which is a method that reduces issues with lighting changes. I programmed the camera to effectively recognize multiple different colored blobs at the same time and determine the distance between the camera and the object if the object's dimensions are known. The error associated with this calculation is about 20 millimeters from a range of less than a meter. AprilTags are recognized by the unique pattern of the tag, and I determined that the range of detection is dependent on the tag size. I used the AprilTag recognition capability to determine the relative position of the robot. The calculation of the distance between the camera and the tag has an average error of about 40 millimeters at a range of 3 meters, which is a relatively insignificant amount. We then applied these capabilities to robot swarm autonomy, using them to recognize a target object, calculate distances between robots, and perform other swarm behavior.works include using active cooling systems to increase thermal performance and conducting real-world magnetic tests with the PCB designs.

Visual Processing for Autonomous Robot Swarms

Marisa Duran, Dr. Ankur Mehta
Laboratory for Embedded Machines and Ubiquitous Robots
UCLA Electrical and Computer Engineering Department

Samueli Research Scholars

UCLA Samueli School of Engineering
SUMMER UNDERGRADUATE RESEARCH PROGRAM

LEMUR

Objective: To use colored blob detection and AprilTag detection to control low-cost robot swarms

Introduction
- Visual processing provides robots with information that is used to make decisions
- In robot swarms, there is a need to find each robot's relative position
- I used AprilTags to determine the relative position
- I used colored blobs to identify other robots and target objects
- We then applied these capabilities to autonomous robot swarms

Key Terms
Computer Vision: When computers interpret information from images and videos
Feedback Control: When sensors on a robot (such as a camera) collect information and then robots take action based on that information
Robot Swarm: A group of robots that work together towards a common goal
Color Thresholding: A method that groups together similarly colored pixels, if they are within a certain constraint or threshold that represents a color

Detecting Colored Blobs and AprilTags

Materials

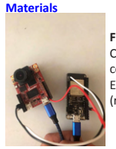

Figure 1: OpenMV Camera (left) connected to an ESP32 Featherboard (right)

Experimental Setup

Figure 2: Measuring reliability, range, and error of AprilTag detection

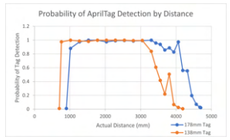

Figure 3: Graph displaying the range and reliability of AprilTag detection for differently sized tags

Using Vision to Control Robots: Methods

Colored Blob Detection (Figure 4)
- Recognizes multiple colors
- Achieved with color thresholding
- Finds blob position
- Calculates z-distance

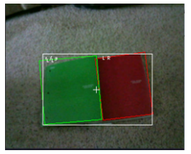

Figure 4: Colored blob recognition

AprilTag Detection (Figure 5)
- Recognizes unique tags
- Finds relative position and orientation
- Calculates distance
- Reliable detection (see Figure 3)

Figure 5: AprilTag recognition

Applying Visual Processing to Robots

Paper Boats (Figure 8)
- Detecting a colored cup

Paper Cars (Figure 6)
- Finding the location of a colored car
- Detecting AprilTags from above the car to determine the relative position

Blimps (Figure 9)
- Tracking a colored box

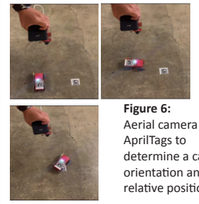

Figure 6: Aerial camera using AprilTags to determine a car's orientation and relative position

Limitations
- The AprilTag distance calculation has an associated error

Figure 7: Graph displaying the error for the calculated distance

Camera = red arrow

Figure 8: Paper boat tracking a red cup with color detection

Figure 9: Blimp turning to follow a green box using colored blob detection

Conclusion

Visual processing provides many capabilities for autonomous robot swarms.
Colored Blob Recognition and AprilTag Recognition
- Recognizes landmarks, other robots, and target objects
- Determines distance between two robots
- Determines orientation

When integrated into a robot swarm, camera sensing and visual processing provides the robots with all the necessary information in order for the robots to work cohesively as a group.

Acknowledgements

- Dr. Ankur Mehta
- Bhavik Joshi, Grace Kwak, Jillian Pantig, Sudarshan Seshadri, Jaehoon Song, Shahrul Kamil bin Hassan, and LEMUR
- William Herrera and the Summer Undergraduate Research Program
- Samueli Research Scholars

Virginia Garcia

Chemical Engineering
Freshman, UCLA

Developing Predictive Abilities for Cancer Cell Growth

FACULTY ADVISOR

Jun Park

DAILY LAB SUPERVISOR

Kris Park

DEPARTMENT

Chemical Engineering

ABSTRACT

Cancer, being a leading cause of death, is a highly researched topic, yet researchers have struggled to understand the relationship between metabolism and cancer cell growth. Glycolysis and gluconeogenesis are the two most important pathways in cancer metabolism. In a low glucose environment, only gluconeogenesis can be performed. A challenge in analyzing cancer's metabolic pathways is measuring what happens inside cells. Cells are dynamic beings which reside in dynamic environments. Traditional measurement techniques are limiting because they rely on a snapshot of the cell and environment, which is a crude representation of the dynamic processes. In order to understand the internal workings, this project sought to measure metabolic fluxes and dynamic metabolic pathway usage. The approach involved conducting flux balance analysis within Cobra Toolbox. First, experimental measurements of cellular nutrient requirements and gene expression data from The Cancer Genome Atlas were mapped in Rstudio. By incorporating those experimental measurements, the human Recon3D model was tailored to model non-small cell lung cancer. Conducting flux balance analysis on the model using appropriate parameters will yield an approximate growth rate of lung cancer cells. Data collection has not yet been completed. This research is important because if it is possible to predict whether or not cancer cells can complete gluconeogenesis, specific therapies for distinct cancer cells can be developed. The predictive abilities that will be gained from completing this project will provide much needed insight into the dynamic systems of cancer cell growth.

UCLA Samueli School of Engineering

Developing Predictive Abilities for Cancer Cell Growth

LILLY GARCIA, KRIS PARK, JUN PARK

Samueli Research Scholars

UCLA Samueli School of Engineering

SUMMER UNDERGRADUATE RESEARCH PROGRAM

UCLA Samueli School of Engineering

INTRODUCTION

Cancer is a leading cause of death and a very important disease to understand. Yet, the dynamic nature of cells and their environment make them difficult to study. This project aims to better understand the dynamic nature of cells by measuring metabolite fluxes and predicting cancer cell growth rates.

APPLICATION

If it is possible to predict whether or not cancer cells can complete gluconeogenesis, specific therapies for distinct cancer cells can be developed.

KEY TERMS

- Tumor Microenvironment-Where Cells survive and proliferate. Different conditions can stifle or help growth
- Gluconeogenesis- Important pathway for Cancer cell growth in low glucose environment. Opposite of glycolysis with some exceptions
- Flux Balance Analysis (FBA)- Mathematical approach for predicting metabolic phenotypes, growth rates, and pathway utilization
- Recon3D- Genome scale model for the entire human body including protein and metabolite structure and atom-atom mapping

pyr
↓
glc

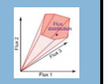

METHODS

1. Download Data from The Cancer Genome Atlas (TCGA) database
2. Determine gene expression patterns for Lung Squamous Cell Carcinoma in RStudio
3. Impose constraints on nutrient uptake
4. Complete FBA on Recon3D model in Cobra Toolbox to determine growth rate

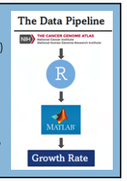

GOAL

- Develop predictive abilities of cancer cell growth using flux balance analysis
  - Predict which types of cancer can survive in low glucose environments
- Create better understanding of cancer metabolism
- Understand where to interfere in metabolic pathways in order to stop growth

RESULTS AND DISCUSSION

Modeling growth with FBA is possible for microbes

```
>> model=readCbModel('iAF1260.xml');
model=changeRxnBounds(model, 'EX_glc__D_e', -18.5, 'l');
model = changeRxnBounds(model,'EX_o2_e',-1000,'l');
model = changeObjective(model,'BIOMASS_Ec_iAF1260_core_59p81M');
FBAsolution = optimizeCbModel(model,'max');
FBAsolution.f

ans =

    1.7478
```

Figure 1: MATLAB code which establishes the lower bounds for glucose and oxygen exchange and maximizes the established objective reaction.

The E. coli model is one of the simplest model systems. Model iAF1260 can be found in the BIGG database and represents a strain of E. coli. After loading the model into MATLAB, Cobra Toolbox was used to change constraints of specific reactions within the model and maximize the flux rate of the Biomass reaction. The growth rate was found to me 1.7478 hr^-1, which corresponds to a doubling time of 0.3966 hours, a reasonable doubling time for this strain. Therefore, modeling growth with FBA was successful for E. coli.

It is possible to incorporate experimental data

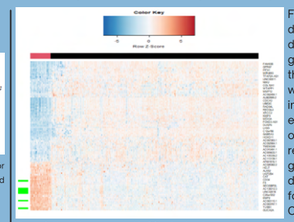

Figure 2: Heat Map generated in RStudio showing gene expression patterns of Lung Squamous Cell Carcinoma based on patient data.

From the TCGA patient data, the 100 most differently expressed genes were mapped and their fold change values were identified. This information was exported to MATLAB in order to find associated reactions for metabolic genes. Experimental data of gene expression for Lung Squamous Cell Carcinoma was successfully complied for use with the Recon3D model.

Gene-Protein-Reaction Associations

	1 Protein Name	2 Gene ID	3 Fold Change Value	4 rxn1	5 rxn2	6 rxn3	7 rxn4	8 rxn5	9 rxn6
1	'GPD1'	'2819_AT1'	0.0169	'r0202'	'G3PD1e'	'G3PD2'	[]	[]	[]
2	'HSD17B6'	'8630_AT1'	0.0493	'HMR_2041'	'HMR_6633'	[]	[]	[]	[]
3	'NPR1'	'4881_AT1'	0.0487	'GUACYC'	[]	[]	[]	[]	[]
4	'CA4'	'762_AT1'	0.0076	'HCO3Ee'	'HCO3E'	'GMAND'	[]	[]	[]
5	'SLC6A4'	'6532_AT1'	0.0064	'SRTN6_2_r'	[]	[]	[]	[]	[]
6	'GGTLC1'	'92086_AT1'	0.0046	'GTHRDHt_syn'	'GGTAe2'	'r0648'	'r0641'	'r0649_1'	[]
7	'ABCA8'	'10351_AT1'	0.0274	'TCHOLABCtc'	'ESTRAABCtc'	'ESTRSABCtc'	'LEUKABCtc'	[]	[]
8	'AK1'	'203_AT1'	0.1628	'DADK'	'HMR_0765'	'HMR_6545'	'FBP'	'FBP26'	'ADK1'
9	'PLA2G1B'	'5319_AT1'	0.0108	'PLA2_2e'	[]	[]	[]	[]	[]

Table 1: This table represents the Gene-Protein-Reaction Associations between the most differently expressed genes in Lung Squamous Cell Carcinoma and reactions in the Human Recon3D model. It also includes associated Fold Change Values which were found in Rstudio.

We are continuing to tailor this approach to the Recon3D model

```
%% Setting initial constraints

%sets the lower bound of all exchange reactions that are not initially 0 to
%be -0.0074
ind1=find((model.lb==0)&(~cellfun(@isempty,strfind(model.rxns,'EX_'))));
model.lb(ind1)=-0.00074;

%sets the lower bound of all sink and demand reactions to be 0
ind2=find(~cellfun(@isempty,strfind(model.rxns,'DM_')));
model.lb(ind2)=0;
ind3=find(~cellfun(@isempty,strfind(model.rxns,'SK_')));
model.lb(ind3)=0;

%based on the given constraints, maximizes the
%flux rate of the Biomass reaction
model=changeObjective(model,'BIOMASS_reaction');
FBAsolution = optimizeCbModel(model,'max');
FL= FBAsolution.f;
doubling_time=log(2)/FL;
```

FL =

0.0289

doubling_time =

24.0135

Figure 3: MATLAB code which sets lower bounds of Sink and Demand reactions equal to 0 and the lower bounds of all exchange reactions that are not 0 to be -0.0074. It then finds the flux rate of the objective reaction.

The Recon3D model has been set up to represent healthy tissue. The lower bounds have been so that the doubling time of the objective reaction is about 24 hours. The next step will be to integrate the experimental data and to determine which amino acids have the most effect of the growth rate, especially in low glucose environments.

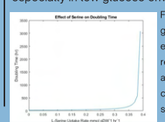

Figure 4: Example of the graphs that will be made for each amino acid to represent the effect of amino acid exchange rate on cell growth rate. This graph shows Serine exchange rate vs. doubling time

CONCLUSION

Because the experiment has not been competed, it is unclear whether experimental data paired with FBA is enough to be able to predict cancer cell growth rates. This experiment showed that it is possible to predict growth rates for microbes and it is possible to incorporate experimental data, but more research is necessary to know if this approach is viable with more complex models such as the Human Recon3D model.

FUTURE GOALS

- Integrate this approach with lab experiments in order to verify the model, and use it to guide experiments. These experiments include using isotope tracing and LCMS to measure
  - nutrient uptake rates
  - cell growth rates
  - intercellular flux
- Refine this computational approach enough to have predictive power for individual patients solely based on a tumor biopsy and rna-sequencing

ACKNOWLEGEMENTS

- Thank you to the Samueli Research Scholars for choosing me to participate in Research
- Thank you to Will Herrera and SURP for academic, career and research guidance
- Thank you to Kris Park for the technical support
- Thank you to Doctor Jun Park for the guidance, support, and encouragement

Sources:

Brunk, E., Sahoo, S., Zielinski, D. C., Altunkaya, A., Dräger, A., Mih, N., Gatto, F., Nilsson, A., Preciat Gonzalez, G. A., Aurich, M. K., Prlić, A., Sastry, A., Danielsdottir, A. D., Heinken, A., Noronha, A., Rose, P. W., Burley, S. K., Fleming, R., Nielsen, J., Thiele, I., ... Palsson, B. O. (2018). Recon3D enables a three-dimensional view of gene variation in human metabolism. Nature biotechnology, 36(3), 272–281. https://doi.org/10.1038/nbt.4072

Kahn, Daniel. "Introduction to Flux Balance Analysis". http://ibis.inrialpes.fr/people/dejong/courses/coursINSA/2016/Introduction_to_FBA

Murfin, Kelley. "3 Things to Know about the Tumor Microenvironment." MD Anderson Cancer Center, MD Anderson Cancer Center, 6 Apr. 2021, www.mdanderson.org/cancerwise/what-is-the-tumor-microenvironment-3- things-to-know.h00-159460056.html.

Sahiti Gavva

Chemical Engineering
Freshman, UCLA

Thermodynamic Simulations Using Industrial Waste Streams for CO2 Mineralization

FACULTY ADVISOR
Dante Simonetti

DAILY LAB SUPERVISOR
Steven Bustillos

DEPARTMENT
Chemical Engineering

ABSTRACT

CO_2 mineralization is a viable alternative CO_2 emissions mitigation strategy in which CO_2 is captured by the precipitation of thermodynamically favorable carbonate phases. For CO_2 mineralization, industrial waste streams with large cation concentrations (e.g., Ca^{2+} [0.01 - 1.0 mol/L]) react with dissolved CO_2 under alkaline conditions (pH > 9). An ion-exchange process has previously been proposed to provide the alkalinity required for CO_2 mineralization while utilizing industrial waste streams. In this work, thermodynamic simulations were performed using Gibbs Energy Minimization Selektor (GEMS) program to predict yields and purities of calcite ($CaCO_3$) formed. The alkaline solution produced via ion-exchange and industrial waste streams were simulated to predict the final compositions of the solution to see how the final composition would affect the overall process. Industrial waste stream compositions were identified using the United States Geological Survey database. Simulations were performed at varying CO_2 concentrations (100%, 50% 20%, 12%, 5%) at fixed waste stream compositions to quantify the effect CO_2 concentrations have on calcite yields, purities, and final solution compositions. The data collected shows acceptable yields (0.14 - 1.3 g/L calcite) and purities (>90%) for calcite using industrial waste streams at each respective CO_2 concentration. Final divalent cation concentrations were predicted following treatment via nanofiltration and reverse osmosis, which resulted in total divalent cation concentrations less than <0.001 mol/L. The low divalent cation concentrations following mineralization and the large yields and purities of calcite simulated confirm that the overall mineralization process is viable using industrial waste streams.

THERMODYNAMIC SIMULATIONS USING INDUSTRIAL WASTE STREAMS FOR CO_2 MINERALIZATION

Sahiti Gavva, Steven Bustillos, Professor Dante Simonetti
Department of Chemical Engineering at University of California, Los Angeles

UCLA Samueli School of Engineering
SUMMER UNDERGRADUATE RESEARCH PROGRAM

Introduction

Today's emissions, specifically CO_2, have terrible consequences on the globe. Emissions need to be prevented or captured to prevent further damage. While there are other ways to prevent or capture emissions, mineralization proves promising because of the stability of minerals and their potential profitability.

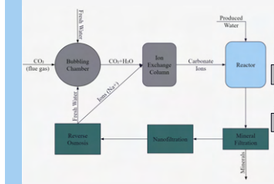

Figure 1: The overall process for mineralization. Steps of the process are defined below.

Bubbling Chamber Dissolving CO_2 in water, produces an acidic solution.

Ion Exchange Column Uses resin and zeolites to increase pH and form carbonate ions (CO_3^{2-}) needed in reaction.

Reactor Minerals are formed with the carbonate ions and Produced Water (PW). Produced Water stream refers to industrial waste streams that are rich in cations needed for the mineralization reaction.

Mineral Filter A vacuum filter is used to separate any minerals formed.

Nanofiltration Removes any unreacted divalent ions with 95% efficiency.

Reverse Osmosis Separates water from any remaining ions.

- The water is reused in the bubbling chamber, and
- the other stream, which is rich in Na^+, is reused in the Ion Exchange Columns to prep the resins and zeolites for reaction to increase pH and form carbonate ions.

Mineralization Reaction

$$Ca^{2+}{}_{(aq)} + CO_3{}^{2-}{}_{(aq)} \rightarrow CaCO_{3\,(s)}$$

- Thermodynamically favorable; reactions happens spontaneously
- Process has the potential to be integrated in a power plant without requiring extra money or energy.

Calcite, or more commonly limestone, is used in building materials, such as cement and can be further expanded to other processes depending on purity.

Objective

It is important to understand if the mineralization process is viable for power plants. The objective of this research is to simulate the mineralization reaction to predict if highly pure calcite could be formed at a large yield and if filtration of leftover ions would allow for regeneration.

Materials & Methods

Gibbs Energy Minimization Selektor (GEMS) software

- Simulates reaction between the Carbonate and Produced Water streams
- Predicts formation and yields based on initial inputs, allowing for the minerals formed and unreacted ions to be analyzed.

Method

Run simulation for a specific PW composition and CO_2 concentration.

↓

Graph yields of calcite and purities of calcite against the amount of PW.

↓

Calculate the concentration of leftover ions after nanofiltration and reverse osmosis.

↓

Repeat for other CO_2 concentrations.

References

Bustillos, Steven, Alturki, Abdulaziz, Prentice, Dale, La Plante, Erika Callagon, et al. (2020) Implementation of Ion Exchange Processes for Carbon Dioxide Mineralization Using Industrial Waste Streams. *Frontiers in Energy Research. 8.* https://www.frontiersin.org/article/10.3389/fenrg.2020.610392

Results

Using waste stream data from the United States Geological Survey (USGS), the values of ions was averaged to produced a Produced Water composition (Figure 2) which was run through the GEMS simulation to predict the calcite produced and the ions leftover.

	Concentration (mmol/L)
$CaCl_2$	20.7
NaCl	339.2
$MgCl_2$	7.5
$FeCl_2$	0.28
KCl	3.15
$CaSO_4$	1.68

Figure 2: Produced Water Composition in mmol/L that was input into GEMS.

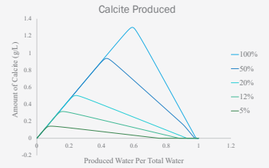

Figure 3: The amount of calcite formed with varying levels of CO_2 concentration. The focus is the peak of each curve (the max amount of calcite produced).

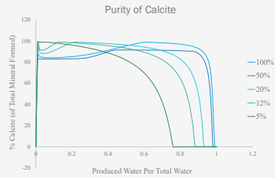

Figure 4: The percentage of calcite formed out of total minerals formed. The focus is, again, the point where amount of calcite produced peaks (from Figure 3).

20% CO_2

	Initial (mmol/L)	Filtered (mmol/L)
Na^+	91.630	164.934
Ca^{2+}	0.411	0.041
Mg^{2+}	1.802	0.180

12% CO_2

	Initial (mmol/L)	Filtered (mmol/L)
Na^+	60.748	109.346
Ca^{2+}	0.474	0.047
Mg^{2+}	1.202	0.120

Figure 5: Concentration of leftover ions predicted by GEMS and calculated concentration of ions after nanofiltration (95%) and reverse osmosis in mmol/L.

Discussion

Yield
Good
Ranges from 0.14 – 1.3 g/L calcite for CO_2 concentrations

Purity
Highly pure
greater than 90% when calcite yield is at its peak for all CO_2 concentrations.

Filtered Ions
Ideal for the regeneration stream of Na^+
Ion concentration of Ca^{2+} and Mg^{2+} are less than 1 mmol/L after filtration. The leftover ions in Figure 5 are reflective of the leftover ions for the other CO_2 concentrations not show in the table.

The mineralization process appears to reliably produce calcite with acceptable yield and purity. With little leftover ions after filtration, the regeneration streams of Na^+ and fresh water are also practical for the process.

Conclusion

By producing calcite, a significant amount of CO_2 can be captured. This process enables power plants to decrease their emissions generated, instead producing minerals that could be used elsewhere.

Future Directions

1. Further Validate Experimentally:
This data will confirm the viability of mineralization on power plants.

2. Secondary Mineralization:
Using the ion concentrate that is produced as a waste product of nanofiltration, a secondary reaction may produce a significant amount of mineral, allowing the process to capture more CO_2.

Acknowledgements

Samueli Engineering Summer Undergraduate Research Program

Women in Engineering at UCLA

Steven Bustillos (DLS)

Professor Dante Simonetti (PI)

Nicholas Hamakami

Electrical Engineering
Freshman, UCLA

Evaluation of Network Topologies in Challenging Environments

FACULTY ADVISOR
Christina Fragouli

DAILY LAB SUPERVISOR
Mine Dogan

DEPARTMENT
Electrical and Computer Engineering

ABSTRACT

Finding the optimal network topology for wireless sensor networks is an important problem that has a wide variety of applications in the field of environmental and earth sensing. This is because issues with connectivity and routing can arise if the environment a topology is in contains obstacles that impede the communication between nodes – examples of such environments being towns or cities. As such, our research focuses on synthesizing wireless sensor networks that satisfy certain sensing and communications requirements in these challenging environments. Towards this end, we created occupancy grids based on satellite images that display the locations of obstacles and free space. For different placements of sensor nodes on the occupancy grids, we assessed the performance of the resulting networks based on our sensing requirements and the maximum flow that can be sent from a source to a destination. The data that we collected will be the basis for a new algorithm that can determine effective sensor network topologies for high-obstacle environments.

Evaluation of Network Topologies in Challenging Environments

Nicholas Hamakami, Mine Dogan, Christina Fragouli

Department of Electrical and Computer Engineering, University of California – Los Angeles

FAST TRACK TO SUCCESS
UCLA Electrical and Computer Engineering

UCLA Samueli School of Engineering
SUMMER UNDERGRADUATE RESEARCH PROGRAM

Introduction

Context:
Finding the optimal network topology for wireless sensor networks is an important problem because issues with connectivity and routing can arise if the environment a topology is in contains obstacles that impede communication between nodes.

Main goals:
- Optimize a sensor network topology in a difficult environment – e.g., city or neighborhood – using occupancy grids and minimum cuts
- Criterion: Maximize the network flow rate for a given network

Motivation:
- Sensor networks have a wide variety of applications in environmental and earth sensing
- Need data as a foundation for a new algorithm that can determine effective topologies in high-obstacle environments

Materials

Google Maps API
- Occupancy grid creation

Python
- Occupancy grid creation
- Node placement with sensing constraints
- Calculations: link capacities, minimum cuts

NumPy

Methods

Create occupancy maps with the Google Maps API and other image editing software. Then transform maps into proper grids with Python.

Google Maps image (left) to occupancy image (right)

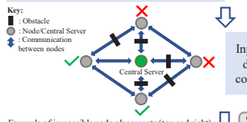

Input occupancy grids into algorithm to determine node placements based on constraints of distance and line of sight.

Example of impossible node placements (top and right) vs. possible node placements (bottom and left).

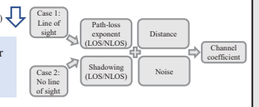

Find channel coefficients for each pair of nodes through the channel coefficient equation.

Link capacity equation:

$$L = \log(1 + P|h|^2)$$

Key:
L: Link capacity
P: Transmission power
h: Channel coefficient

Channel coefficients: Subsume the effects of distance, shadowing, and path-loss at a reference distance of 1 meter

Link capacities: Measurement of how much data can be sent through a link between two nodes

Calculate link capacities based on channel coefficients through the link capacity equation.

Water analogy:
Higher link capacity synonymous with higher water flow

Low (left) vs. high (right) link capacity

Use finalized link capacities to calculate minimum cuts – and thus maximum network flow – through the Gomory-Hu Tree Algorithm.

Gomory-Hu Tree Algorithm: Takes in link capacities and returns a Gomory-Hu tree. To find a minimum cut for a pair of nodes from the Gomory-Hu tree, find the smallest edge on the path between the nodes.

Node Placement Algorithm

Choosing a selection of nodes that meet sensing constraints:

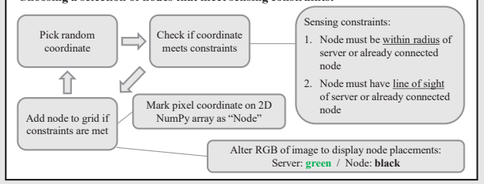

Results

Example satellite image to network flow process:
Location: UCLA – Manning, Malcom, La Conte Ave intersection

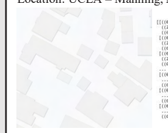

Input: Google Maps satellite image

Figure 1: Occupancy grid represented as a 2D NumPy array. Each coordinate is marked as either "Occupied," "Not Occupied," or "Node"

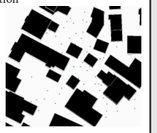

Figure 2: Final distribution of 50 nodes and a single central server

Key observations:
- Vast majority of nodes were placed either near the central server or in an open area where there is access to other nodes
- As expected, few nodes were placed near the edge of the grid

Calculating the maximum network flow from minimum cuts:
- Minimum cuts – act as a restrictor to the maximum flow. In other words, the flow of a network can only be as large as its minimum cut
- Flow rate given in unambiguous units of flow

Conclusion

Next steps – data collection:
Our next objective is to use this algorithm to create node distributions for a variety of maps, with the main goal being to compare the network flow of the different maps.

Closing thoughts:
Having created a method to generate node distributions and quantifiably measure their effectiveness, we are one step closer to our end goal of developing an algorithm that can determine effective network topologies for high-obstacle environments.

References

Gomory, Ralph E., and Tien Chung Hu. "Multi-terminal network flows." *Journal of the Society for Industrial and Applied Mathematics* 9.4 (1961): 551-570.

Acknowledgements

I would like to thank Professor Christina Fragouli, the Summer Undergraduate Research Program, the Fast Track to Success Program, and the National Science Foundation for the opportunity to conduct this research. I would also like the thank William Herrera, Mine Dogan, and Jonathon Bunton for their continued support throughout the program.

Vanessa Huaco

Chemical Engineering
Freshman, UCLA

Analysis of Scattering Data Using Bayesian Optimization

FACULTY ADVISOR
Samanvaya Srivastava

DAILY LAB SUPERVISOR
Divya Iyer

DEPARTMENT
Chemical Engineering

ABSTRACT

Polyelectrolyte complexation between oppositely charged macromolecules is primarily driven by non-covalent (electrostatic) interactions. These self-assembled materials find applications as bio-adhesives, encapsulants, delivery and purification agents. Analytical techniques such as small angle x-ray scattering (SAXS) and dynamic light scattering (DLS) offer insights about the size, structure and behavior of these materials, all of which are influenced by the polymer backbone, intermolecular interactions and solution conditions. In this project, we focus specifically on obtaining size and structure estimates of these materials via light scattering measurements, to explain structure-property relationships. We propose a Bayesian optimization model that will best describe and fit the size and structure estimates found. We are working to fit our equation

$$P(q) = (9 * scale * V * \Delta\rho^2) * \left[\frac{sin\,(qr) - qrcos(qr)}{(qr)^3}\right]^2$$

for a spherical model to our data. We are looking at the relationship between their form factor $(P(q))$ and length scale (q), where the form factor is the dependent variable, and the length scale is the independent variable. Our model will be constructed using the Statistics and Machine Learning toolbox in MATLAB, as well as the Parallel Computing toolbox. The effectiveness of toolboxes offered by MATLAB, to perform Bayesian Optimization, was tested with preexisting generic examples. The terms involved in the optimization process have been learnt and understood.

UCLA Samueli School of Engineering

ANALYSIS OF SCATTERING DATA USING BAYESIAN OPTIMIZATION

Samueli Research Scholars
UCLA Samueli School of Engineering

Vanessa Huaco, Divya Iyer, Professor Samanvaya Srivastava
Chemical and Biomolecular Engineering Department -
University of California, Los Angeles

UCLA Samueli School of Engineering
SUMMER UNDERGRADUATE RESEARCH PROGRAM

INTRODUCTION

Polyelectrolyte complex coacervates are unique polymer-rich materials that can serve many purposes but are yet poorly understood.[1]

Analytical techniques such as small angle x-ray scattering (SAXS) and dynamic light scattering (DLS) offer insights about the size, structure and behavior of these materials, all of which are influenced by the polymer backbone, intermolecular interactions and solution conditions.

Prior research utilizes Bayesian methods to analyze small angle scattering data of these materials. Understanding the properties and behaviors of these materials will help us harness self-assembly as a tool for material design.

OBJECTIVE

We aim to find the model that best fits and explains the size and structure estimates data obtained experimentally so that we may harness self-assembly as a tool for material design.

KEY TERMS

Small Angle X-Ray Scattering

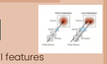

A technique for studying structural features of colloidal size[2]

Dynamic Light Scattering

A technique in physics that can be used to determine the size distribution profile of small particles in suspension or polymers in solution

Bayesian Regression Analysis

A statistical process for estimating the relationships between a dependent variable and one or more independent variables in which the hypothesis is updated as more data becomes available

MATERIALS

MATLAB

- Statistics and Machine Learning Toolbox
- Parallel Computing Toolbox

METHOD

Obtain scattering curves from SAXS and DLS → Partition Data and Remove Outliers → Input data into MATLAB and preprocess the data set → Use curve fitting tools to find regression model that fits or data

RESULTS

Sphere model : $P(q) = I(q)/V = (9 * scale * V * \Delta\rho^2) * \left[\frac{sin\,(qr) - qrcos(qr)}{(qr)^3}\right]^2$

Equation inputted into MATLAB: $I(q) = a * r^3\left[\frac{sin(qr) - qrcos(qr)}{(qr)^3}\right]^2$

a = 1.978e-05
r (radius) = 104.9
r-square = 0.9927

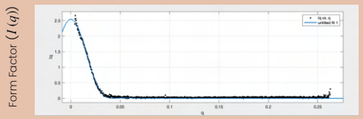

DISCUSSION

We utilized the curve fitting application in MATLAB to try and fit our equation for a sphere model to our data set. This resulted in the blue line displayed in the graph above. This model also gave us the value of the "a" coefficient and the value of the radius.

This fit yielded an r-squared value of 0.9927 which is a relatively good value, indicating that this is an okay fit for our data. However to obtain a customized equation that would better explain different datasets, especially in the low q region, which is the area of interest we must further refine our model using Bayesian Optimization.

CONCLUSION

- Regression Analysis and Bayesian Optimization were learnt and understood
- Effectiveness of MATLAB toolboxes were tested using generic examples
- Curve fitting tools were utilized to generate a model for our data

Further Steps:

- Extend this process to spherical systems
- Optimize our equations by building our own Bayesian algorithm
- Find the model that best fits and explains the size and structure estimates

References

[1] "Srivastava Lab." Research, www.srivastava-lab.net/research.
[2] Glatter O; Kratky O, eds. (1982). Small Angle X-ray Scattering. Academic Press. ISBN 0-12-286280-5. Archived from the original on April 21, 2008
[3] Kline, Steve, and Alan Munter. "Sphere Model." NIST Center for Neuron Research , ncnr.nist.gov/resources/sansmodels/Sphere.html.

Acknowledgments

I would like to thank the Samueli Research Scholars for funding our research through the Summer Undergraduate research Program. I would also like to thank Professor Srivastava, Divya Iyer and Holly Senebandith for their resources, guidance and support. Finally, I would like to thank Will Herrera and the SURP staff for putting together this program.

Tricia Jain

Civil and Environmental Engineering
Freshman, UCLA

Development of a Relational Database for Seismic Response Data from Instrumented Buildings Subjected to Historical Earthquakes

FACULTY ADVISOR
Henry Burton

DAILY LAB SUPERVISOR
Eusef Abdelmalek-Lee

DEPARTMENT
Civil and Environmental Engineering

ABSTRACT

The instrumentation of buildings with measuring devices, such as accelerometers, enables rapid assessments of building damage and functionality following an earthquake. However, in a typical urban context, only certain buildings are instrumented due to the associated costs. Fortunately, statistical and machine learning methods can utilize the response data collected from a limited number of sensors to predict seismic demands in uninstrumented structures. Currently, there exists a large inventory of seismic response data, but no standardized system of organization, hindering data analysis. As a result, this study seeks to develop a relational database to streamline the storage and retrieval of seismic response data, along with associated building and earthquake parameters. An efficient database schema, which eliminates data redundancy and simplifies links between tables, was designed. Appropriate data types for attributes, particularly vectors of time-series data, were researched and implemented. Code to accurately extract, organize, and insert over 2.5 GB of remote sensing data into the database was written. Finally, Python scripts were designed to enable data querying and analysis of extracted results. The relational database and accompanying python scripts that were developed create the framework for performing advanced data analysis. In the context of this dataset, this can improve post-earthquake building damage assessments, mitigating the socio-economic toll of earthquakes on communities.

UCLA Samueli School of Engineering
SUMMER UNDERGRADUATE RESEARCH PROGRAM
Samueli Research Scholars

Development of a Relational Database for Seismic Response Data from Instrumented Buildings Subjected to Historical Earthquakes

Tricia Jain, Eusef Abdelmalek-Lee, Henry Burton Ph.D., S.E.
Department of Civil and Environmental Engineering— University of California, Los Angeles

Introduction

- The instrumentation of buildings with measuring devices enables rapid assessments of building damage and functionality following an earthquake.
- In a typical urban context, only certain buildings are instrumented.
- Statistical and machine learning methods can utilize the response data collected from a limited number of sensors to predict seismic demands in uninstrumented structures.

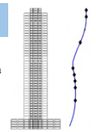

Figure 1. Measured Seismic Response

Objective

- Develop a relational database to streamline the storage and retrieval of seismic response data along with associated building and earthquake parameters.
- Design Python scripts to execute queries and analyse the extracted data.

Relational Database

- Utilizes tables to store data, which are related through shared fields (foreign keys).
- Reduces data redundancy and provides better scalability.
- Data extraction is performed by executing queries, which are requests for data.

Materials and Methods

- Designed and revised the database schema
- Introduced a junction table to reduce data redundancy
- Selected the MEDIUMTEXT data type to store time-updated data vectors

Extracted and wrote scalar value data into spreadsheets

Exported vectors of time-updated data into individual text files

Generated SQL statements for data insertion

- Implemented the database schema
- Ran queries to insert data into the database
- Performed tests for insertion accuracy

Created a notebook of example queries to facilitate database use

Performed statistical analysis of data using Python machine learning libraries

Published the database

Conclusion

- A relational database facilitates access to and analysis of large inventories of remote sensing data, providing the foundation for advanced data analysis.
- The DesignSafe cyberinfrastructure allows the greater natural hazards community to utilize the database in their research.
- The database can be continually updated with data from new earthquakes to better calibrate models.

Acknowledgements

I would like to thank Professor Burton and Eusef Abdelmalek-Lee for their guidance throughout this project, the Samueli Research Scholar Award for funding this research, and all SURP staff for their support.

Database Schema

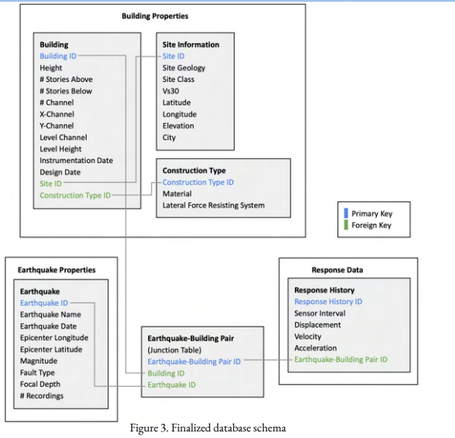

Figure 3. Finalized database schema

Results

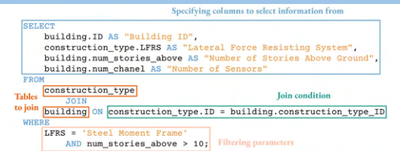

Figure 4. Example query

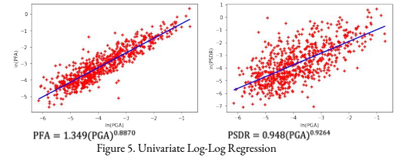

Figure 5. Univariate Log-Log Regression

$$PFA = a(PGA)^b(S)^c$$

Figure 6. Multivariate Log-Log Regression Equation

References

Brandenberg, Scott J., et al. "Next-Generation Liquefaction Database." Earthquake Spectra, vol. 36, no. 2, May 2020, pp. 939–959, doi:10.1177/8755293020902477.
Omoya, Morolake; Ero, Itohan; zaker esteghamati, mohsen; Burton, Henry; Brandenberg, Scott; Nweke, Chukwuebuka (2021) "Relational database for post-earthquake damage and recovery assessment: 2014 South Napa earthquake." DesignSafe-CI. https://doi.org/10.17603/ds2-3nvj-4127.
Sun, H, Burton, H, Wallace, J. Reconstructing seismic response demands across multiple tall buildings using kernel-based machine learning methods. Struct Control Health Monit. 2019; 26:e2359. https://doi.org/10.1002/stc.2359
Zaker Esteghamati, Mohsen & Lee, Jeonghyun & Musetich, Matthew & Flint, Madeleine. (2020). INSSEPT: An open-source relational database of seismic performance estimation to aid with early design of buildings. Earthquake Spectra. 10.1177/8755293020919857.

Bhavik Joshi

Computer Engineering
Freshman, UCLA

Multi-Hop Mesh Networking with Frequency Diversity as Robust Communication Infrastructure for Robotic Swarms

FACULTY ADVISOR
Ankur Mehta

DAILY LAB SUPERVISOR
Ankur Mehta

DEPARTMENT
Electrical and Computer Engineering

ABSTRACT

Robotic swarms are groups of autonomous robots that work together in order to perform tasks through cooperative behavior and interactivity with their environments. In order for robotic swarms to collaborate, they must have a reliable way of communicating with one another. Thus, we created a robust network infrastructure to allow autonomous robots to work together through peer-to-peer communication even in difficult environments. As a means of doing so, we used the painlessMesh Arduino library to implement a multi-hop mesh network, or a network topology that allows each node to relay signals to nodes too far away by routing packets across intermediate nodes. Additionally, we added 433 MHz packet radios onto our hardware stack and sent each message between robots over multiple, distinct frequencies; this keeps interference on one frequency band from preventing successful communication. Through this infrastructure, we enabled our robots to successfully communicate with any other robot. We also saw that for certain messages, when one frequency became unusable, our diversity maintained the infrastructure's ability to communicate reliably. In the future, this work can be used to bring robotic swarms one step closer to becoming ubiquitous and useful in daily life, improving their communication so that together they can accomplish tasks previously and independently impossible.

UCLA Samueli School of Engineering

Multi-Hop Mesh Networking with Frequency Diversity as Robust Communication Infrastructure for Robotic Swarms

LEMUR
Bhavik Joshi, Dr. Ankur Mehta, The Laboratory for Embedded Machines and Ubiquitous Robots, UCLA

FAST TRACK TO SUCCESS
UCLA Electrical and Computer Engineering

UCLA Samueli School of Engineering
SUMMER UNDERGRADUATE RESEARCH PROGRAM

Objective

We are creating a **robust network infrastructure** with a multi-hop mesh network and frequency diversity for robotic swarms to communicate over.

Goal:
- Robots can communicate, even in difficult environments

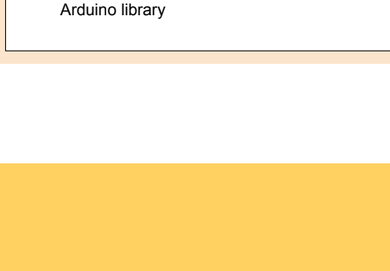

Robotic Swarms:
- Collaborative robots
- Environment interactivity
- Must communicate reliably

Infrastructure Elements

Hardware used:

ESP32 Featherboard, 433 MHz Packet Radio

Software used:
- painlessMesh
  - Mesh over WiFi
- Radiohead library
- Arduino IDE

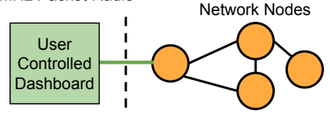

We created a software package that implements:
- 433 MHz radio into a multi-hop mesh network
- A bridge node that relays packets between an external network and other nodes
- Swarm communication into a simple to use Arduino library

Network Robustness

Multi-Hop Mesh Network:
- Any node to any node
- Intermediates relay signals to unreachables

↓

Why: to allow our robots to **communicate with any other** robot

Frequency Diversity
- Using multiple, distinct frequencies (2.4 GHz and 433 MHz)

↓

Why: our robots **communicate over both** so interference on one doesn't stop communication

Results and Conclusions

The network enabled our robot swarms to:
- Work autonomously
- Respond to commands

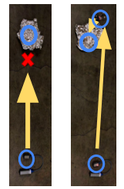

Because of the reflective obstacle, the signal has to hop across nodes

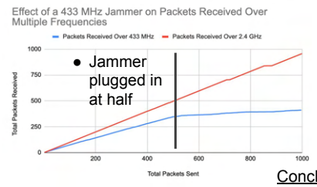

The network is robust:
- Works when one frequency fails
- Indirect nodes can communicate

Conclusions and Future

This research advances swarm communication

↓

Swarms can do harder tasks in more difficult environments

↓

Robotic swarms become ubiquitous

Acknowledgements

- William Herrera, Summer Undergraduate Research Program
- Dr. Ankur Mehta, Grace Kwak, Jaehoon Song, Jillian Pantig, Marisa Duran, Shahrul Kamil Hassan, and Sudarshan Seshadri, UCLA Lemur

Kim Kha

Mathematics
Junior, Mount Saint Mary's

Enoch Huang

Electrical Engineering
Freshman, UCLA

Amanda Hacker

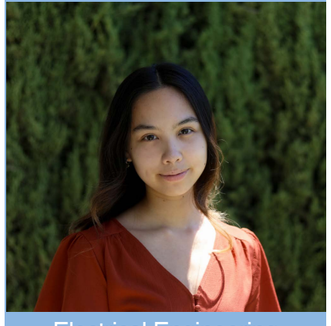

Electrical Engineering
Freshman, UCLA

Wearable & Mobile Bioanalytical Technologies for Personalized Medicine

FACULTY ADVISOR
Sam Emaminejad

DAILY LAB SUPERVISOR
Hannaneh Hojaiji

DEPARTMENT
Electrical and Computer Engineering

ABSTRACT

Exponential growth in Internet of Things (IoT) devices and wearable sensing technologies has created an unprecedented opportunity to enable personalized medicine through real-time individual biomonitoring. Although these commercialized platforms are capable of tracking physical activities and vital signs, they fail to access molecular-level biomarker information which provide insight into the body's dynamic chemistry. Thus, as sweat is a rich source of biomarkers that can be retrieved unobtrusively, sweat-based wearable biomonitoring has emerged as one of the most promising candidates to merge this gap. By designing and integrating compact electrochemical sensors into wearable electronic devices, we can non-invasively and accurately track specific biomarkers in sweat and provide actionable feedback about users' health status. We develop a signal modulation strategy to stimulate our electrochemical sensors for wearable biomarker monitoring. We also design a novel sensor readout methodology for improved and accurate biomarker tracking. Then, we integrate these designs into a wireless electrochemical readout circuitry to noninvasively track intended biomarkers. As a result, we successfully demonstrate our signal modulation solution's efficacy through electrodeposition of prussian blue films. Additionally, we show this sensing methodology improves signal readout and sensitivity by 3 times. Thus, we can non-invasively track subjects' biomarkers and underlying health status in a wireless and wearable format. This platform can further be utilized for real-time glucose monitoring in diabetic patients without requiring conventional painful extraction methods, or monitoring lithium levels in bipolar patients for drug abuse/compliance.

UCLA Samueli School of Engineering

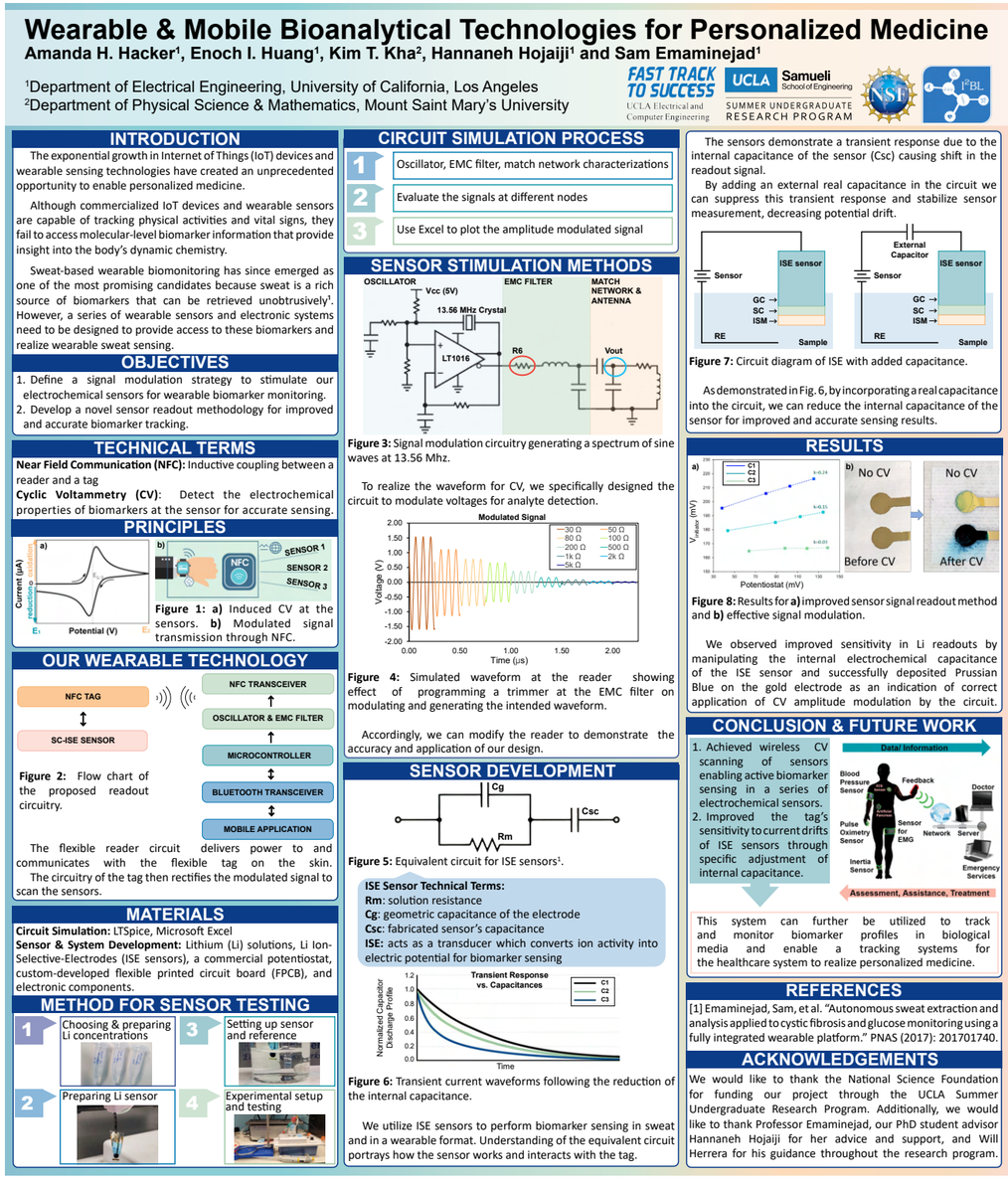

Sarah Kimak

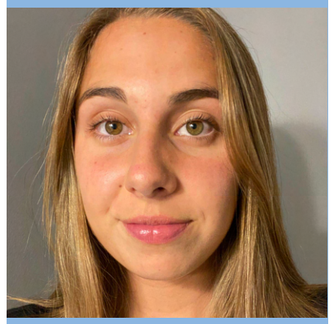

Computer/Cognitive Science
Freshman, University of
Delaware

Analyzing the Effectiveness of Social Robots in Children's Speech Assessments

FACULTY ADVISOR
Abeer Alwan

DAILY LAB SUPERVISOR
Alexander Johnson

DEPARTMENT
Electrical and Computer Engineering

ABSTRACT

Speech recognition devices have vastly transformed people's way of life, as everyone knows of "hey google" and "Alexa," but there are greater possibilities with such systems including improving the early education of children. Many children are behind in their reading and speech acquisition skills, a direct result of lack of exposure to vocabulary and oral skills. While other companies have created intelligent tutoring systems, they do not possess the ability to pick up on the acquisition of children. In order to determine the success of a young child interacting with a social robot, a series of tasks were completed and recorded with an instructor, child and the robot JIBO. These sessions were analyzed to quantify patterns in interactions such as boredom, excitement, and frustration. The data concluded that boredom and prompts from the instructor occurred most often, showing that young children struggle the most with staying focused during the long tasks. The more interjections from the instructor, the longer the sessions lasted since they kept the children on track, but it was found only 18.7% of the recordings were a child speaking. It's suggested the tasks be shortened so that there can be more success in the students completing all of the tasks to be recorded and analyzed for future sessions. Social robots can be used in classrooms, clinician offices and even at home to develop learning at a young age that is most beneficial for the future.

UCLA Samueli School of Engineering

Analyzing the Effectiveness of Social Robots in Children's Speech Assessments

Sarah Kimak - Speech Processing & Auditory Perception Lab
Department of Electrical and Computer Engineering
Professor Abeer Alwan & DLS Alexander Johnson
University of California, Los Angeles

UCLA Samueli School of Engineering
SUMMER UNDERGRADUATE RESEARCH PROGRAM

Introduction & Background

- Tech giants lack major focus on the articulation of children when creating and developing speech recognition devices
- Intelligent tutoring systems only have success with kids over 10 years old, after their crucial developmental education years [1]
-The goal of this project is to analyze how children interact with a social robot in order to determine what improvements need to be made so they can successfully conduct a session of tasks
- Robots can conduct individual and specialized lessons that benefit the child's reading, speech and language acquisition skills, which many kids are falling behind in today

Materials & Methods

1. Sessions conducted and recorded by social robot JIBO with a child aged 4-7 and an instructor [1]

2. Transcripts analyzed for patterns of boredom, excitement, needing assistance from the instructor, etc.

3. Anaconda Jupyter Notebook and Python coding language used to quantify and compare patterns

Results & Discussion

Quantifying Patterns (by hand):

- Incompletion of tasks and interjections from the instructor were the most frequent patterns that occurred.
- Analyzing by hand reveals specifics that are hard to identify with code since all sessions are unique to the student and instructor.
- The instructor interjected to move the session along when JIBO couldn't, by helping the student to get back on track or understand the assignment, and in order to get the student to give more details in the explanation task (where they had to answer personal questions about themselves and their life).

Figure 1 Instructor Interjections v Session Length

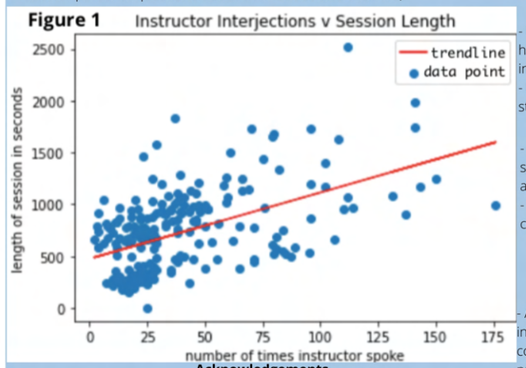

Quantifying Patterns (with code):

A function was used to go through transcripts and total the occurrences of exact phrases showing instructor interjections:
[i]: 8730 the instructor was speaking in the format of the transcripts, but there is no way of knowing if they are helping the child or just making casual conversation
anything else: 654 - a popular secondary prompt in the explanation tasks when the instructor desired more details
what is this: 1920 - used as a prompt, but was also how JIBO asked children to identify images, letters and numbers

- Using the NumPy library, the Figure 1 graph was created to display how more prompts by the instructor increased session length, as indicated by both the by hand and with code analyzations.
- Use of prompts such as 'anything else?' and 'what is this?' helped students to refocus on the task and continue answering questions.

- In using code to calculate the average percentage of student's speaking throughout all of the transcripts it was found that **only** about **18.7%** of the recordings were actually the students.
- This finding demonstrates how often JIBO or the instructor were conducting the task or prompting the student.

Conclusions

- Analyzing the transcripts both by hand and with code was insightful in seeing how students interacted with JIBO, situations where JIBO could not successfully move the session along, as well as the trend of prompts by instructors increasing the length of the session.
- Students mostly struggled with the explanation tasks because they required them to form complex sentences whereas in other tasks they simply had to identify images, letters and numbers.
- A suggestion for future experiments is to adjust the length so that the students remain engaged and can actually complete the tasks. It is important for them to finish the sessions successfully in order to collect data more specific to the articulation of children, after their interaction with JIBO the social robot is improved.

Acknowledgements

- I am grateful for NSF for sponsoring my position in the 2021 SURP, which has been an amazing opportunity for me to expand my knowledge, interests, and possibilities for the future.
- A special thank you to Dr. Alwan and prior researchers for giving me an incredible project to work on and learn from this summer and my DLS Alexander Johnson for teaching and guiding me in my research and new topics of interest in the field.

References

[1] Gary Yeung, Alison L. Bailey, Amber Afshan, Marlen Q. Pérez, Alejandra Martin, Samuel Spaulding, Hae Won Park, Abeer Alwan and Cynthia Breazeal "Towards the Development of Personalized Learning Companion Robots for Early Speech and Language Assessment", AERA, 2019, DOI: 10.302/1431402
[2] Gary Yeung, Alison L. Bailey, Amber Afshan, Morgan Tinker, Marlen Q. Pérez, Alejandra Martin, Anahit A. Pogossian, Samuel Spaulding, Hae Won Park, Manushage Muco, Abeer Alwan and Cynthia Breazeal, "A robotic interface for the administration of language, literacy, and speech pathology assessments for children", SLATE, 2019, pp. 41-42..
[3] "Jibo Robot - He can't wait to meet you," Boston, MA, 2017. [Online]. Available: https://www.jibo.com

Ash Kuhlmann

Chemical Engineering
2nd Year, El Camino College

Designing a Pseudo-Solid Electrolyte

FACULTY ADVISOR
Bruce Dunn

DAILY LAB SUPERVISOR
Patricia McNeil

DEPARTMENT
Materials Engineering

ABSTRACT

Demand for rechargeable electronics has increased reliance on lithium (Li) metal batteries. Unfortunately, repeated plating and stripping of Li metal results in dendrite formation, limiting safe and reliable use of Li as an electrode. Our project seeks to develop a free standing mono-lithic ionogel separator, which would function as an electrolyte while suppressing dendrite formation for long term cycling. We synthesized ionogel materials consisting of MTMOS, TMOS, VTMOS, formic acid, and LiFSi in ionic liquid using typical ionogel synthesis procedures. Galvanostatic measurements in coincells revealed consistent plating and stripping for up to 250 hours (for spin coated Cu) and up to 30 hours (for infiltrated celgard) without evidence of Li dendrite formation or short-circuiting. These results represent a “proof-of-concept” for the production of free-standing pseudo-solid electrolytes and suggests promising results for Li dendrite suppression.

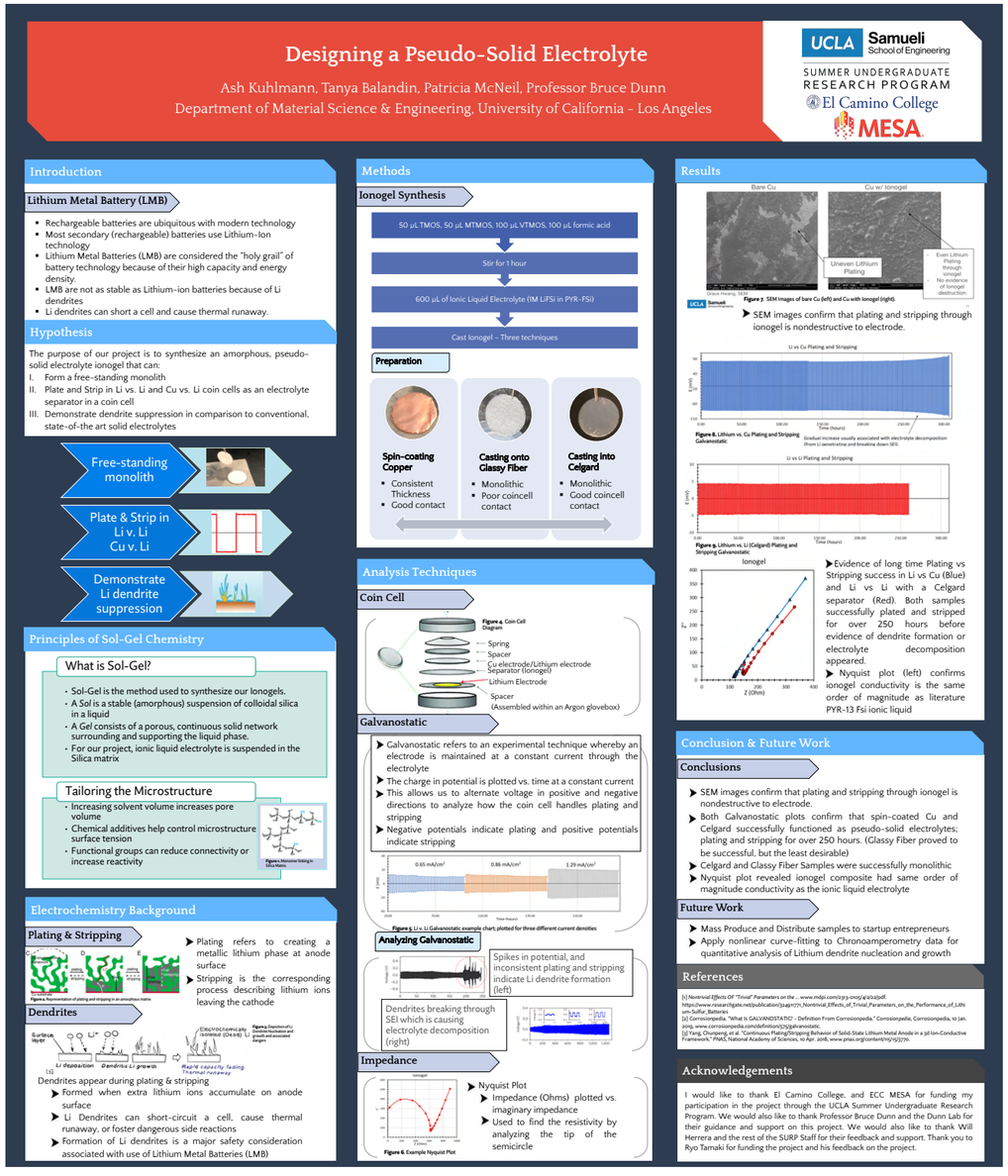

Grace Kwak

Electrical Engineering
Freshman, UCLA

Printable Robotic Boat Swarms with Actuation and Sensing Capabilities

FACULTY ADVISOR

Ankur Mehta

DAILY LAB SUPERVISOR

Ankur Mehta

DEPARTMENT

Electrical and Computer Engineering

ABSTRACT

The design and development of robotic devices remains limited to those with considerable time, funds, and technical expertise. Our goal is to increase the accessibility of robotics so that the average person can design and create their own robotic boats. I set out to provide a variety of boat hull morphologies with three new actuation capabilities: a propeller, paddlewheel, and rudder. After designing the 2D layout of these origami-inspired boats, I implemented them in the Robot Compiler (RoCo) framework for generating foldable robotic designs, thus allowing a user to add any actuation capability to any boat hull by setting parameters in code. I then used a paper cutter to cut out inexpensive thin plastic sheets into foldable boats with actuators driven by continuous rotation servos and DC motors. I found that the propeller produces fast linear motion, the paddlewheel enables motion that is linear and rotational, and the rudder adds more precise steering capabilities. In order to test my boats' autonomous capabilities such as following a colored object, I integrated my boats with OpenMV cameras and inertial measurement units (IMUs), which provided basic feedback-controlled movement. I found that given this relatively small set of tools and materials, it's possible to generate a wide variety of robotic boats. This work establishes a foundation for the community at large to rapidly, easily, and inexpensively create novel types of robotic boats.

Printable Robotic Boat Swarms with Actuation and Sensing Capabilities

Grace Kwak, Ankur Mehta
Laboratory for Embedded Machines and Ubiquitous Robots
UCLA Electrical and Computer Engineering Department

LEMUR

UCLA Samueli School of Engineering
SUMMER UNDERGRADUATE RESEARCH PROGRAM

NSF

Introduction

We build upon a framework for foldable robotic designs in order to allow users to build printable robotic boats with driven propellers, paddle-wheels, and rudders.

Materials

Microcontroller Motors Polyester film

Source: adafruit.com, eplastics.com

Design Process

Sketch Create Fold

Rapid, simple, low-cost

- Origami-like straight folds
- Tab-and-slot connections
- Single-sheet fabrication

Prototypes

Results

Paddlewheel **Propeller** **Rudder**

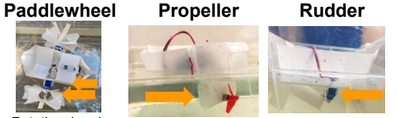

Rotational and linear motion

High linear speed

More precise rotation

Parameterized
Adjustable dimensions and actuator positioning

Modularized
Designs can be cut and pasted

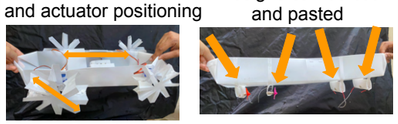

Additional features

- User-controllable via dashboard
- Feedback control using vision processing

Conclusion

Modularity + Parameterization → New Designs

Future work

- Amphibian vehicles
- Boat sails and masts

Acknowledgements

- William Herrera, SURP
- UCLA ECE Fast Track
- Ankur Mehta, UCLA LEMUR
- National Science Foundation

Sung Gyung Lee

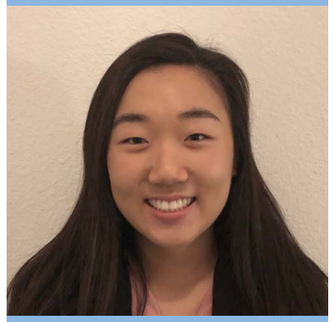

Chemical Engineering
Junior, UCLA

Gallic Acid Upregulates Glycolysis and Depletes Tricarboxylic Acid Cycle Intermediates in H1299 Human Non-small Cell Lung Cancer Cells

FACULTY ADVISOR

Junyoung Park

DAILY LAB SUPERVISOR

Sevcan Erşan

DEPARTMENT

Chemical and Biomolecular Engineering

ABSTRACT

A major hallmark of cancer is metabolic reprogramming, characterized by the upregulation of glycolysis to fuel cancer cells' energy demand. Targeting altered cancer metabolism is an emerging strategy for developing new chemotherapeutics for cancer treatment. Phenolic compounds, plant-derived bioactive natural products, are potential metabolism modulators with their broad range of interactions with enzymes and proteins and their potential interference with cellular activities. However, the potential mechanisms by which phenolic compounds affect cancer metabolism remain unclear. To address this research gap, we treated a human non-small cell lung cancer H1299 cell line with 50 μM of gallic acid, a dietary phenolic compound, for 3 h. Gallic acid-induced metabolite changes in H1299 cells were determined via metabolomic profiling using liquid chromatography-high-resolution mass spectrometry and stable-isotope tracing using [1,2-^{13}C] glucose. After 3-h gallic acid exposure, increased glucose uptake and accumulation of intracellular glycolysis intermediates, such as hexose-biphosphate, phosphoglycerate, and pyruvate, were observed. Citrate, an intermediate of the tricarboxylic acid (TCA) cycle interconnected to glycolysis, was accumulated in gallic acid-treated cells while remaining downstream metabolites, including alpha-ketoglutarate and succinate, from the same pathway were depleted. These results may indicate that glycolysis is upregulated to feed increased energy need of cells after gallic acid treatment, possibly due to increased gallic acid-induced oxidative stress and blockage of metabolic pathways providing energy. Upon feeding cells with stable-isotope [1,2-^{13}C] glucose, we observed higher enrichment in M+2 isotopic fraction in intracellular pyruvate and extracellular alanine, a metabolite exchanged with intracellular pyruvate, in gallic acid-treated cells than that of the controls, further supporting our hypothesis on upregulation of glycolysis. These results taken together suggest gallic acid may be a promising anticancer agent, altering metabolism in H1299 by affecting downstream glycolysis and TCA pathways, consequently reducing energy supply. Through our metabolomic findings, we hope to further understanding of gallic acid's anticancer activity.

UCLA Samueli School of Engineering
SUMMER UNDERGRADUATE RESEARCH PROGRAM

UCLA Samueli School of Engineering

Gallic Acid Upregulates Glycolysis and Depletes Tricarboxylic Acid Cycle Intermediates in H1299 Human Non-small Cell Lung Cancer Cells

Sung Gyung Lee, Sevcan Erşan, Junyoung Park
Chemical and Biomolecular Engineering Department, University of California, Los Angeles

Gallic Acid as an Anticancer Therapeutic

- Gallic acid (GA), a plant-derived bioactive natural product, is suggested to have anticancer activity across various human cancer cell lines.
- A major hallmark of cancer is altered metabolism. GA may be a valuable chemotherapeutic through its potential to modulate metabolism.
- The mechanisms by which GA affect cancer metabolism remain unclear. We aim to address this research gap through metabolomics — the comprehensive analysis of metabolites for biomarker discovery.

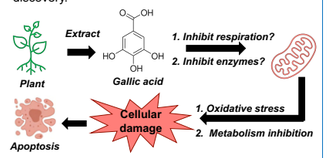

Figure 1. Proposed theories behind GA's anticancer activity. GA may inhibit mitochondrial respiration, producing damaging reactive oxidative species.[1] Alternatively, GA's inhibition of metabolism, such as glycolysis, can lead to cellular energy depletion.[2]

Principles of Metabolomics-guided Analysis

- We employed liquid chromatography-high-resolution mass spectrometry (LC-HRMS) and stable-isotope tracing to investigate metabolic activity of GA for cancer treatment.

Overview of LC-HRMS

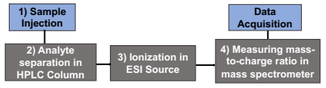

Figure 2. Simplified workflow of LC-HRMS. LC-HRMS differentiates compounds based on their physical and mass properties to separate and identify metabolites in a biological system.

Overview of stable-isotope tracing

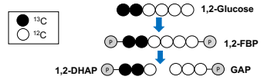

Figure 3. Application of stable-isotope tracing. Glucose with its carbon atoms replaced by a stable isotope is introduced into a system. This technique allows for *in vivo* assessment of metabolic changes and quantitation of metabolic reaction rates (flux).

Materials & Methods

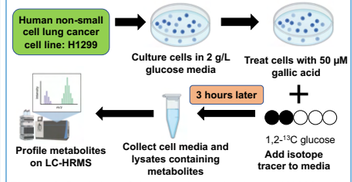

Figure 4. Depiction of the experimental scheme. H1299 cells were cultured until reaching 80% confluence. Cells were then treated with 50 μM of GA, and [1,2-^{13}C] glucose tracer was introduced. After 3 hours, metabolites were extracted. Samples were analyzed using LC-HRMS and MAVEN.

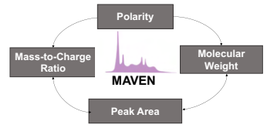

Figure 5. Depiction of necessary information for metabolite identification using MAVEN interface. MAVEN is an open-source software that allows for identification of metabolites and quantitation of isotope-labeling patterns between different biological conditions.[3,4]

Gallic Acid-induced Differential Metabolite Levels

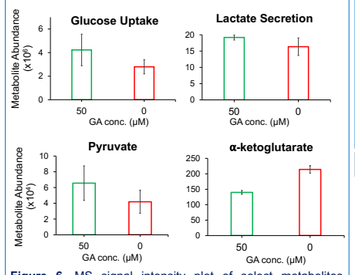

Figure 6. MS signal intensity plot of select metabolites obtained using MAVEN. Error bars indicate standard deviation between 3 biological replicates.

- For GA-treated H1299, we observed marginally increased glucose uptake and lactate secretion in media, accumulation of intracellular glycolysis metabolites, and depletion of most intracellular tricarboxylic acid cycle metabolites compared to those of the control.

Enrichment of M+2 in Pyruvate and Alanine

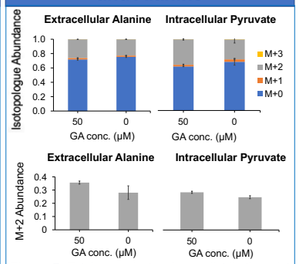

Figure 7. Total mass isotopologue distribution plot and M+2 isotopologue abundance plot for extracellular alanine and intracellular pyruvate, respectively.

- We observed higher enrichment of M+2 (2 atoms replaced by isotope) in intracellular pyruvate, the end product of glycolysis, and extracellular alanine, a metabolite exchanged with pyruvate in GA-treated cells.

Conclusions & Future Directions

- The accumulation of glycolytic intermediates may indicate GA-induced blockage of glycolysis, or alternatively, upregulation of glycolysis to compensate for GA-induced oxidative stress.
- Depletion of tricarboxylic acid cycle intermediates suggest this pathway may be dysfunctional or blocked in GA-treated H1299 cells, leading to their energy depletion.
- Differential isotopic labeling patterns indicate differential [1,2-^{13}C] glucose metabolism between GA-treated cells and control.
- In the future, we plan to quantify metabolic fluxes using computational tools to identify regulatory mechanisms (proteins, enzymes, etc.) involved in H1299 metabolism.

References

[1] Guerra, A.R, Duarte, M.F., Duarte, I.F. Targeting Tumor Metabolism with Plant-Derived Natural Products: Emerging Trends in Cancer Therapy. *Journal of Agricultural and Food Chemistry* **2018,** *66* (41) , 10663-10685.

[2] Liu, C., Lin, J.J., Yang, Z.Y. *et al.* Proteomic study reveals co-occurrence of gallic acid-induced apoptosis and glycolysis in B16F10 melanoma cells. *Journal of Agricultural and Food Chemistry* **2014,** 62(48), 11672-11680.

[3] Melamud, E., Vastag, L., Rabinowitz, J.D. Metabolomic Analysis and Visualization Engine for LC-MS Data. *Analytical Chemistry* **2010,** 82(23), 9818-9826.

[4] Clasquin, M.F., Melamud, E., Rabinowitz, J.D. LC-MS Data Processing with MAVEN: A Metabolomic Analysis and Visualization Engine. *Current Protocols in Bioinformatics* **2012,** 37:14.11.1-14.11.23.

Acknowledgements

Special thank you to the members of the Park Lab and UCLA Samueli Engineering Summer Undergraduate Research Program for their valuable guidance and support.

Ella Levine

Chemical Engineering
Freshman, UCLA

Annual Energy Output for Multijunction Solar Cells In Los Angeles County

FACULTY ADVISOR

Carissa Eisler

DAILY LAB SUPERVISOR

Lindsey Parsons

DEPARTMENT

Chemical Engineering

ABSTRACT

Implementing renewable energy sources is necessary to combat climate change. Typical solar panels use single junction cells (which use one material to absorb and convert light) instead of more expensive multijunction cells (which use multiple materials and convert sunlight more efficiently). Annual power production estimations are often based on efficiency, representing the power converted for a standard spectrum (AM1.5G), without accounting for spectral changes due to climate and season. These changes significantly impact annual energy generation, but data constraints and geographic variations hamper effective modeling. We hypothesized that a multijunction cell design employing a low-cost flat concentrator would generate significantly more energy from rooftop installations than current estimations of efficiency improvements. We applied Warmann's[1] spectral binning method and data from Los Angeles to detailed balance calculations with realistic concentrator and cell properties to predict the power output. Then, we applied developable residential roof area to calculate LA's annual solar energy generation for households. We found that our dual-junction solar cell design is 39.5% efficient while the record silicon single junction cell is 26.8% efficient. However, when accounting for annual spectral changes for LA, our design has a yearly maximum energy production of 472 kWh/m²—which is only 6.14% higher than the silicon cell (445 kWh/m²). This is lower than the percent increase in efficiency (47%). This demonstrates the importance of comparing designs through annual energy produced rather than efficiency so we can idealize designs for specific locations.

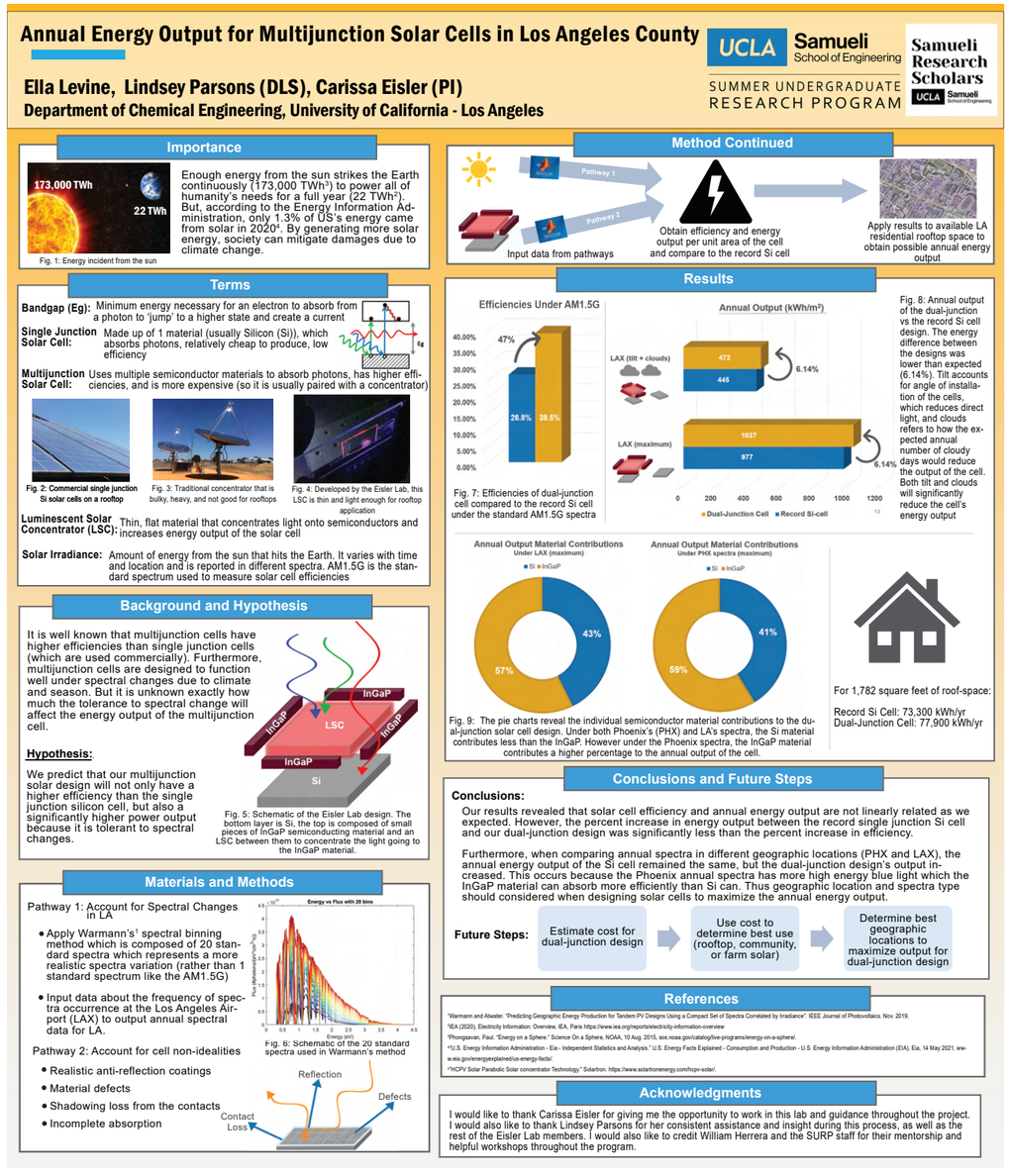

Sandra Li

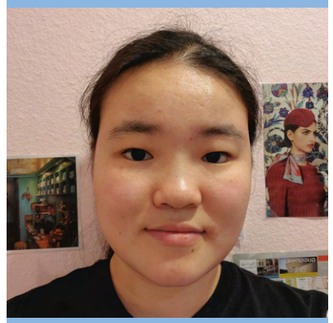

Electrical Engineering
Junior, UCLA

Modeling Terahertz Quantum-Cascade VECSELS with Randomized Metasurface Ridges Widths

FACULTY ADVISOR

Benjamin Williams

DAILY LAB SUPERVISOR

Eilam Morag

DEPARTMENT

Electrical and Computer Engineering

ABSTRACT

Speckle is an imaging artefact that arises from interference in high-coherence sources, such as conventional single-mode lasers. Thus, one approach to removing speckle in imaging is using spatially incoherent multi-mode lasers. For this reason, we are interested in achieving multi-mode lasing in the terahertz frequency range – a frequency range that is promising for imaging applications due to its non-ionizing yet penetrative nature. Using quantum-cascade vertical-external-cavity surface-emitting lasers (QC-VECSELs) – lasers in which in one reflecting end of the laser cavity is combined with metal-topped ridges that are filled with quantum-well gain material – our lab has previously achieved single-mode terahertz lasing. However, multi-moding is more difficult to achieve due to gain competition and spatial hole burning. In this work, we present a 2D model of QC-VECSEL metasurfaces with random ridge widths, based on our hypothesis that randomizing the ridge widths will localize lasing modes to different areas of the metasurface, reducing spatial hole burning. To investigate the validity of this approach, we generated various random metasurfaces and simulated their cavity fields using COMSOL Multiphysics. We then extracted all modes lasing under a fixed gain threshold and calculated their mutual spatial overlap across all biased ridges. In these simulations, we demonstrated that randomizing the metasurface increased the number of lasing modes and decreased spatial overlap significantly, at the cost of increased thresholds. In addition, uncertainty remains in how accurately our 2D models will represent 3D devices, and in how much we actually need to reduce spatial overlap for successful multi-moding.

UCLA Samueli School of Engineering

Modeling Terahertz Quantum-Cascade VECSELs with Randomized Metasurface Ridge Widths

Sandra Li, Eilam Morag, Professor Benjamin S. Williams
Terahertz Devices and Intersubband Nanostructures Laboratory
UCLA Department of Electrical and Computer Engineering

UCLA Samueli School of Engineering
SUMMER UNDERGRADUATE RESEARCH PROGRAM

INTRODUCTION

Speckle is an imaging artefact that arises from interference in high-coherence sources, like single-mode lasers. Speckle can be removed using spatially incoherent, multi-mode lasers, as the speckle patterns from different spatial modes will average each other out and reduce grain.

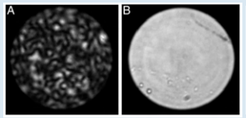

Fig. 1. A. Speckle from a coherent source. **B.** Speckle-free imaging from a multi-mode laser. *Original figure reprinted from [3].*

We are interested in achieving multi-mode lasing in the terahertz frequency range using our quantum-cascade vertical-external-cavity surface-emitting lasers (QC-VECSELs)[1]. However, achieving significant multi-moding is often challenging due to spatial hole burning.

OBJECTIVE

Inspired by random laser[2] and chaotic cavity[3] work, we hypothesize randomizing the metasurface ridge widths will localize lasing modes to different areas of the metasurface, reducing spatial hole burning. We aim to test the validity of this hypothesis by simulating the cavity fields of randomized metasurfaces in two dimensions.

BACKGROUND

Threshold gain – the amount of amplification gain material needs to provide for a mode to lase. Different modes have different thresholds.
Metasurface – reflective QC-VECSEL structure with metal ridges filled with quantum-well gain material laid on top.

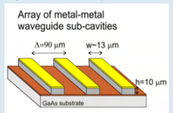

Fig. 2. The ridges of a QC-VECSEL metasurface act like antennas to help propagate emitted waves. In the base design, all ridges are of uniform width. *Original figure reprinted from [1].*

Spatial hole burning – Strong modes in a laser cavity will eat up the gain in the area they occupy spatially, reducing the availability of gain for other modes in that area.

MATERIALS

- **COMSOL Multiphysics** with LiveLink scripting module
  - For running simulations
- **MATLAB**
  - For writing scripts and calculations

METHODS

Building the metasurface
- A script automatically constructs a randomized 30-ridge metasurface in COMSOL and sets up the studies.

*randomized 2D metasurface obtained with MATLAB RNG

COMSOL simulations
- **Eigenfrequency simulation:** Searches for all lasing modes from 3.6 – 4.0 THz
- **Parametric sweep:** Repeats simulations for two different gain values (50 1/cm and 60 1/cm)

Calculating threshold gain (g_{th}) for lasing modes
- Using data from the parametric sweep, we can calculate g_{th}.
- Modes lase where the imaginary part of the eigenfrequency is 0

Using linear extrapolation with two eigenfreq. of different gain:

```
>>polyfit([imag50, imag60], [50, 60], 1);
```

Calculating spatial overlap factor $f_{i,j}$
- Run calculation between all lasing modes
- Spatial overlap factor quantifies how much spatial overlap two modes have.

For the set of all two modes i and j, calculate overlap factor $f_{i,j}$ as inner product of E_y fields over all ridges:

$$\langle a \mid b \rangle = \int_{\text{ridges}} ab \, dxdy$$

$$I = \frac{|E_y|^2}{\sqrt{\langle |E_y|^2 | |E_y|^2 \rangle}} \quad f_{i,j} = \langle I_i \mid I_j \rangle$$

RESULTS

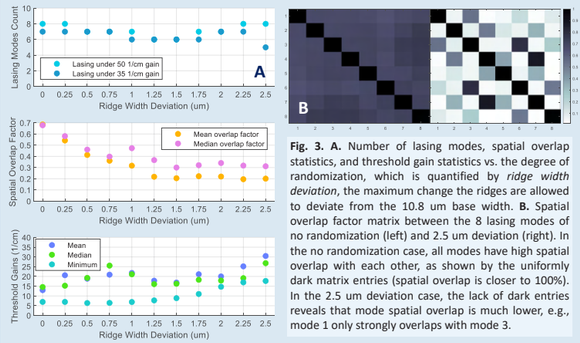

Fig. 3. A. Number of lasing modes, spatial overlap statistics, and threshold gain statistics vs. the degree of randomization, which is quantified by *ridge width deviation*, the maximum change the ridges are allowed to deviate from the 10.8 um base width. **B.** Spatial overlap factor matrix between the 8 lasing modes of no randomization (left) and 2.5 um deviation (right). In the no randomization case, all modes have high spatial overlap with each other, as shown by the uniformly dark matrix entries (spatial overlap is closer to 100%). In the 2.5 um deviation case, the lack of dark entries reveals that mode spatial overlap is much lower, e.g., mode 1 only strongly overlaps with mode 3.

CONCLUSIONS

We demonstrated that randomizing the metasurface significantly decreased spatial overlap, at the cost of increased thresholds. There is still some uncertainty as to how much we'll actually need to reduce spatial overlap for multi-moding. In the future, we plan to fabricate randomized patch metasurfaces and perform experiments to see if the model predictions are reflected.

ACKNOWLEGE MENTS

I would like to thank the National Science Foundation for funding this project. I would also like to thank Eilam Morag and Prof. Benjamin Williams for their help and guidance. I thank UCLA SURP for their support this summer.

REFERENCES

[1] Appl. Phys. Lett. 107, 221105 (2015); https://doi.org/10.1063/1.4936887

[2] Molen, Karen L. van der, et al. "Spatial Extent of Random Laser Modes." Physical Review Letters, vol. 98, no. 14, 2007.

[3] Redding, Brandon, et al. "Low Spatial Coherence Electrically Pumped Semiconductor Laser for Speckle-Free Full-Field Imaging." Proceedings of the National Academy of Sciences, vol. 112, no. 5, 2015, pp. 1304–09.

Dehao Lin

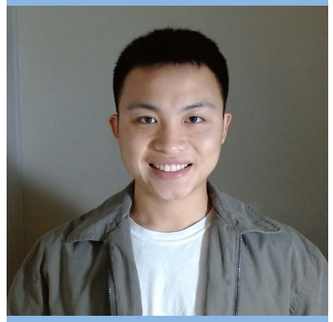

Mechanical Engineering
Sophomore, El Camino College

Scott Cao

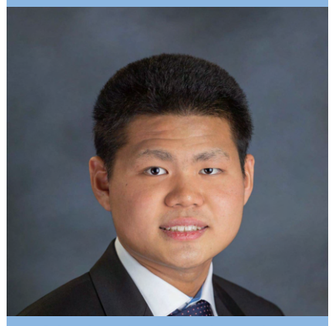

Mechanical Engineering
Freshman, UCLA

Exploring Viscoelastic Properties of Liquid Crystal Elastomers (LCEs)

FACULTY ADVISOR

Lihua Jin

DAILY LAB SUPERVISOR

Chen Wei

DEPARTMENT

Aerospace and Mechanical Engineering

ABSTRACT

Recently, soft materials have been under increasing study due to their high flexibility. We are studying a soft material known as liquid crystal elastomers (LCEs). With the ability to change shape when exposed to heat or light, LCEs have found applications in artificial muscles, biomedical devices, and more. These materials are made of liquid crystals (LCs) embedded in the backbone of a polymer, and their LCs can reorient in the direction of an applied stress. Our goal is to experimentally study the mechanical properties of LCEs and further explain their constitutive behavior by focusing on LCEs whose LCs are oriented in the same direction, called monodomain LCEs. We conducted relaxation tests and uniaxial stress-strain measurements at different loading rates on monodomain LCEs that we fabricated with different LC orientations. Effects of stress on LC reorientation were measured using transmission circular polariscopy (TCP), which characterizes the rotation of LCs during deformation. In addition, digital image correlation (DIC) was used to study the shear strain distribution in stretched LCEs. Our results show that the stress-strain relation of LCEs highly depends on loading rate and LC orientation. At low strain rates, the hysteresis in stress-strain curves is small, and LCs can reorient with strain, while at high rates, the hysteresis is large, and there is a lag of LC reorientation. Also, our DIC tests show that LC reorientation causes shear strain within LCEs. These experiments further contribute to the development of theoretical models of LCEs and drive forward LCE technologies.

UCLA Samueli School of Engineering

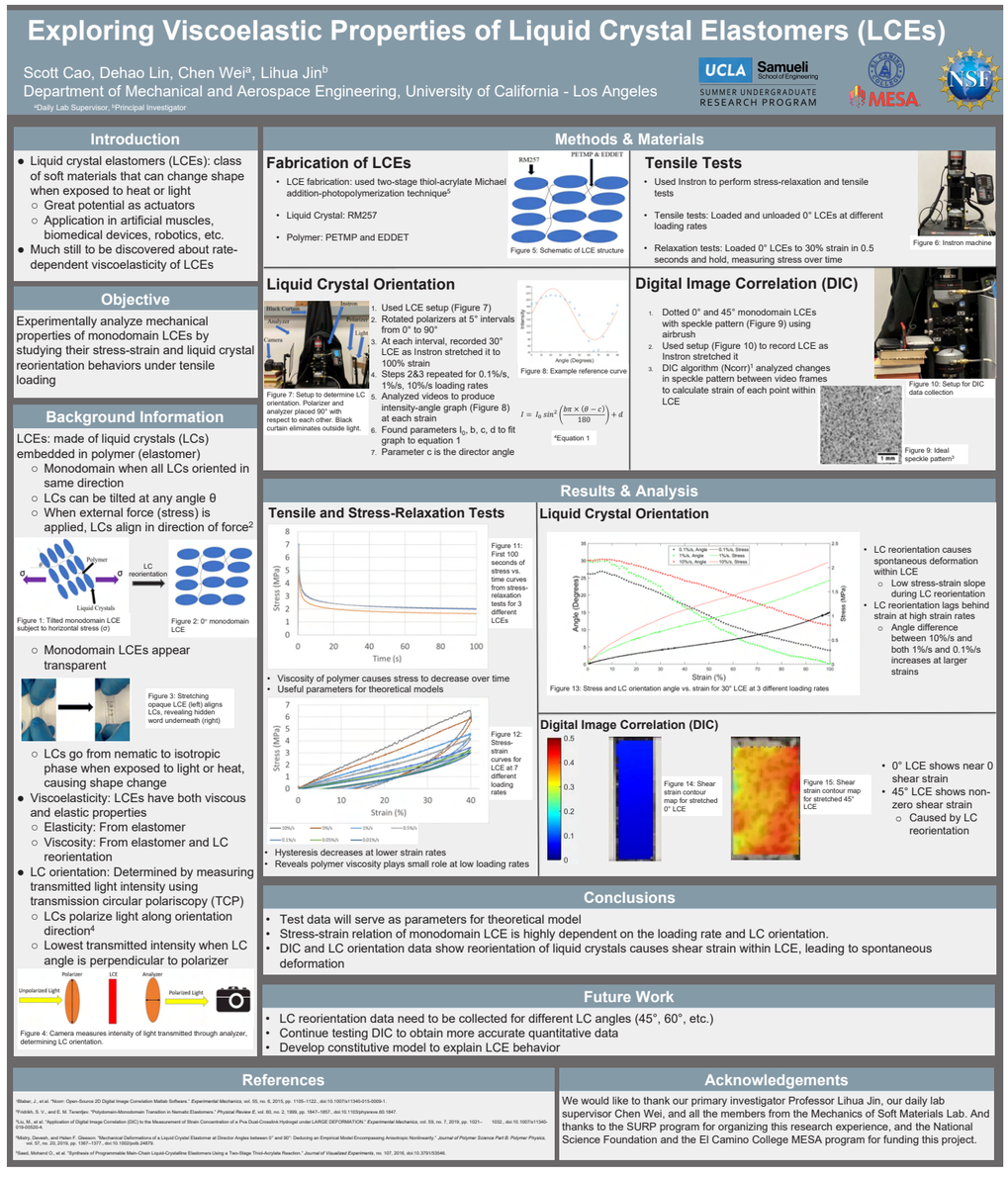

Angela Liu

Chemical Engineering
Freshman, UCLA

Integrating data-driven and Mechanistic Approaches in Cell Regulatory Pathway Analysis

FACULTY ADVISOR

Aaron Meyer

DAILY LAB SUPERVISOR

Farnaz Mohammadi

DEPARTMENT

Bioengineering

ABSTRACT

Targeted therapies eliminate cancer cells by inhibiting specific dysregulated pathways. While these treatments have proven to extend and save lives, drug resistance is a prevalent issue for currently available drugs. Previous work has identified sets of genes in melanoma that are disproportionately expressed in cancer cells that go on to become resistant after treatment with targeted therapy. However, how these genes form a coordinated pathway is not understood. We used a previously proposed non-linear form of gene regulatory network identification to convert perturbation experiments into an inferred pathway for these genes. Extending this work, we developed an iterative matrix solving method, making this algorithm scalable to many thousands of genes and knockdown conditions, along with allowing us to reason about its statistical properties. We applied this model and then analyzed its results to reveal drivers of melanoma drug resistance development. The matrix was visually represented by a weighted directed diagram, which was analyzed for clustering using the Bellman-Ford distance algorithm for pairs of pre-resistant, resistant, and randomized nodes. In total, this work provides a scalable approach to reasoning about the pathway mechanisms revealed in perturbation experiments.

UCLA Samueli School of Engineering

Integrating data-driven and Mechanistic Approaches in Cell Regulatory Pathway Analysis

Angela Liu, Farnaz Mohammadi, Aaron S. Meyer
University of California Los Angeles

SUMMER UNDERGRADUATE RESEARCH PROGRAM

Introduction

While cancer can be treated using drugs that inhibit dysregulated pathways, resistance to such drugs is a prevalent issue. Previous studies have identified genes that are disproportionately expressed in melanoma cells that were more likely to become resistant when exposed to treatment drugs, as well as those that are disproportionately expressed in known resistant cells. These are referred to as pre-resistant and resistant genes, respectively. However, how these genes form a pathway from pre-resistant to resistant is not understood. This can be tested in perturbation experiments, in which cells are exposed to various compounds and gene expression is recorded to measure the reaction of target genes.

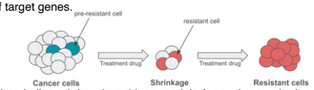

Recent work[2] has indicated that data-driven models for such perturbation studies are a valid way to predict untested interactions, effectively lowering research costs and facilitating large scale studies. Our goal is to build on this work in order to identify and analyze the genetic drivers of melanoma drug resistance for use in combination cancer treatment development. This is achieved by creating and training a model of gene expression in the form of a system of ordinary differential equations.

Dataset and Tools

The premise of the model is that gene expression can be measured as the level of mRNA produced by target genes and assumed to be at steady-state in order to create an ODE representation of the effects of each perturbation on each gene.

The perturbation data examined came from Torre *et al.*'s melanoma study, which contains 83x84 individual interactions of melanoma cells with various perturbagens. Genes were designated as pre-resistant or resistant based on a comparison of their frequency of NGFR^{high} cells and the number of resistant colonies, also from Torre *et al.*

Package in Python used to calculate cost function of perturbation model

Package in Python used to create directed weighted graph of gene interactions

Perturbation Model

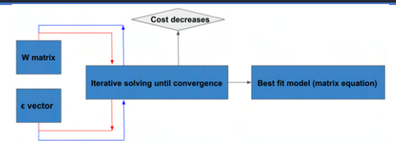

Figure 1. Iterative solving process

- The **W matrix** is created in Python by importing RNA sequencing data in which the gene expression levels of target genes in melanoma cells were measured after being exposed to various perturbagens. This data is then normalized and any genes with zero expression are removed. The resulting matrix is shown in Figure 1, where each value represents the interaction level between the genes in the corresponding row and column.

Figure 2. Partial w matrix with columns as gene knockouts and rows as gene expression

```
>>> print(w)
              ADCK3      BRD2      BRD8      BUB1B      CBFB     CDK11B      CHD7  ...         TPT1       USO      VEZF1      YBX1     ZBTB37      ZEB2      ZF
ADCK3     -1.874883  3.593628  1.840833  2.253157  24.750587 -41.165722  8.843573  ... -0.183811  8.876440   7.774188  285.853624  0.005056  9.895317  1.188251
BRD2      -0.687308 -20.416828 -19.410441 -24.978237 -168.515468 -7.596359  297.854279  ... -6.755139 -6.898346   8.648346  926.392857 -1.115138  76.153195 -6.898346
BRD8      -0.687308 -20.416828 -19.410441 -24.978237 -168.515468 -7.596359  297.854279  ... -6.755139 -6.898346   8.648346  926.392857 -1.115138  76.153195 -6.898346
BUB1B      1.537934  13.001224  4.538141  2.953647  25.161772  1.856490  15.980084  ... -5.451473  8.023696   7.726698  116.316187  0.717879  11.049148  1.549394
CBFB      13.567506 -20.283089  8.203663  6.968631 -6.853193  5.213904 -62.763355  ... -4.358172  8.122791  86.252775 -846.595242 -2.688598 -37.513852 -7.896532
...
VEZF1     43.454682  82.289855  30.123015  10.982214  39.154455  3.664839 -9.435556  ...  4.380476 -6.194501 -135.333562  611.267965  8.285584 -61.875210 -3.486473
YBX1     -68.784598 -583.498965 -56.197576  7.240826 -605.180653 -5.662862 -29.285891  ... -6.524228  8.864853 -44.312674 4857.005089 -4.242440 -338.754823 -9.467354
ZBTB37    15.555414  25.158986  -6.449397  29.497635 -5.167032  58.521145 -9.819859  ...  8.848852  72.729528  5834.985158  2.247638  178.638617  4.354423
ZEB2       8.473225 -5.147089  6.974821 -6.528838 -18.371383  8.983171  7.967446  ... -6.268057  8.883154 -5.748669  15.877681 -8.653782 -3.342259 -5.639611

[78 rows x 78 columns]
```

- W is a parameter of the **matrix equation** below, the solution of which describes the RNA sequencing data. It is co-dependent with the parameter eta, which is found by taking the average value of each column from the ratio of αX and 1+tanh(WU)

$$\bar{\epsilon}\,(1+\tanh\,(WU)) = \alpha X$$

- The solution of the matrix equation is found using an **iterative matrix solving method:** starting with a random value of W, we iterate between eta and W, using one to solve for the other until they converge. In each iteration, the model becomes closer to the experimental data, which we quantify using the cost function shown below.

$$cost = norm(\epsilon \cdot (1 + tanh(\omega \cdot U)) - \alpha \cdot D)$$

- The **cost**, or the difference between the model and the data, is calculated in order to quantify how well the model fits the RNA sequencing data.

Results and Discussion

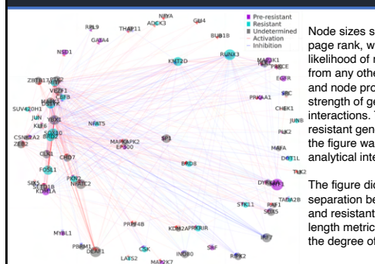

Figure 2. Directed weighted graph displaying gene-gene interactions.

Node sizes show the strength of page rank, which is a metric of the likelihood of reaching that node from any other node. Edge weight and node proximity reflect the strength of gene-gene interactions. The clustering of resistant genes on the left side of the figure was of particular analytical interest.

The figure did not clearly indicate separation between pre-resistant and resistant genes, so a path length metric was used to quantify the degree of clustering.

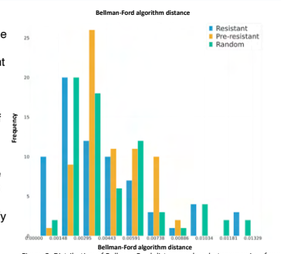

Figure 3. Distribution of Bellman-Ford distance values between pairs of pre-resistant, resistant, and random gene nodes on the network diagram.

Pre-resistant	Resistant	Random
Mean: 4.413E-3	Mean: 4.462E-3	Mean: 4.248E-3

The Bellman-Ford distance algorithm for weighted graphs was used to find the separation in interaction between pre-resistant and resistant nodes. We used the inverse of edge weight so stronger interactions resulted in shorter distances. The distance between randomized pairs of nodes was also calculated for comparison.

The pairs of genes across types turned out to be more closely connected than those within their own type.

Conclusions

The distribution of distance values suggests that the assumption that pre-resistance and resistance are separate genetic programs is false, or that they each contain multiple pathways. In order to confirm these results, we are working to analyze additional cell lines in hopes of finding patterns in the gene interactions.

Future work includes test the model's ability to predict data it hasn't previously seen by taking away indices and filling back them in while iterating over a fitting function. The results of this function will guide future model improvements.

References and Acknowledgement

1. Torre, E.A., Arai, E., Bayatpour, S. *et al.* Genetic screening for single-cell variability modulators driving therapy resistance. *Nat Genet* **53,** 76–85 (2021). https://doi.org/10.1038/s41588-020-00749-z
2. Yuan *et al.* CellBox: Interpretab;e Machine Learning for Perturbation Biology with Application to the Design of Cancer Combination Therapy. *Cell Systems*, 128-140 (2021). https://doi.org/10.1016/j.cels.2020.11.013

I would like to thank Dr. Aaron Meyer and Farnaz Mohammadi for their supervision and guidance. Additionally, I would like to thank the SURP program for the organizing and funding this research opportunity and for their support.

Matthew Lopez

Civil and Environmental Engineering Freshman, UCLA

The Risk of Liquefaction and Sea Level Rise on California's Coastal Communities

FACULTY ADVISOR

Timu Gallien

DAILY LAB SUPERVISOR

Margit Maple

DEPARTMENT

Civil and Environmental Engineering

ABSTRACT

Liquefaction occurs when a high water content soil loses strength during an earthquake and enters a liquid-like state. Sea level rise will elevate local beach groundwater tables and may substantially increase liquefaction risk along the California coastline. Studies have been conducted in Hawaii and Connecticut to understand the combined risk of liquefaction and sea level rise, however studies for the California coastline are limited, as are the publicly available groundwater well data required to make these risk assessments. This research highlights liquefaction risk within specific sites, how sea level rise affects these risks, and considers the impact at various urbanized coastal California sites. Sunset Beach and Newport Beach serve as case studies. Information such as population, number of buildings, and building type are compiled. Geospatial surface terrain data and tidal elevations are then compiled in ArcGIS to create elevation maps for the sites and used to make a general assessment of potential liquefaction damage. For the Sunset Beach site the areas currently within liquefaction zones include 403 buildings and $849 million in housing while Newport Bay includes 6,934 buildings and $26.6 billion in value. Limited groundwater data suggests that groundwater tables within the sites are at a moderate depth. This, combined with the extent that SLR could temporarily increase groundwater levels at the sites through direct inundation suggests that these coastal communities may become increasingly susceptible to liquefaction. Study results emphasize the severity of liquefaction risks and highlight the need to monitor local beach groundwater tables and potential liquefaction conditions to reduce current and future threats to infrastructure.

UCLA Samueli School of Engineering

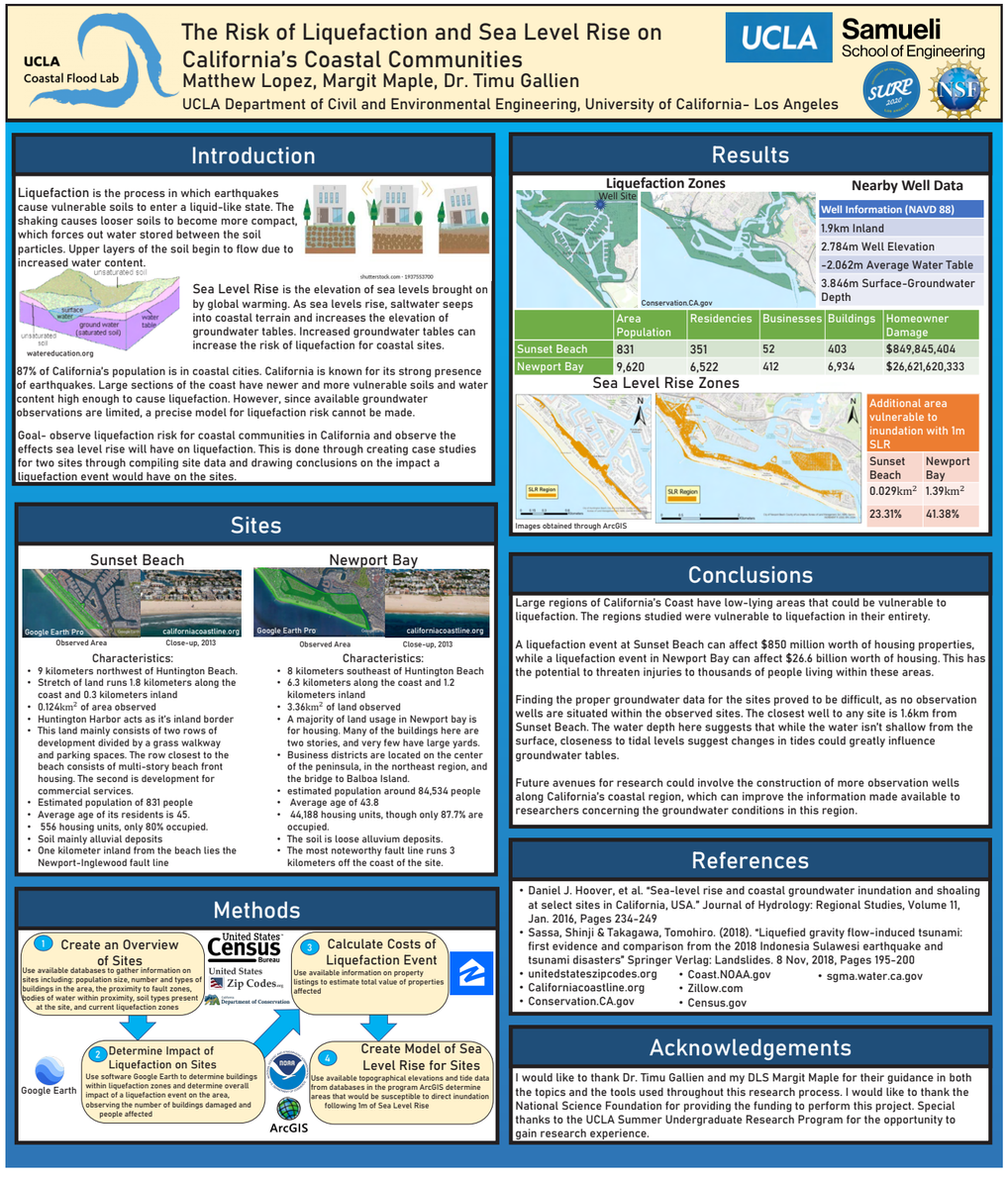

Arthur Lovekin

Mechanical Engineering
Junior, UCLA

Design and Implementation of an Autonomous Weed-Spraying Robot

FACULTY ADVISOR

Khalid Jawed

DAILY LAB SUPERVISOR

Yayun Du

DEPARTMENT

Aerospace and Mechanical Engineering

ABSTRACT

Precision farming is a hotly pursued field in modern agriculture that seeks to target individual weeds as opposed to entire fields, thereby dramatically reducing the application of herbicide and mitigating the negative impact of herbicides on human and environmental health. In this project we present an autonomous weed-spraying robot which utilizes computer-vision-based navigation and weed-identification algorithms in order to spray weeds with high efficiency for a variety of stages of plant growth. This compact platform is the first (to our knowledge) to autonomously spray row crops such as flax and canola where row spacing is as small as one foot, and offers an inexpensive alternative to larger industrial robots that have difficulties with smaller row spacings. The robot identifies flax plants using an implementation of the YOLOv4 neural network, and uses the plant locations both to navigate and to spray weeds. Furthermore, a novel self-charging station design and sprayer system allows the robot to operate for the entire day. This robot was extensively tested in the flax fields surrounding the North Dakota State University. Preliminary results indicate that the weeds are successfully killed in the center of rows, but they persist immediately next to the cropline where the robot cannot access without trampling the flax. Additionally, further development of the autonomous navigation and weed identification algorithms is needed for dependable performance in the field. However, overall this platform provides a strong basis on which to build a robust platform that could substantially decrease the amount of labor and herbicide required to grow crops, and increase the health of both humans and the environment.

UCLA Samueli School of Engineering
SUMMER UNDERGRADUATE RESEARCH PROGRAM

Design and Implementation of an Autonomous Weed-Spraying Robot

Name: Arthur L. Lovekin[1] DLS: Yayun Du[1] PI: Professor M. Khalid Jawed[1]
[1] Structures-Computer Interaction Lab, Department of Mechanical Engineering, University of California - Los Angeles

Background

Precision farming is a hotly pursued field in modern agriculture that seeks to target individual weeds as opposed to entire fields, thereby dramatically reducing the application of herbicide and mitigating the negative impact of herbicides on human and environmental health. Current industrial robots tend to be expensive, and rely on GPS to navigate which is unsuitable for crops with small row-spacings (eg. flax and canola). We seek to fill the niche of small, inexpensive autonomous robots that take an under-canopy perspective of crops with small row-spacings. This versatile platform can increase spraying efficiency for a variety of crops, and ultimately revolutionize the way we produce agricultural products.

Naio Technologies: Dino[3] $220,000
- GPS RTK guidance
- Wide row spacing

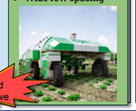

Big and Expensive

Objectives

- Low cost (<$1000)
- Able to travel between 25cm croplines
- Full-Day Autonomy
- All weather conditions and stages of plant growth
- Computer-vision based navigation and plant identification

Methods

The Robotic Operating System (ROS) is used as a framework to organize each independent process (ie. sensor or algorithm) into a graphical structure. Each independent process is represented by a node which can publish it's output (eg. sensor data or algorithm output) to a topic. Other nodes can then subscribe to that topic to use the data. The algorithms were written primarily in Python. The hardware was designed in Solidworks, and manufactured out of 3D-printed PLA or Aluminum.

Autonomous Charging

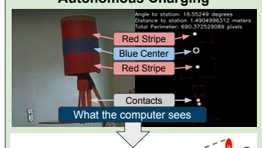

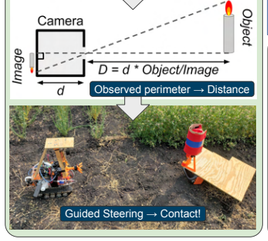

Field Testing

Location: North Dakota State University experimental flax fields

[Jul 7] "Piggybot"
- Sprayed all fields without getting stuck

[Jul 22] "Franky"
- Improved Nozzle height and spray consistency

[Aug 2] "Jetbot"
- Fully incorporated all sensors simultaneously

[Aug 16] "Turtlebot"
- Improved cameras and camera stabilization

Autonomous Navigation … A Work in Progress

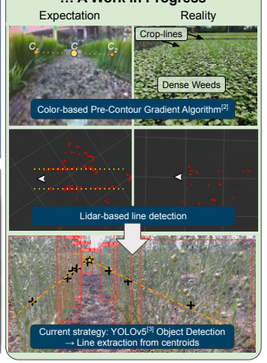

Robotic Operating System Communication Graph

- (1) Herbicide Pumps
- (2) Motors With Encoder
- (3) Gimbal Moves around to identify and spray weeds
- (4) LIDAR
- (5) Cameras Raspberry Pi V2
- (6) Jetson Xavier
- (7) Autonomous Charging
- Navigation
- Weed Identification
- (8) Arduino Uno Connects algorithms and low-level components

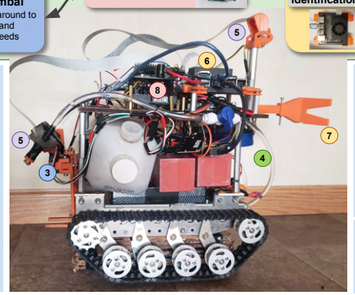

Results

Weeds are successfully killed in the center of rows, but they persist where the robot cannot access without trampling the flax. Hardware upgrades to address this are under development.

Conclusions

Overall, great strides have been made towards accomplishing our goal of a robust weed-spraying platform. Through extensive testing we demonstrated that the robot is able to overcome most obstacles despite its small size, and charge itself as needed to operate throughout the day. We are also very close to a framework that can accomplish robust autonomous navigation. Our contribution of a flax and weed library, as well as our hardware successes and failures, will hopefully open the door to scalable automation for under-canopy weeding of a variety of crops.

Future Work

- Multi-herbicide spray
- Resilience to rain and large obstacles
- Improved navigation and weed-detection
- Expand to other crops

Acknowledgments

Many thanks to my mentors Dr. Yayun Du and Professor Jawed for guiding me in my work, as well as the other SCI Lab undergraduates for always putting in hard work. Additionally, thanks to the Samueli School of Engineering Student Undergraduate Research Program, the US Department of Agriculture, and the National Science Foundation for making this research possible.

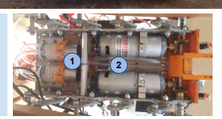

References

[1] "Dino Vegetable Weeding Robot for Large-Scale Vegetable Farms." *Naio Technologies*, www.naio-technologies.com/en/dino/.
[2] Du, Yayun, et. al. "A Low-Cost Robot with Autonomous Recharge and Navigation for Weed Control in Fields with Narrow Row Spacing." International Conference on Intelligent Robots and Systems.
[3] Jocher, G. (2020, May). *GitHub - ultralytics/yolov5*. GitHub. https://github.com/ultralytics/yolov5

Quinlan McKnight

Civil Engineering
Sophomore, UCLA

Presence of Microplastics in Stormwater Wetlands Delays Microbial Methane Production

FACULTY ADVISOR

Sanjay Mohanty

DAILY LAB SUPERVISOR

Renan Valenca

DEPARTMENT

Civil and Environmental Engineering

ABSTRACT

Wetland environments are home to biological processes that emit methane - a greenhouse gas that accelerates climate change. Methanogens, methane-producing bacteria, are commonly present in these wetlands that receive stormwater runoff containing a range of contaminants including microplastics (MPs). MPs are known to suppress microbial activity, but their effect on the methanogenesis process and on the diversity of microbial communities in wetland environments remains unknown. To identify the impact of MPs on the methane production from wetland sediments, we performed a series of laboratorial batch experiments where different wetland sediment sizes were exposed to MPs under aerobic and anaerobic conditions while monitoring the production of methane. The batch experiments were kept in incubators at optimum conditions for methane production. Our results show that, under aerobic conditions, large sediments (> 2.0 mm) produced 100 times more methane than fine sediments (< 2.0 mm), possibly due to the decomposition of organic matter present only within large sediments. Under anaerobic conditions, fine particles increased their production by more than 40 times when acetate was present in solution, proving that wetland sediments have the capacity for methane production when nutrients are available. The presence of MPs among fine sediments with acetate caused a delay and suppressed methane production, possibly due to the direct interaction between MPs and methanogens, as well as the indirect interaction between MPs and acetate, as both processes could suppress methane production. Overall, the results furnish the understanding of methane fluxes in relation to microplastic transport in wetland environments.

UCLA Samueli School of Engineering

Samueli Research Scholars
UCLA Samueli School of Engineering

Presence of Microplastics in Stormwater Wetlands Delays Microbial Methane Production

Quinlan McKnight, Renan Valença, Dr. Sanjay K. Mohanty
Department of Civil and Environmental Engineering – University of California, Los Angeles

UCLA Samueli School of Engineering
SUMMER UNDERGRADUATE RESEARCH PROGRAM

Introduction

Images: Flatiron.com

Wetlands (WLs) are biologically diverse environments; however, methanogens (methane-producing bacteria) there are the main source of methane emissions into the atmosphere, a climate change accelerator.

WLs receive stormwater runoff that contain emerging contaminants such as microplastics (MPs). It is known MPs suppress microbial activity, but the effect of MPs on wetland methane production is unknown.

What is the effect of MPs on methane production and microbial communities in wetlands?

Materials and Methods

WL sediments were collected from the Ballona Wetlands in Los Angeles, CA. On the same day as collection, sediments were sieved to separate the fine sediments (< 2.0 mm) from large (> 2.0 mm) and used in the following experiments:

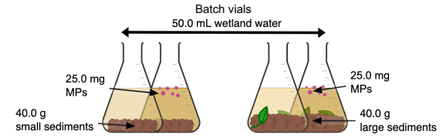

Fig. 1: Experiment 1 -- Control and MP batch vials containing small or large sediments under aerobic conditions. Vials were kept in an incubator at optimum conditions; gas samples were extracted in the same manner as **Fig. 2** to measure methane concentration.

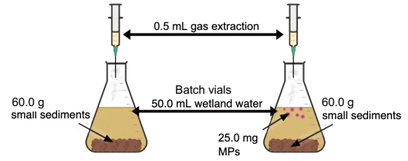

Fig. 2: Experiment 2 – Control and MP batch vials containing fine sediments and nutrients (acetate) under anaerobic conditions as achieved by **Fig. 3**. Vials were kept in an incubator at optimum conditions; gas samples were extracted periodically and analyzed using gas chromatography.

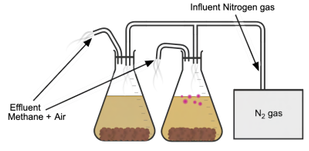

Fig. 3: Nitrogen gas purged into batch vials to achieve anaerobic conditions.

Results

Fig. 4: Experiment 1 – Large sediments produced significantly more methane ($p < 0.05$) than fine sediments under aerobic conditions in both the control and MP batch vials.

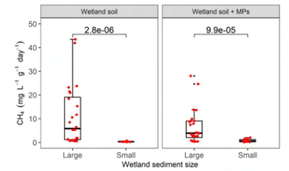

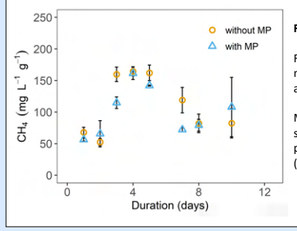

Fig. 5: Experiment 2 -- Fine sediments produced more methane when acetate was present.

MPs delayed and suppressed the production of methane (day 2 – day 8).

Conclusions

In Experiment 1, the decay of organic matter only present among large sediments may have caused the magnitude difference of methane production. For this reason, future experiments will only utilize small sediments, as the research focus is on microbial production of methane.

In Experiment 2, results suggest that fine sediments have the capacity to produce methane when nutrients are available. MPs delayed and suppressed methane production, possibly due to the direct interaction between MPs and methanogens, and/or between MPs and acetate.

Future Work

Microbial DNA analysis will be performed on the sediments to connect the varying methane concentrations with bacterial health.

Since rising global temperatures cause wildfire frequency to increase, Experiment 2 will be recreated with wildfire residues to understand the effect of these contaminants on methane production.

Acknowledgements

Thank you to my Daily Lab Supervisor, Renan Valença, and my faculty advisor, Dr. Sanjay Mohanty, for the invaluable support I have received. Thank you to the Summer Undergraduate Research Program, the Samueli Research Scholars Program, and the Samueli Foundation for this research opportunity.

Damian Meza

Aerospace Engineering
Sophomore, UCLA

3D Printing of Anisotropic and Curved Structures

FACULTY ADVISOR

Lihua Jin

DAILY LAB SUPERVISOR

Shivam Agarwal

DEPARTMENT

Aerospace and Mechanical Engineering

ABSTRACT

Direct-ink writing (DIW) 3D printing as a means of fabrication allows for the deposit of viscous fluids to create three-dimensional structures along a computer-guided print path. In this work, 3D-printed anisotropic structures were fabricated by customizing the direction of extruded filament, and the mechanical properties were studied. A polydimethylsiloxane (PDMS) ink mixture was prepared with optimal rheological properties for DIW printing. We tune the printing parameters, such as pressure and print height to reduce various defects such as stretching and overhanging of the extruded filament. A MATLAB script was developed to orient the print direction at any given angle within any convex polygon; print instructions were converted to G-Code using a Python script with the Mecode module. Planar rectangular structures were printed with filaments aligned along the horizontal, vertical, and diagonal directions. Printed structures were subjected to uniaxial tensile tests and stress-strain curves were obtained for quasistatic loading and unloading. Results suggest that the stiffness has a strong dependence on the print angle. Methods used here, specifically G-Code creation, will facilitate the fabrication of active morphing structures by DIW printing of Liquid Crystal Elastomers (LCEs) in the future.

UCLA Samueli School of Engineering

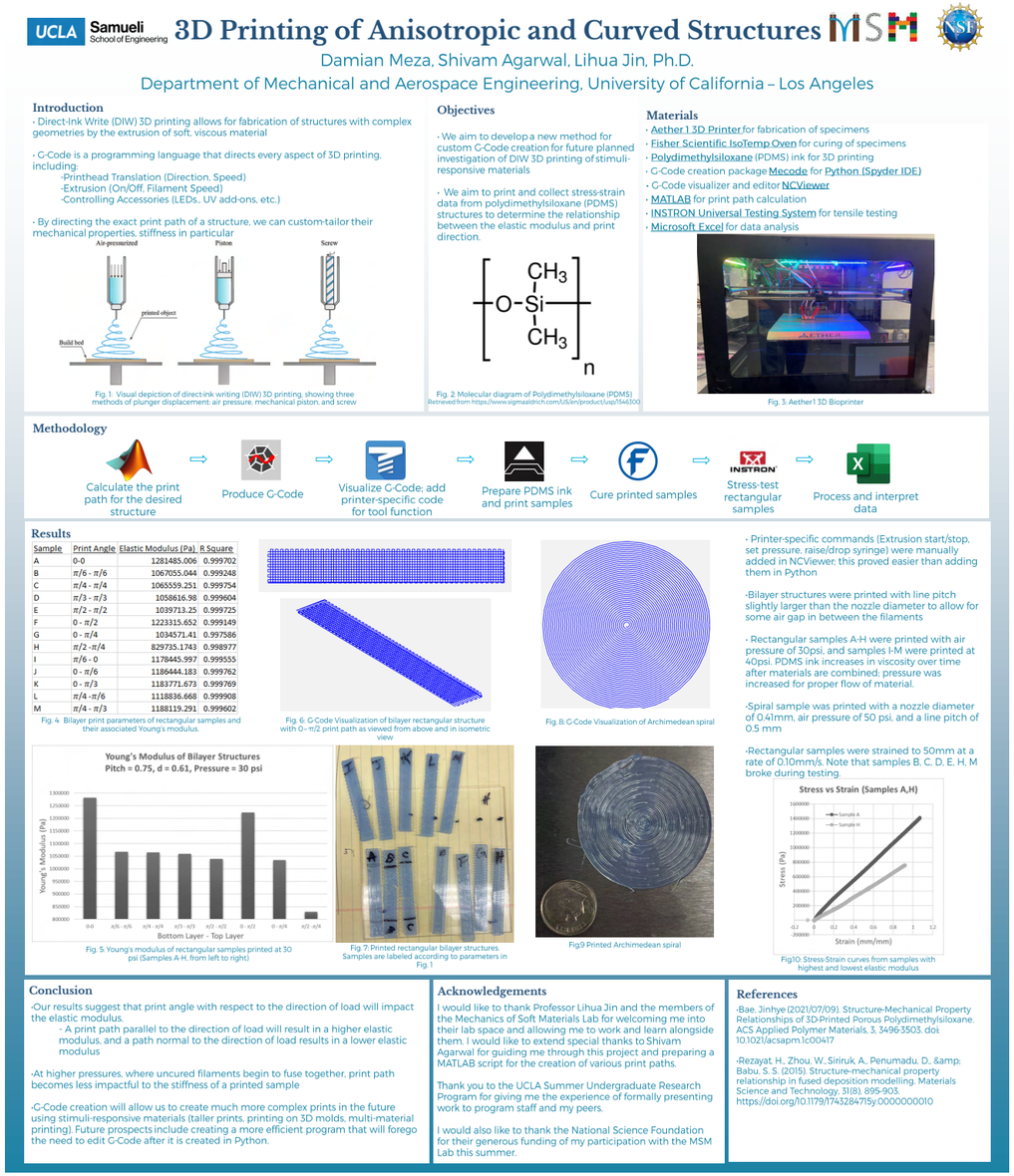

Krisha Minocha

Computer Engineering
Freshman, UCLA

Camera-based Heart Rate Estimation Focused on Mitigating Bias

FACULTY ADVISOR

Achuta Kadambi

DAILY LAB SUPERVISOR

Pradyumna Chari

DEPARTMENT

Electrical and Computer Engineering

ABSTRACT

The COVID-19 pandemic has led to an influx of telehealth appointments, causing difficulty in assessing vital signs virtually. Our work focuses on remote photoplethysmography (R-PPG), the concept of measuring heart rate using color fluctuations in the face. Many different algorithms already exist with varying levels of success; however, one major gap is the lack of performance of these existing algorithms on darker skin tones, which, given the prevalence of cardiovascular disease in African American communities, creates a pressing issue. We have employed a VGG-style convolutional network known as DeepPhys to learn different spatial masks and increase robustness across the board. My work has focused on improving this existing network to increase medical accuracy by manipulating the structure of the network along with training parameters.

Camera-based Heart Rate Estimation Focused on Mitigating Bias

Krisha Minocha, Pradyumna Chari, Professor Achuta Kadambi
Department of Electrical and Computer Engineering - UCLA

Introduction

There has recently been a notable influx in telehealth visits due to the COVID-19 pandemic. While telehealth has created a way to provide patient care remotely, it is extremely difficult to assess vital signs such as heart rate, breathing rate, etc., indicating that there is clearly a need for contactless heart rate sensing solutions. While there are existing computer vision solutions available, they exhibit a bias against darker skin tones.

Key Concepts

Remote Photoplethysmography (R-PPG)
- Type of algorithm focused on using subtle color variations in the face to measure a blood volume pulse and, consequently, estimate heart rate.

Convolutional Neural Network
- A computer system modeled on the human brain and nervous system, specifically focused on mimicking the optic nerve and image processing

Objective

I aim to implement an improved computer vision model for measuring heart rate using deep learning. My goal is to increase performance specifically on darker skin tones.

VITAL Dataset

Vital-sign Imaging for Telemedicine AppLications developed by Visual Machines Group at UCLA
- At least 432 videos of 54 subjects
- Focus on a diverse dataset in terms of gender, race, age, skin tone, etc.
- Using two different camera angles and four different lighting conditions with only a smartphone camera

I will be working to train the algorithm on this dataset in order to ensure optimal performance across the board.

Figure 1. Experimental Setup for creation of VITAL dataset

Proposed Algorithm

My proposed algorithm will build off the existing DeepPhys algorithm developed by W. Chen and D. McDuff consisting of:
- A VGG-Style Convolutional Neural Network (up to 19 layers)
- Learns spatial masks for regions of interest to maximize performance and robustness
- Emphasis on diffuse component, ignoring the mirror-like reflections of the skin
- Uses two streams: Motion and Appearance in order to maximize performance

This algorithm was able to improve performance with motion and talking. However, there is still a bias in terms of skin tone. My proposed changes will be to the structure of the model to hopefully improve performance across the board. I plan on doing this by using different activation and loss functions and observing the results.

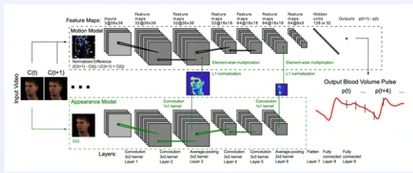

Figure 2. Proposed Algorithm Structure Using Both Appearance and Motion Streams to Increase Robustness

Conclusion and Results

Activation/Loss Function Combination	Mean Absolute Error (bpm)
rrelu/softmarginloss	18
tanh/MSE	13.166
selu/pearson	12.73
relu/MSE	12.57
relu/L!Loss	12.57
rrelu/MSE	11.257
rrelu/L1Loss	11.257
rrelu/pearson	11.251

Table 1. Table of experimental results of loss/activation function manipulation

This work furthers previous algorithmic advances such as the existing DeepPhys algorithm to increase accuracy. We can see that regardless of loss function, the rrelu activation function creates the best results. However, there is still a large margin of error, which needs to be corrected. This work can also be extended outside of the medical realm into reducing bias in other computer vision applications such as facial recognition, etc.

References

1. Chari, Pradyumna, et al. "Diverse R-PPG: Camera-Based Heart Rate Estimation for Diverse Subject Skin-Tones and Scenes." *ArXiv*, 2020. https://arxiv.org/pdf/2010.12769.pdf
2. Chen, Weixuan, and Daniel McDuff. "DeepPhys: Video-Based Physiological Measurement Using Convolutional Attention Networks." *ArXiv*, 2018, https://arxiv.org/pdf/1805.07888.pdf

Acknowledgements

We would like to thank the UCLA Summer Undergraduate Research Program for organizing this research internship and the Samueli Research Scholars Program for funding it. We would also like to thank the UCLA Fast Track to Success Electrical and Computer Engineering Program for their continued guidance and support. I would also like to thank Pradyumna and Professor Kadambi for challenging me and creating such a supportive and creative atmosphere for learning.

Zofia Orlowski

Mechanical Engineering
Sophomore, UCLA

Internet of Things (IoT) Technology for Electrowetting-on-dielectric (EWOD) Devices

FACULTY ADVISOR

Chang-Jin Kim

DAILY LAB SUPERVISOR

Qining Wang

DEPARTMENT

Aerospace and Mechanical Engineering

ABSTRACT

Electrowetting-on-dielectric (EWOD) is a mechanism that enables the manipulation of droplets through electrical signals alone. Due to its advantages for droplet-based microfluidics, such as the simplicity in both device design and fabrication, EWOD has demonstrated its utility in numerous biochemical and biomedical applications, especially lab-on-a-chip. However, currently the EWOD technology is being utilized by only a small number of labs who have proper engineering backgrounds, enough resources to design and fabricate devices to fulfill their goals, and control systems and software to operate the devices. To combat this barrier, the UCLA Micro and Nano Manufacturing Laboratory is developing a cloud-based cyber-manufacturing platform for common users to gain easy access to the EWOD technology. In furthering the mission, the lab is exploring a remote operation of the EWOD control system by introducing an Internet of Things (IoT)-based intermediate system. This remote operation will serve as a gateway to an envisioned lab-on-cloud that will help democratize EWOD technology. Acting as a broker for information exchange between a backend server and EWOD control system, the intermediate system is designed to run users' instruction files, communicate its messages to the EWOD control system, and operate alongside a camera for users to remotely monitor their experiments. My work has involved developing a proof-of-concept demonstration that one can operate an EWOD control system by sending the necessary commands from a remote location.

Jillian Pantig

Computer Engineering
Sophomore, Irvine Valley College

A Process for Implementing Accessible Cardstock-made Robot Cars Equipped with A Variety of Robotic Behaviors

FACULTY ADVISOR

Ankur Mehta

DAILY LAB SUPERVISOR

Ankur Mehta

DEPARTMENT

Electrical and Computer Engineering

ABSTRACT

As the world rapidly turns to robots, it is important to make robot creation ubiquitous, but there are barriers – accessibility and limitation of resources – that inhibit such phenomena. In this study, we proposed and tested a possible solution that can lessen those barriers by building origami robots made with accessible resources. Origami is defined as the Japanese art of folding. To test our hypothesis, we implemented a process that fabricates origami robot cars made from single-layered materials like cardstocks while ensuring that these cars can still carry out several robotic behaviors. The process includes gathering accessible hardwares, programming behaviours using Arduino, designing the origami-inspired body of the car using LEMUR's RoCo, and testing the car to determine if its origami-structure can handle the programmed robotic functionalities: driving on a variety of surfaces, using differential and pivot steering, detecting obstacles, implementing PID control through IMU and visual sensors, and enabling communication with other robots through mesh networking. The scheme yielded robot cars that are useful and fairly accessible with cardstock-made bodies and with a variety of robotic behaviours as mentoned above. The result of our study justifies that the implementation of origami robots has a huge potential in terms of lessening the resource-related barriers of robot creation which increases both the number of people who can build robots and the probability of robot creation being ubiquitous.

Mateen Rabbani

Mechanical Engineering
Sophomore, UCLA

Fabrication of 3D Printed Thermoplastic Polyurethane Lattices via Fused Deposition Modeling

FACULTY ADVISOR

Lihua Jin

DAILY LAB SUPERVISOR

Shivam Agarwal

DEPARTMENT

Aerospace and Mechanical Engineering

ABSTRACT

Thermoplastic polyurethane (TPU) is a class of material that combines the desirable elastic properties of rubbers with the ease of manufacturing of plastics, and are widely used in various industries sectors. The objective of this study is to fabricate TPU lattice structures as light-weight energy-absorbing materials by fused deposition modeling (FDM) 3D printing. Since the extrusion of TPU from the nozzle and adhesion on the surface is fraught with challenges, dog-bone samples were first printed to characterize the correct printing parameters, such as temperature, printing height, and printing speed. It was observed that increasing the print temperature and reducing the extrusion rate improve the print quality, (i.e. reduction in missing material, burning and clogging). To further print TPU lattices full of overhanging structures, water-soluble Polyvinyl alcohol (PVA) is used as the supporting material. Unit cells of an octet truss lattice were printed, and it was found that by increasing layer thickness, disabling retraction, and enabling sacrificial nozzle wiping structures provide the best prints.

UCLA Samueli School of Engineering

Fabrication of 3D Printed Thermoplastic Polyurethane Lattices via Fused Deposition Modeling

UCLA Samueli School of Engineering
SUMMER UNDERGRADUATE RESEARCH PROGRAM

Mateen Rabbani, Shivam Agarwal, Lihua Jin, Ph.D.
Mechanics of Soft Materials Lab
Department of Mechanical and Aerospace Engineering - University of California, Los Angeles

Introduction

Thermoplastic polyurethane (TPU) is a polymer that combines the highly elastic properties of rubber with the ease of manufacturing of plastics[1].

However, to maximize the energy absorbing properties of TPU, it is essential that it can be printed into complex lattice structures with ease. Specifically, it is important that it can be printed into an octet truss lattice, which is an ideal structure for energy absorption.

Prior research has primarily focused on either the constitutive material properties of TPU itself or on the properties of different lattice structures, but has yet to concentrate on the ideal manufacturing methods used to create TPU lattices.

Objective

The objective of this study is to reliably fabricate TPU lattice structures as light-weight energy-absorbing materials by fused deposition modeling (FDM) 3D printing.

Fused Deposition Modeling

Fused deposition modeling (FDM) is a 3D printing technology whereby a solid filament is pushed through a heated chamber, melted, and extruded onto a build plate. By the incremental layering of the material on top of itself, FDM allows a user to create complex forms in three dimensional space.

To print lattices full of overhanging structures, water-soluble Polyvinyl alcohol (PVA) is used as the supporting material and is subsequently dissolved leaving the TPU behind.

Unlike more common 3D printable plastics, TPU is fraught with challenges. TPU is not only highly sensitive to the print temperature, but it is also hygroscopic. Additionally, subsequent layers of TPU tend to have difficulty adhering to the previous layer.

Dog-Bone Samples

Printing

Dog-bone samples were first created to characterize the optimal printing conditions before creating larger 3D structures. In order to find these conditions, multiple dog-bone samples were produced each with different printing parameters. More than twelve parameters including layer height, printing speed, and printing temperature were varied to hone in on the optimal printing parameters.

Figure 1: Dog-bone sample

Results

By varying the print conditions and printing multiple samples, it was observed that increasing the print temperature and reducing the extrusion rate were the primary factors in improving the print quality, (i.e. reduction in missing material, burning and clogging).

Annealing Samples

Annealing

Annealing is the process by which a sample is raised to an elevated temperature (below the melting point) for a prolonged period of time. This is done to reduce internal stress, reduce printing defects, and improve the stress-strain characteristics of the TPU dog-bone samples[2]. To explore annealing on 3D printed TPU, a pair of reference dog-bone samples, a pair of samples annealed at 70°C for twelve hours, and a pair of samples annealed at 160°C were stretched to 30% strain using an Instron five times.

Results

Annealing the print for twelve hours at 70°C seemed to yield the greatest improvement in the energy absorbing characteristics of the sample.

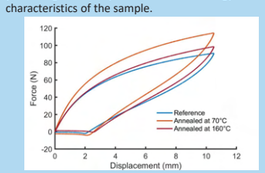

Figure 2: Tensile Testing of Annealed Samples

The energy dissipated within the first cycle of the samples annealed at 70°C was 28.13% greater than the reference. The energy dissipated within the first cycle of the samples annealed at 160°C was 4.48% greater than the reference.

Octet Unit Cell Samples

Printing

Using the print settings from the dog-bone samples as a starting point, octet truss unit cells were printed. Due to the necessity of PVA in order to support the overhangs of the octet truss, a new set of printing conditions would be required. To find these optimal conditions, a similar series of parameters were varied the addition of unit cell density as well as new sacrificial structures to help ease the transition between printing PVA and TPU.

Results

By varying the print conditions and printing multiple samples, it was found that by increasing layer thickness, disabling retraction, increasing density, and enabling sacrificial nozzle wiping structures provide the best prints. All of these factors created a reliable method for making unit cells as small as 10 mm^3.

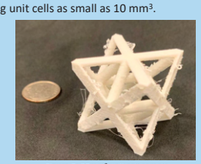

Figure 3: 30mm^3 unit cell sample

Octet Lattice Samples

Printing Lattices

Using the same optimized print settings as the unit cell resulted in a reliable method for printing larger lattices. Additionally, these lattices printed well at smaller unit cell sizes due to the added stability of the neighboring cells.

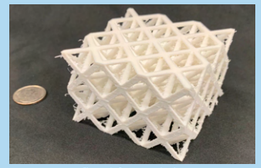

Figure 4: Octet truss lattice

Findings

Conclusion

In optimizing the print quality of both the dog-bone and unit cell samples, it is clear that a denser lattice made from thick layers is ideal for producing high quality FDM prints. It is also evident that using sacrificial structures to prime and clean the print nozzle between printing TPU and PVA significantly improver the quality of the final lattice.

Future Work

The next steps in studying TPU lattices would be to focus on quantifying the energy absorbing properties of the lattice via compression testing. It is also important to look at how the structure of the lattice (whether it is periodic or aperiodic or it is bending or stretching dominant) affects the properties of the lattice. This can further be extended to an analysis of the behavior of randomly generated stochastic lattices.

References

[1] Qi, H.J., and M.C. Boyce. “Stress–Strain Behavior of Thermoplastic Polyurethanes.” Mechanics of Materials, vol. 37, no. 8, 2005, pp. 817–839., doi:10.1016/j.mechmat.2004.08.001.

[2] Amirkhosravi, Mehrad, et al. “Designing Thermal Annealing to Control Mechanical Performance of Thermoplastic Polyurethane Elastomers.” Polymer, vol. 214, 2021, p. 123254., doi:10.1016/j.polymer.2020.123254.

Acknowledgements

I would like to think both Dr. Lihua Jin and Shivam Agarwal for taking the time out of their schedule to teach me, to mentor me, and to guide me in creating this research project. Without there support, none of this would have been at all possible. I would also like to thank Mr. William Herrera and the entire SURP program for providing their professional guidance and expertise throughout the entirety of the program.

Samantha Rafter

Electrical Engineering
Freshman, UCLA

Optimization of Double Ridge Metasurface for Quantum Cascade External Cavity Laser

FACULTY ADVISOR

Benjamin Williams

DAILY LAB SUPERVISOR

Eilam Morag

DEPARTMENT

Electrical and Computer Engineering

ABSTRACT

Terahertz light has demonstrated the ability to identify complex molecules via spectroscopy. However, its potential to do so has been largely untapped due to a lack of capable, broadband, non-dispersive sources. The double ridge design of the metasurface is a viable path toward bridging this gap by broadening the amplification bandwidth of metasurfaces, which may then be used to create widely tunable quantum cascade external-cavity lasers with low group delay dispersion (GDD). The design consists of repeating units of two differently sized ridges, each of which corresponds to a resonant frequency, at which there is a peak in reflectance (a measure of the amplification of light). Altering the widths of the ridges and the separation between them allows for manipulation of the resonant frequencies so that they are near each other, creating a continuous range of frequencies where amplification is high. Previously, the ridge widths and separation of the ridges were determined by running simulations where tested dimensions were manually decided by the user, who would then analyze the collected data to determine favorable geometries. To more efficiently and accurately find a geometry that could be considered optimal, MATLAB functions representing broadband reflectance and GDD were written in order to quantify the values to be optimized. The simulation software COMSOL Multiphysics as well as its associated optimization module were then used with these functions to create and run optimization studies that determined the geometry of the ridges that minimized dispersion while maintaining broadband reflectance. Initial results suggest that GDD could be improved upon by 1.72% while maintaining the same broadband performance as a previous design, and could be improved upon by 7.48% at a slight cost (0.125 THz) to the bandwidth.

UCLA Samueli School of Engineering

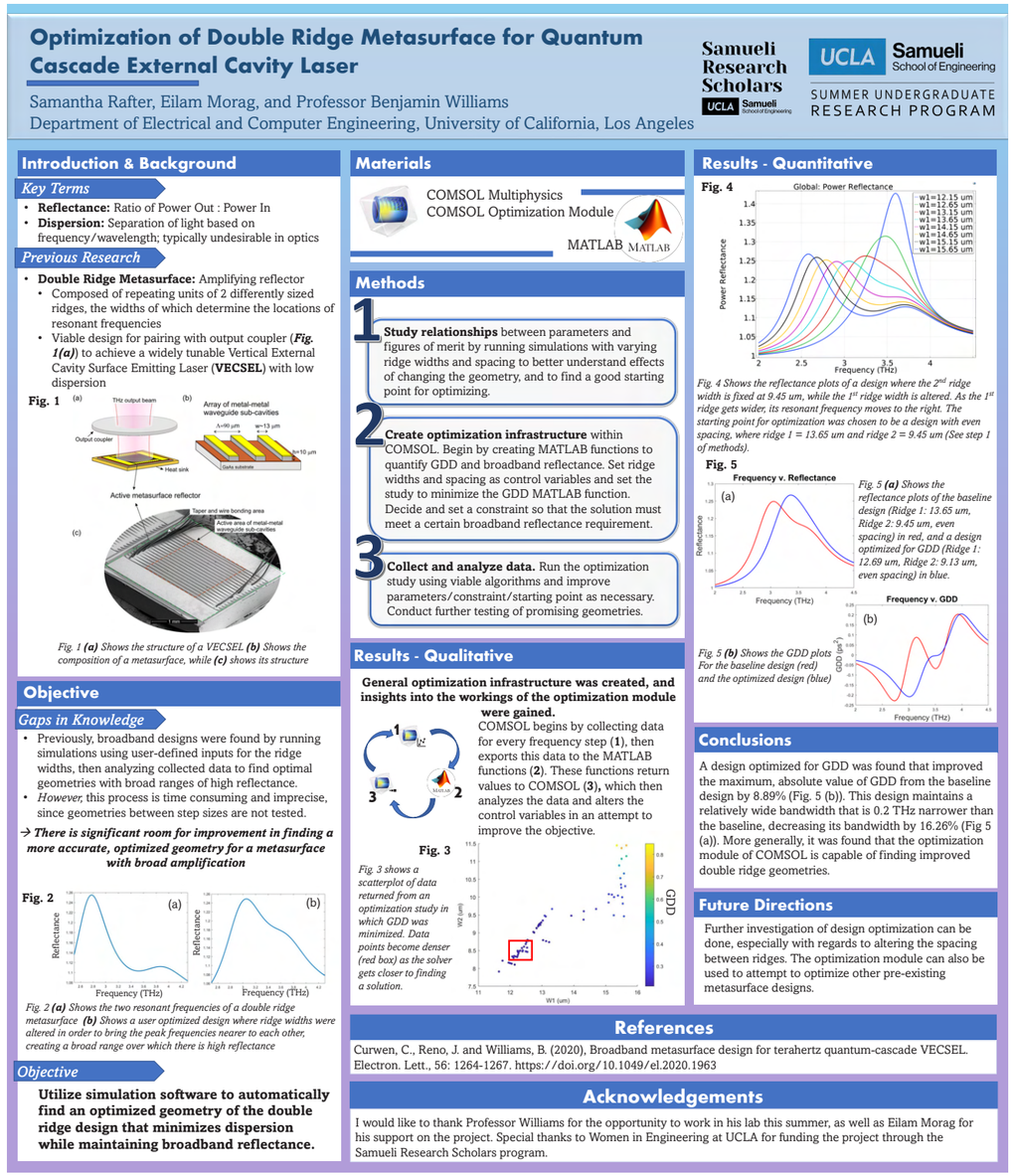

Aadhidhya Ravikumar

Electrical Engineering
Freshman, UCLA

Jenna Kim

Electrical Engineering
Freshman, UCLA

Deep Learning Approaches for Transmitter Classification

FACULTY ADVISOR

Danijela Cabric

DAILY LAB SUPERVISOR

Danijela Cabric

DEPARTMENT

Electrical and Computer Engineering

ABSTRACT

Wireless signal classification plays an important role in the security of a wireless communication system since it can be used for transmitter authorization, the process by which authorized transmitters are distinguished from non-authorized transmitters based on transmitter-specific traits in their signals. Current systems have only investigated authorization for a closed set scenario, where the algorithm classifies among a finite set of known transmitters. This has several limitations, the most significant of which is that transmitters outside of the known set may be misclassified. In this project, we attempt to remedy this issue by performing authentication in an open set scenario, where the number of transmitters is not known. To do this, we generated and transmitted signals from eleven different ADALM Pluto Software Defined Radios using MATLAB software. We also simulated 5 unique transmitters by artificially adding different I/Q imbalance impairments to the signals. The signals were transmitted in the form of packets (active transmission separated by idle moments), which were then extracted using pre-written code. Finally, the extracted packets were inputted into an existing deep learning algorithm called One Vs. All, where the algorithm was tested and modified until a satisfactory accuracy was found. With this algorithm, wireless communication security can be significantly improved, since it minimizes the risk of misclassification by solving the previous weakness of authorization only under closed set conditions.

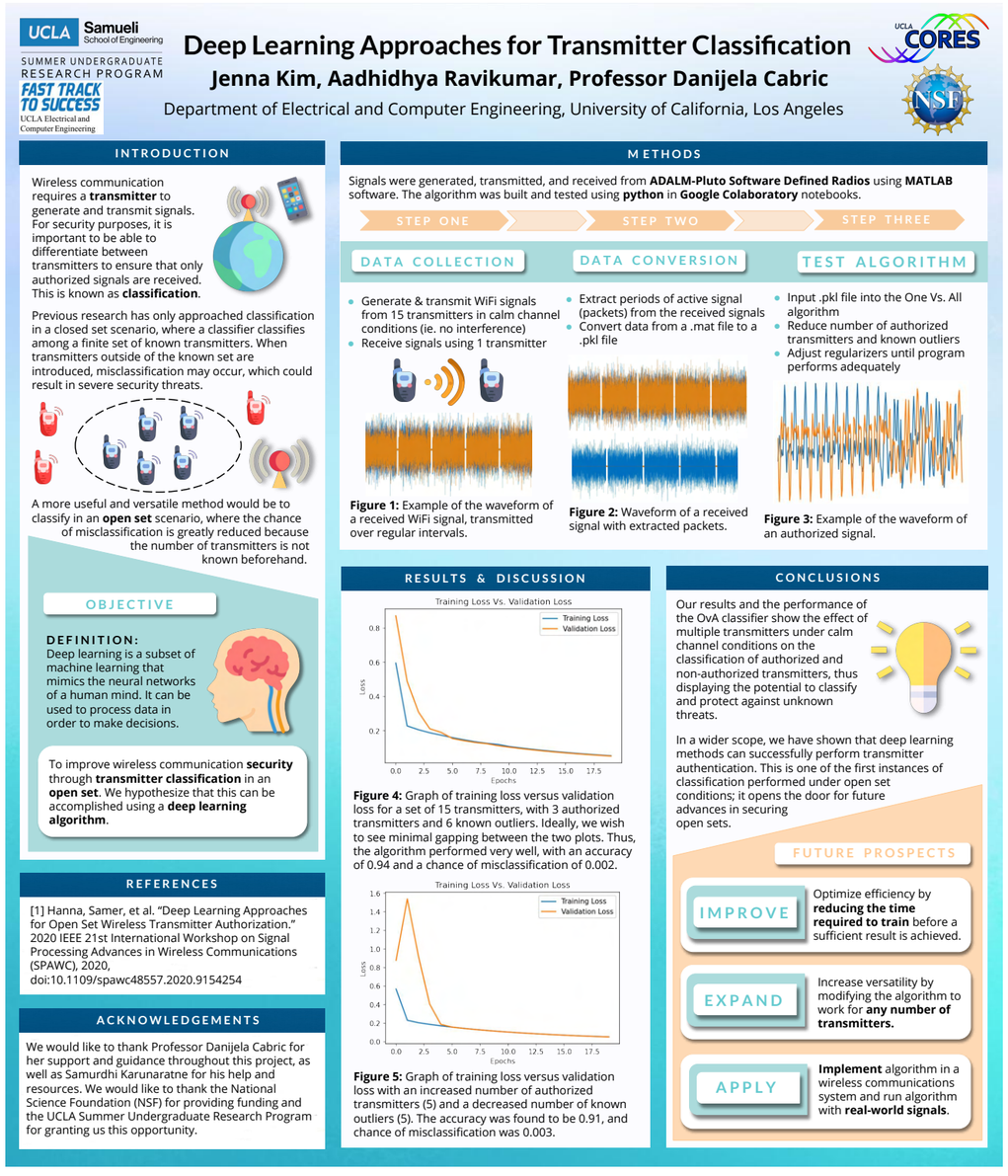

Dolores Rodriguez

Chemical Engineering
Junior, UCLA

The Effects of Mass Transfer on CO2 Reduction

FACULTY ADVISOR

Carlos G. Morales-Guio

DAILY LAB SUPERVISOR

Joonbaek Jang

DEPARTMENT

Chemical Engineering

ABSTRACT

Carbon dioxide is the most abundant greenhouse gas in the atmosphere emitted through human activities. However, through an electrochemical process CO2 can be converted into more useful products such as fuels and feedstock chemicals. To improve this process so that selectivity is increased towards these more desirable products, this study will explore how mass transport affects the product distribution of the electroreduction of CO2. We alter the mass transportation of CO2 to the catalytic surface by rotating the catalyst. A cylindrical Cu catalyst is used and rotation speeds of 200 and 400 rpm are tested. The applied potential is also varied from -1.31 V vs SHE to -1.67 V vs SHE. This study provides new insights into what may be the optimal rotation speed that will produce the highest selectivity towards more desirable products, in turn opening up the possibility of CO2 reduction being a new avenue of renewable energy.

UCLA Samueli School of Engineering

The Effects of Mass Transfer on CO_2 Reduction

By Dolores Rodriguez with Joonbaek Jang and Dr. Carlos G. Morales-Guio
Laboratory of Electrochemical Systems Engineering
Department of Chemical Engineering, University of California, Los Angeles

Samueli Research Scholars UCLA Samueli School of Engineering

UCLA Samueli School of Engineering
SUMMER UNDERGRADUATE RESEARCH PROGRAM

Introduction

CO_2 is the most abundant greenhouse gas in the atmosphere emitted through human activities. This study contributes to the ongoing research on how to reduce CO_2 into fuel and feedstock chemicals in a carbon neutral process. The reduction of CO_2 could prove to be a very useful and new avenue of renewable energy.

Objective

The objective of this study is to explore how mass transport affects the product distribution of the electrochemical reduction of carbon dioxide. More specifically, we will be looking into how rotating the catalyst, and in doing so, changing the mass transfer of carbon dioxide to the catalyst surface affects the product distribution.

Principles

Current Density

- Current density which is the density of electrons flowing from the catalyst
- This is how we measure the activity of a catalyst
- The more active a catalyst is, the more electrons that will be transferred, and therefore a higher current density

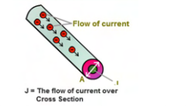

Figure 1[1]: Flow of current through a cross-sectional area

Mass Transfer

- Mass transfer is the net movement of mass from one location to another
- We will be looking at the mass transfer of CO_2 to the catalyst surface.

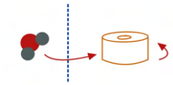

Figure 2: Carbon dioxide molecule traveling to a rotating catalyst

Materials

The electroreduction of carbon dioxide occurs in a custom rotation cell.

The programs Peaksimple [2] and Bruker Topspin [3] are used to identify and quantify the resulting products.

PeakSimple BRUKER

Results

Partial Current Density vs Potential at 200 rpm

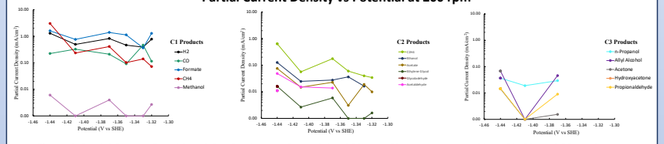

Figure 4: Partial Current Densities of Gas Products vs Potential at 200 rpm. Plots are separated into C1, C2, and C3 products.

Partial Current Density vs Potential at 400 rpm

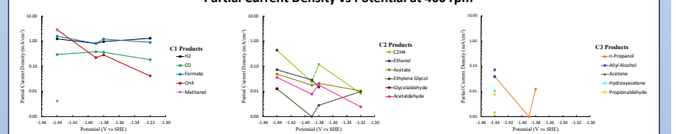

Figure 7: Partial Current Densities of Gas Products vs Potential at 400 rpm. Plots are separated into C1, C2, and C3 products.

Methods

1. Prepare the Catalyst Surface

The catalyst is first mechanically polished and then electropolished.

2. Running the experiment

The catalyst is placed in the cell where it rotates. The rotation speeds and potentials applied to the system are varied.

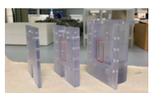

Figure 3: The custom rotation cell

3. Product Quantification

After the experiment is finished, the liquid products are analyzed using Bruker Topspin while the gas products are analyzed using Peaksimple.

Conclusions

Our results don't show a great difference in the range of partial current densities of each product between the two rotation speeds. However, there are noticeable differences in the onset potential of each product between the two rotation speeds. The onset potential is the lowest overpotential at which the product is detected. At 400 rpm, most C3 products have a higher onset potential than at 200 rpm.

For future experiments, data should be collected at more potentials to better depict and define what the partial current density looks like at each rotation speed.

References

[1] Current Density, https://byjus.com/physics/current-density/

[2] Peaksimple Logo, https://www.sri-instruments-europe.com/en/products/software/peak-simple.php

[3] Bruker Topspin Logo, https://nmr.wp.st-andrews.ac.uk/bruker-topspin/

Acknowledgements

I would like to thank to my P.I., Dr. Carlos G. Morales-Guio and my daily lab supervisor, Joonbaek Jang for their guidance and mentorship. I would like to thank William Herrera and the rest of the SURP program administrators for their resources. I would also like to thank Samueli Research Scholars for funding this research.

Nicolas Schmidt

Electrical Engineering
Junior, UCLA

Terahertz polarization imaging using quantum-cascade laser with switchable polarization

FACULTY ADVISOR

Benjamin Williams

DAILY LAB SUPERVISOR

Anthony Kim

DEPARTMENT

Electrical and Computer Engineering

ABSTRACT

We are using a terahertz quantum-cascade vertical external cavity surface emitting laser (QC-VECSEL) with switchable polarization for polarization difference imaging. Terahertz radiation's non-damaging nature gives it several applications such as cancer detection, bomb detection, and drug detection. Furthermore, polarimetric imaging can show various features not shown by traditional images, such as roughness, edge details, and birefringence. To optimize imaging, we first found the focal point of the laser, meaning where the gaussian beam spot size is minimum. Next, we investigated the signal to noise ratio through a wide range of parameters. We found the parameters with the strongest signal to noise ratio and from there we could move on to imaging. The beam goes through a biconvex lens, the sample, a rotating polarizer and finally two off-axis parabolic mirrors focus it onto the detector. Then we use Stokes-Mueller formalism to conveniently model the partially polarized light. Our images suggest that polarization difference can show edge features with high contrast for samples transparent in the terahertz frequency range.

UCLA Samueli School of Engineering

UCLA Samueli Electrical & Computer Engineering

Terahertz polarization imaging using quantum-cascade laser with switchable polarization

Nicolas Schmidt[1], Anthony D. Kim[1], Benjamin S. Williams[1]
[1]Department of Electrical and Computer Engineering, University of California Los Angeles (UCLA), Los Angeles, CA 90095

Terahertz Devices and Intersubband Nanostructures Laboratory

Introduction

- **Terahertz (THz) radiation** is able to penetrate through a wide range of non-metals. Furthermore, due to its low energy it is known to cause no detectable damage to matter.
- **THz imaging** shows promise in medicine (cancer detection), security (illegal drug and bomb detection), agriculture (water content detection) and more.
- Imaging via polarization can show various features not shown by traditional images. It is significantly more sensitive than conventional imaging, showing features such as **roughness, edge details, and birefringence**.

Terahertz illumination

- **We use a teraquantum-cascade (QC) vertical-external-cavity surface-emitting-laser (VECSEL) with switchable polarization.**
- Our laser uses a metasurface with two different arrays of antennae and quantum-cascade gain which are respectively activated via an electrical bias.
- The two sets have quasi-orthogonal linear polarizations with set 1 emitting a beam at about 45° and set 2 at about 135°. The two sets also show excellent beam quality.
- We operate our QC-VECSEL at operating temperature 77K, 10% duty cycle, at 3.2 THz, 0.7mW average power for the top set and 0.5 mW for the bottom set

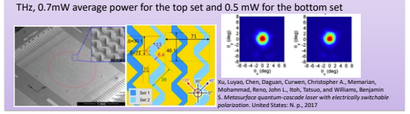

Xu, Luyao, Chen, Daguan, Curwen, Christopher A., Memarian, Mohammad, Reno, John L., Itoh, Tatsuo, and Williams, Benjamin S. *Metasurface quantum-cascade laser with electrically switchable polarization*. United States: N. p., 2017

Experimental setup and detection methods

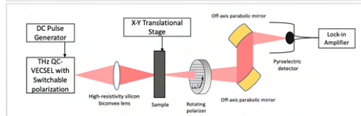

Diagram of optical setup.

- **The pulsed QC-VECSEL with linear polarization goes through a high-resistivity silicon biconvex lens to be focused onto a sample.**
- **The THz signal coming out of the sample is modulated a linear polarizer rotating at 10 Hz.**
- Lock-in amplifier collects the in-phase and quadrature component of the laser beam, which can be used to calculate the polarization state of the beam after going through the sample.
- We use Stokes-Mueller formalism to analyze the light reaching the detector.

Resolution and noise

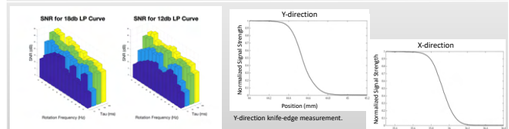

Y-direction knife-edge measurement.

X-direction knife-edge measurement.

SNR testing results.

- 100 samples of the laser are taken while variating the rotating polarizer's frequency, the lock-in amplifier's averaging time (tau) and the frequency the lock-in amplifier uses for the signal (double the rotation frequency).
- Optimal operation parameters for the optical setup are found to, 10 Hz rotation frequency, resulting in a 20 Hz lock-in frequency, and tau of 300ms
- Using knife-edge measurements with the X-Y translational stage we measure the diameter of the focal point of the beam to be $\mathbf{0.28}\ \boldsymbol{mm}$ in both the X and Y direction.
- This measurement corresponds to the transmission drop from 90% to 10% of the laser's maximum transmission

Stokes-Mueller Formalism

- Stokes-Mueller formalism is convenient to model the partially polarized light coming out of our sample

$$\boldsymbol{S} = \begin{pmatrix} S_0 \\ S_1 \\ S_2 \\ S_3 \end{pmatrix} = \begin{pmatrix} \langle E_x^2 \rangle + \langle E_y^2 \rangle = \langle I_{R'} \rangle + \langle I_{RC} \rangle \\ \langle E_x^2 \rangle - \langle E_y^2 \rangle = \langle I_{R'} \rangle - \langle I_{RC} \rangle \\ 2\langle E_x E_y \cos\left(\delta_y(t) - \delta_x(t)\right)\rangle = \langle I_{45'} \rangle - \langle I_{135'} \rangle \\ 2\langle E_x E_y \sin\left(\delta_y(t) - \delta_x(t)\right)\rangle = \langle I_{LC} \rangle - \langle I_{RC} \rangle \end{pmatrix}$$

- Furthermore, our rotator and lock-in amplifier system provides the Stokes parameters.

$$\boldsymbol{M_{rotator}} = \frac{1}{2}\begin{pmatrix} 1 & \cos(2\omega t) & \sin(2\omega t) & 0 \\ \cos(2\omega t) & \cos^2(2\omega t) & \sin(2\omega t)\cos(2\omega t) & 0 \\ \sin(2\omega t) & \sin(2\omega t)\cos(2\omega t) & \sin^2(2\omega t) & 0 \\ 0 & 0 & 0 & 0 \end{pmatrix}$$

- With this we can extract the intensity and the change from the initial polarization-angle at the edges and features of the sample.
- Intensity:

$$S_{out,1} = \frac{1}{2}(S_0 + S_1\cos(2\omega t) + S_2\sin(2\omega t))$$

- Polarization Angle:

$$\psi_{rot} = \frac{1}{2}\tan^{-1}\left(\frac{S_2}{S_1}\right)$$

Results

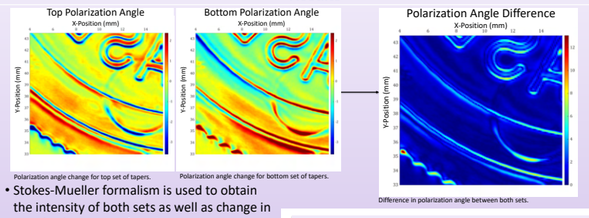

Polarization angle change for top set of tapers.

Polarization angle change for bottom set of tapers.

Difference in polarization angle between both sets.

- Stokes-Mueller formalism is used to obtain the intensity of both sets as well as change in polarization angle of the laser.
- It can be seen by analyzing these images that the orthogonal polarizations show different features more prominently. It is of interest to consolidate these features into one image.
- The clearest image obtained from this specific sample was the difference in polarization angle, as all the features of the sample are most clearly seen.
- It is clear to see the features such as the edges and roughness of the sample

Conclusion

- Our resultant images suggest polarization difference imaging can resolve edge features with high contrast for objects transparent in the terahertz frequency such as plastic

Future Prospects:

- Splitting the initial beam to compare the intensity measured through the sample to the intensity to the full intensity without going through through the sample.
- Vary the optical setup to capture information such as reflection.

Acknowledgements

- Funding support is provided by the National Science Foundation (NSF).

Sudarshan Seshadri

Electrical Engineering
Freshman, UCLA

Gathering and Presenting Sensor and Control Data from Autonomous Agents, Interpreting High Level User Behavior Inputs

FACULTY ADVISOR

Ankur Mehta

DAILY LAB SUPERVISOR

Ankur Mehta

DEPARTMENT

Electrical and Computer Engineering

ABSTRACT

A successful user interface for a group of autonomous robots must have three main characteristics. First, it must be able to easily gather and visualize data as well as send commands to the robotic swarm. Second, because robotic projects constantly evolve, it must be highly modular and display data in many formats. Lastly, it must be able to replay the data as if in real time, which previous systems, such as typical IoT dashboards, cannot do. We were able to create a demo of a swarm of robots that feature mesh networking, autonomy, and vision processing. Using the front end JavaScript library React, I created a dashboard that is able to transfer data over different protocols as well as record data to play back later. I implemented different input methods such as text boxes, sliders, joysticks, and buttons. Members of my lab can now easily visualize robot data in different ways including video feeds, raw text feeds, live graphs, and 3D rotation visualization. Ultimately this project enables users to easily prototype and control a generic swarm of robots. In the event that new controls or interfaces are needed, the modularity of this project makes it easy to implement new functionality.

UCLA Samueli School of Engineering

Assisted Autonomy Dashboard

Gathering and Presenting Sensor and Control Data from Autonomous Agents, Interpreting High Level User Behavior Inputs

Sudarshan Seshadri, Dr. Ankur Mehta,
The Laboratory for Embedded Machines and Ubiquitous Robots, UCLA

FAST TRACK TO SUCCESS
UCLA Electrical and Computer Engineering

Introduction

A successful user interface for controlling a group of robots must:

- Gather and visualize data from multiple sources and sinks
- Be highly modular: any part can be replaced
- Record data for playback, to compare robot runs

Web App Structure

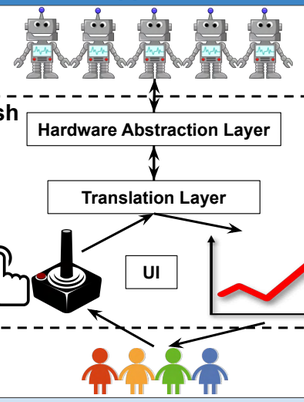

- Split into several parts to increase modularity.
- Each component can be swapped out for an alternative.

Conclusion

- Control any group of robots.
- Add new controls and data visualization elements easily (modularity)
- Future developments:
  - add more input and output components
  - add more troubleshooting/prototyping tools
  - integrate into RoCo (origami robot design tool)

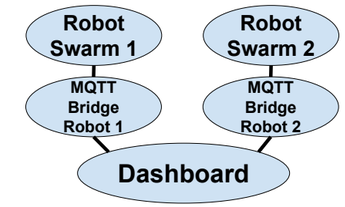

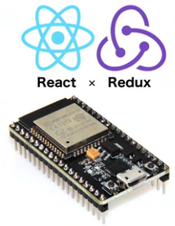

Results

The dash can control boats, cars, Blimps, any new robots developed.

Input Components:

- Text
- Buttons
- Joysticks
- Macros
- Sliders

Display Components:

- Text
- Rotation Display
- Video
- Graphs

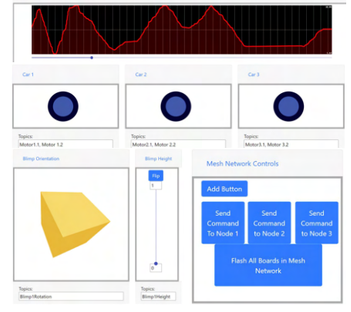

Protocols

- Websockets
  - Full duplex over TCP
  - HTTP initiates connection
- MQTT
  - Publish / subscribe
  - Broker / clients

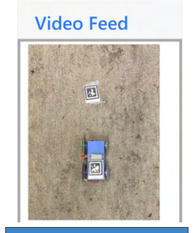

Acknowledgements

- Dr. Ankur Mehta, UCLA LEMUR
- Grace Kwak, Jaehoon Song, Bhavik Joshi, Jillian Pantig, Marisa Duran, Shahrul Kamil Hassan
- William Herrera, Summer Undergraduate Research Program

Krish Shah

Computer Engineering
Freshman, UCLA

Waree Protprommart

Biochemistry
Sophomore, Mount Saint
Mary's University

William Clark

Computer Science
Sophomore, Los Angeles City College

Expanding Human-Computer Interaction via Object Recognition Implemented into a Hand Signal Actuated Robotic Arm (SARA)

FACULTY ADVISOR

Xiang 'Anthony' Chen

DAILY LAB SUPERVISOR

Jiahao Li

DEPARTMENT

Electrical and Computer Engineering

ABSTRACT

Human-computer interaction (HCI) has advanced the efficacy of a multitude of sectors such as communication and consumerism. However, there exists a gap where most HCI research is conducted to improve quality in industrial aspects rather than personal aspects. Our research extends HCI to improve quality of life by designing and implementing a hand signal response AI into a six degree of freedom (6DoF) robotic arm. We call this our hand signal actuated robotic arm, SARA. An implementation of forward kinematics (FK) and inverse kinematics (IK) in python allows the robotic arm to actuate in response to complex hand signals, made possible via our hand recognition software. This software presents a real-time object-tracking process that recognizes hand signals by finger landmark mapping. A rule classifier distinguishes different variations of raised fingers. To confirm mechanical actuation and limitations, we developed a simulator in MATLAB using a virtual robotic arm that parallels SARA. Our research ultimately produced a design that, when implemented, gives SARA the capability to react to diverse hand signals independently. Qualitative demos conducted with a variety of hand signals validated our research design and implementation. A set of thirty-two hand signals was displayed to SARA that resulted in successful actuation in accordance with the simulator. The application of this design aims to assist individuals with physical limitations, making HCI more personal. The success of implementing a hand signal response AI makes the interaction with a robotic arm intuitive, ultimately expanding the scope of HCI to enhance the human experience.

UCLA Samueli School of Engineering

Joonwoo Shin

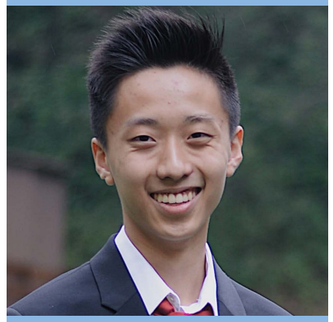

Electrical Engineering
Freshman, UCLA

Viterbi Algorithm for Decoding TCM based PAS

FACULTY ADVISOR

Richard Wesel

DAILY LAB SUPERVISORS

Dan Song, Linfang Wang

DEPARTMENT

Electrical and Computer Engineering

ABSTRACT

The development of a trellis-coded modulation (TCM) based probabilistic amplitude shaping (PAS) coding scheme has the potential to greatly improve the rate of data transmissions to meet the rapidly growing data demands. Previous studies on convolutional codes have determined that there is a theoretical maximum channel noise in the memoryless channels used for data transmission; a TCM based PAS design has the potential to reach a higher maximum threshold in comparison to low-density parity-check (LDPC) codes. To obtain the initial data sequence, we propose an implementation of the maximum likelihood soft decision Viterbi algorithm that calculates the branch metrics using a probability vector for the constellation design in order to determine the survivor path.

Viterbi Algorithm for Decoding TCM based PAS

Joonwoo Shin, Felipce Areces, Dan Song, Linfang Wang, and Richard Wesel

Department of Electrical and Computer Engineering,
University of California, Los Angeles

Fast Track to SUCCESS summer scholars program
Electrical Engineering Department

Introduction

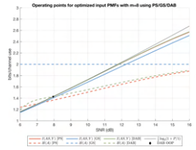

Figure 1. *Theoretical performance limit.*

- **Problem:** There is a theoretical maximum noise threshold in the memoryless channels used for data transmission that has not been achieved at short block lengths.
- **Approach:** Using a nonuniform input and a Trellis-coded modulation (TCM) based Probabilistic amplitude shaping (PAS) system may approach this theoretical limit.
- **This Project:** Implement the maximum likelihood soft decision Viterbi algorithm to determine the original transmitted data from the received data sequence.
- **Significance:** This work seeks to increase the speed and reliability of short transmissions.

Trellis Coded Modulation

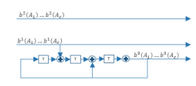

Figure 2. *Rate 2/3 Convolutional Encoder. Two uncoded bits enter the encoder. One input bit is uncoded and does not affect the state of the encoder, and the remaining bit is processed into two coded bits. The T boxes represent the states of the shift register. The + represents an XOR notch that process any two bits.*

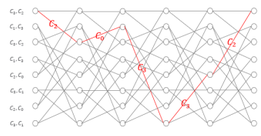

Figure 3. *Trellis diagram of the convolution encoder in Figure 2. Each node indicates a unique state in the shift register. Each path between nodes represents the next possible states, depending on the input symbol. The red lines indicate an example path of encoder states over time. This trellis uses parallel branches.*

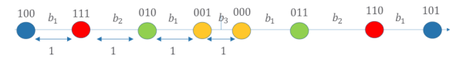

Figure 4. *Constellation diagram for the encoder in Figure 2. The first two bits represent the two coded bits outputted from the encoder. The third bit is the uncoded bit that passes through the encoder.*

- The convolutional encoder:
  - Creates a redundant bit for every 2 bits in the data sequence before transmission.
- The trellis:
  - Stores the next possible states from any given state and the coded output bits for any uncoded input bit.
  - Does not consider the uncoded bit that passes through the encoder.
  - Each path represents two parallel branches for the two possible uncoded bits that passed through the encoder.
- The constellation design:
  - Separates constellation points share two parallel branches, i.e. that differ only in an uncoded bit, to have the maximum possible distance.

Methods

- All code was implemented in MATLAB, using the Communications Toolbox.

MATLAB

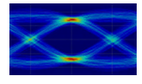

Soft Decision Viterbi Algorithm

- Viterbi Algorithm:
  - Cannot determine the original sequence with complete certainty.
  - Calculates most likely transmitted sequence given the received sequence.
  - The path through the trellis that has the highest probability is selected by the Viterbi algorithm.
- Soft Decision Decoding:
  - Calculates the path metric of each path through the trellis using a priori probabilities of the input symbols, which are not equal in our design.
  - More reliable but also more computationally complex than hard decision decoding, which computes path metrics using Hamming distance.

Design

- Inputs:
  - Vector of encoded channel symbols.
  - Trellis corresponding to the encoder used.
  - Probability vector of the constellation design.
  - Vector of constellation points.
- Output:
  - Vector of decoded bits
- Implementation:
  - Starting from the zero state, traverse each next possible state in the trellis.
  - Calculate the squared Euclidean distance and sum the new path metric for each branch.
  - For converging paths, discard the branch with the greater path metric.
  - Store the input symbols, paths choices, and path metrics of each state in the trellis.
  - Select path having the highest probability, i.e. smallest path metric.
  - Return the sequence of input symbols reshaped as a vector of bits.

Conclusion and Future Work

- The TCM based PAS coding scheme has the potential to greatly improve the rate of data transmissions.
- Examples: performance benefits in any digital video, radio, or mobile communication systems.
- Prospects:
  - Further optimizations of decoder.
  - Translation to C++
  - Measure the performance of TCM based PAS system with this decoder.

Acknowledgements

We would like to thank the National Science Foundation, UCLA ECE Fast Track Program, and UCLA Summer Undergraduate Research Program for funding our project and providing the research opportunity. We would like to thank Professor Wesel, Dan Song, Linfang Wang, and Felipe Areces for the extensive guidance throughout the research process.

References

[1] Ungerboeck, G. (1982). Channel coding with multilevel/phase signals. *IEEE Transactions on Information Theory*, *28*(1), 55–67. https://doi.org/10.1109/tit.1982.1056454
[2] Xiao, D., Wang, L., Song, D., & Wesel, R. D. (2021). Finite-Support Capacity-Approaching distributions for Awgn channels. *2020 IEEE Information Theory Workshop (ITW)*. https://doi.org/10.1109/itw46852.2021.9457608
[3] Wesel, R. D. (2004). Reduced-State representations For Trellis codes Using CONSTELLATION SYMMETRY. *IEEE Transactions on Communications*, *52*(8), 1302–1310. https://doi.org/10.1109/tcomm.2004.833023

Jaehoon Song

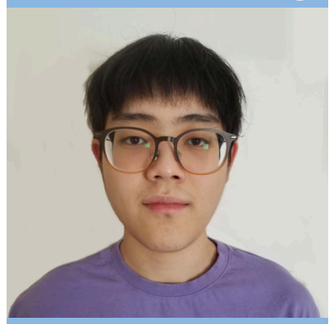

Computer Science
Freshman, Irvine Valley College

Origami Webapp User Interface & Integration of New Designs

FACULTY ADVISOR

Ankur Mehta

DAILY LAB SUPERVISOR

Ankur Mehta

DEPARTMENT

Electrical and Computer Engineering

ABSTRACT

The Origami Design App is a web application that can view, compile, and change the parameters of robots along interfaces. UCLA's LEMUR originally designed this webapp as a means to make robot compiling easier for those that lack the engineering or the programming background. I integrated some of the functionalities such as being able to view necessary component files when inputting a subcomponent into a html form by using a PATH method. This is significant because a user could potentially compile a robot easier or faster than using the standard RoCo application. I also edited some of the existing user interface such as editing the style of transitioning buttons with css files to provide the user with optimal visual experience. For the future, I plan to conduct a user study to observe that the changes I have implemented have benefited the Origami Design App and prove that the changes within the user interface were successful. I also plan to implement the functionality to combine components along interfaces which will most likely reduce the time that a user needs to spend in order to design a robot.

UCLA Samueli School of Engineering
SUMMER UNDERGRADUATE RESEARCH PROGRAM

Origami Webapp User Interface & Integration of New Designs

Jaehoon song, Ankur Mehta, The Laboratory for Embedded Machines and Ubiquitous Robots

LEMUR

Introduction

The Origami Design App is a web application that can view, compile, and change the parameters of robots along interfaces.

Objective

The goal is to improve the user interface of Origami Design App and to create an environment where a user without an engineering or programming background can easily and quickly compile robots.

RoCo

RoCo: Robot Compiler

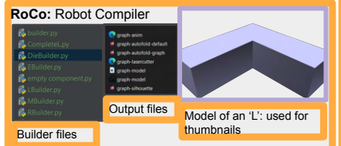

- Standard RoCo application is a set of python scripts
- component files that the webapp uses are generated here

RoCo Library

Rocolibrary: Library that contains pre-built/newly built component/models

- Webapp uses Rocolibrary to render designs

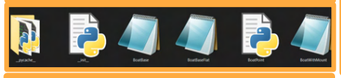

Jinja

By using **Jinja**, a templating engine, I was able to:

- Inherit templates
- Used python codes on html
- Used delimiters to fetch the user input

```
"{{ request.form["nm"] }}";
```

User Interface

CSS Stylesheets:

- Used for general styling and layout
- Bigger and aligned transition buttons

Web Interface Interaction

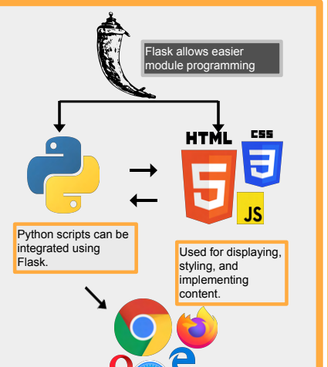

HTML

HTML and **Jinja** was used to inherit templates:

- Used delimiters to inherit the navigation bar

```
{% extends "layout_and_nav.html" %}
```

- Used html tags to create an easily navigable builder option which directs to the builder page

Builder

GET

GET method: fetches data from the server

- Used for rendering designs from thumbnails

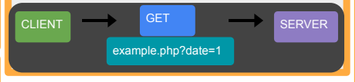

Post

POST method: sends data to the server

- HTML input sends data to the server
- Loads the model that was sent

Results & Discussion

URL: 192.168.86.82:5000/Paperbot#

Loading models using **POST** method:

- Enables loading models much easier
- Can automatically call models within the library
- Load in new designs for better view

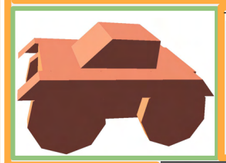

Tank Model:

- Loaded using POST method
- The '#' indicates that it has used POST

- Takes user input and converts it into a component
- the need for compiling two additional python scripts eliminated

Conclusion

- Easier robot compiling for those that lack the engineering or the programming background
- Plan to implement combining components along the interface
- New Interface Design

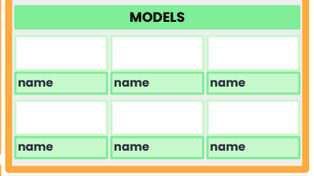

Acknowledgements

- Dr. Ankur Mehta, UCLA LEMUR
- William Herrera, Summer Undergraduate Research Program
- Grace Kwak, Bhavik Joshi, Jillian Pantig, Marisa Duran, Shahrul Kamil Hassan, and Sudarshan Seshadri
- NSF REU

Alethea Sung-Miller

Electrical Engineering
Senior, UCLA

Shakeh Kalantarmoradian

Electrical Engineering
Senior, UCLA

Analysis of Frame Error Rate (FER) and Bit Error Rate (BER) of Viterbi Decoding with Periodic Puncturing

FACULTY ADVISOR

Richard D. Wesel

DAILY LAB SUPERVISOR

Alexander Baldauf

DEPARTMENT

Electrical and Computer Engineering

ABSTRACT

Communications systems are crucial to modern everyday life – whether it be Wi-Fi, satellite communications, or storing and sharing documents digitally. However, imperfect communication channels can result in noise distorting transmitted data. Error correcting codes seek to identify and correct distorted data. Error correction comes at the cost of efficiency – this project's rate-□ trellis encoder outputs three encoded bits per every one information bit, making it three times as inefficient as only sending the original data. By puncturing – omitting certain bits in transmission – higher efficiency can be attained, but the chance of receiving the correctly decoded information decreases. Previous literature has investigated the characteristics of a rate-□ 64-state 8PSK-modulated trellis encoder under puncturing and used these characteristics to develop a bit error rate (BER) union bound on the data. By running BER data simulations using C++ and the Hoffman2 Cluster and comparing them to theoretical union bound plots in MATLAB, this project has confirmed the results found in previous literature. Additionally, this project will extend the BER union bound methods to develop a union bound for the frame error rate (FER), as well as simulating the FER performance for this specific encoder and various puncturing patterns of interest. Whether in satellite transmissions, self-driving cars, streaming, Wi-Fi, memory storage hard drives, 5G, or GPS, our research has countless applications in the modern, digital world.

UCLA Samueli School of Engineering

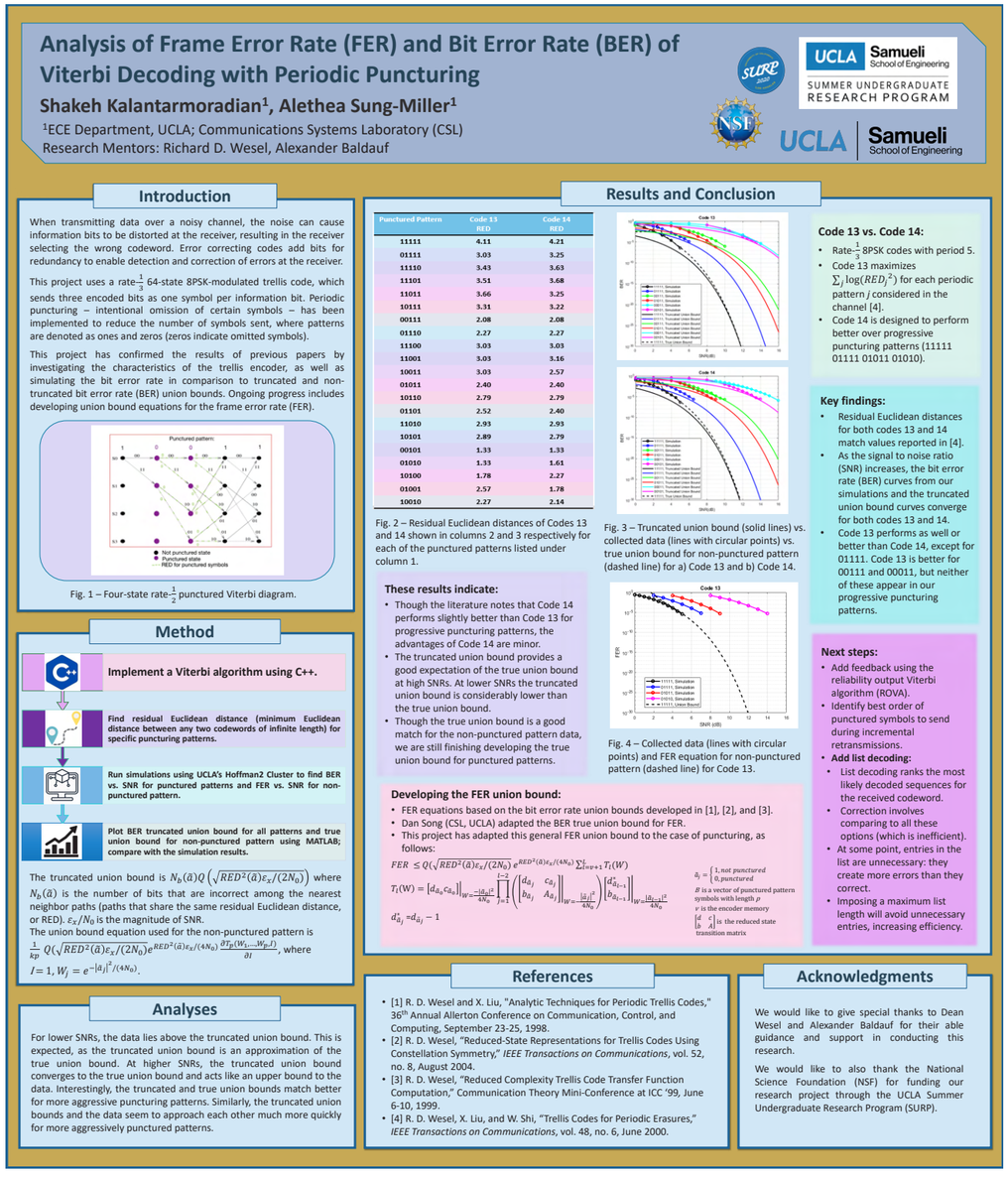

Andrew Tang

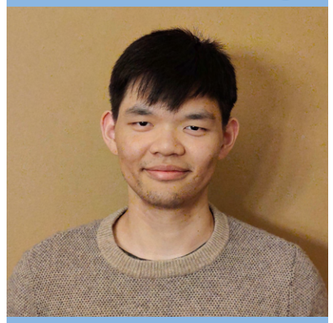

Electrical Engineering
Senior, UCLA

Differentially Private Algorithms for Federated Learning

FACULTY ADVISOR

Suhas Diggavi

DAILY LAB SUPERVISOR

Antonious Girgis

DEPARTMENT

Electrical and Computer Engineering

ABSTRACT

In machine learning, the main objective is to learn a centralized model by exploiting the numerous data which is available from the clients. However, the clients' data might contain personal and sensitive information, and hence, it is required to provide privacy guarantees on the clients' data. In this work, we examine differentially private training algorithms for convolutional neural networks on training practical datasets such as MNIST, ENMIST, and CIFAR10. In order to maximize testing accuracy within a fixed privacy budget, we explore the usage of novel noise functions instead of Gaussian noise in the differential privacy algorithm and transfer learning for CIFAR10 from a network trained on CIFAR100. Furthermore, we consider the problem of retaining privacy while training neural networks in a federated learning framework, where data is stored and accessed locally by the client and a central server builds and updates the neural network model. Also, separately, we examine different mechanisms for updating the global model other than the aggregate average of the local updates.

Differentially Private Algorithms for Federated Learning

Andrew Tang, Antonious Girgis, Professor Suhas Diggavi

Introduction

- The surge in machine learning has necessitated greater amounts of training data. Often times this data contains client's sensitive information, such as medical information or personal images. Without a private training algorithm, attacks such as model inversion can be used on machine learning models and compromise client privacy.
- As such, neural network training algorithms have incorporated differential privacy. Differentially private algorithms provide a robust privacy guarantee based on the probability of discerning the inclusion of any single training example within the training dataset, however they still lag behind in performance compared to the non-private counterpart.
- Furthermore, with the advent of personal computers and smart phones, the notion of a federated learning framework, where a central server never directly accesses client data, becomes very practical. In a federated learning framework, the central server stores and updates a global model based off information provided by clients who train the global model on their local data.
- In this work, we consider training a differentially private neural network in both a conventional central framework and a federated learning framework. Notably, we consider, different L-norms, and implementing a differentially private learning algorithm into a federated learning framework.

Objective

- Explore different L-norms other than the L2-norm in the clipping function
- Test performance of a differentially private federated training algorithm for EMNIST dataset

Materials

- MNIST, EMNIST,
  - MNIST - Handwritten digits from 0 to 9
  - EMNIST - Handwritten digits and characters grouped by client
- TensorFlow Privacy - allows for gradient clipping and Gaussian noise addition
- TensorFlow Federated - allows for neural network training in a federated learning framework

Methods

Differentially Private Stochastic Gradient Descent

Compute Gradients → Clip Gradients → Add Noise → Update Model

Federated Learning Algorithm

Sample Clients → Compute Local Gradients → Transform Gradients → Send transformed gradients to central server → Update Model

Acknowledgements

I would like to thank Antonious Girgis and Professor Suhas Diggavi. Also I would like to thank the National Science Foundation (NSF) for funding this project. This work was funded by a REU supported by National Science Foundation (NSF) grant **# 1740047.**

Results

Layers	Parameters
Convolution	16 filters of 8x8, Stride 2, tanh
Max-Pooling	2x2
Convolution	32 filters of 4x4, Stride 2, tanh
Max-Pooling	2x2
Fully Connected	32 units, tanh
Softmax	10 units

Table 1: Model Architecture for MNIST

Layers	Parameters
Convolution	32 filters of 3x3, Stride 1
Convolution	64 filters of 3x3, Stride 1, ReLU
NA pooling	2x2
Dropout	p = 0.25
Fully Connected	128 units
Dropout	p = 0.5
Softmax	62 units

Table 2: Model Architecture for EMNIST

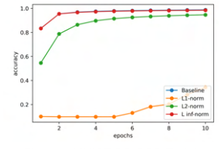

Figure1: MNIST DP-SGD Training

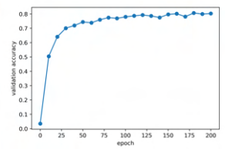

Figure 3: EMNIST Baseline

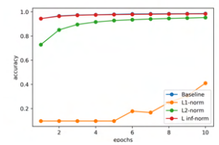

Figure 2: MNIST DP-SGD Validation

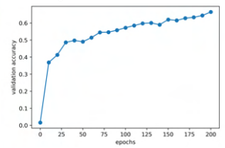

Figure 4: EMNIST with C=1 Clipping

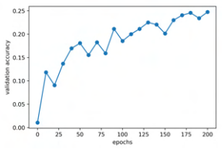

Figure 5: EMNIST with C=1 Clipping and Var=0.5

Conclusion and Future Work

- For MNIST validation accuracy, we see that as the dimension of the L-norm increases, it functions closer to the baseline. A higher dimensional norm is more impacted by a single data point thereby implying the gradient norm is not dominated by a few single points.
- For EMNIST with clipping at C=1 there is a drop in validation accuracy compared to the baseline model. This is expected because the C=1 bound used is the same for the MNIST training, however the EMNIST model has more trainable parameters and therefore more gradients.
- Future work includes use of different mechanisms to send the gradients from the client to the central server and further optimizing the hyper parameters for the federated learning network.

References

- Antonious M. Girgis, Deepesh Data, Suhas Diggavi, Peter Kairouz, & Ananda Theertha Suresh. (2020). Shuffled Model of Federated Learning: Privacy, Communication and Accuracy Trade-offs.
- Nicolas Papernot, Steve Chien, Shuang Song, Abhradeep Thakurta, & Ulfar Erlingsson. (2020). Making the Shoe Fit: Architectures, Initializations, and Tuning for Learning with Privacy.
- Abadi, M., Chu, A., Goodfellow, I., McMahan, H., Mironov, I., Talwar, K., & Zhang, L. (2016). Deep Learning with Differential Privacy. Proceedings of the 2016 ACM SIGSAC Conference on Computer and Communications Security
- Sashank Reddi, Zachary Charles, Manzil Zaheer, Zachary Garrett, Keith Rush, Jakub Konečný, Sanjiv Kumar, & H. Brendan McMahan. (2020). Adaptive Federated Optimization.

Esha Thota

Computer Engineering
Freshman, UCLA

Sraavya Pradeep

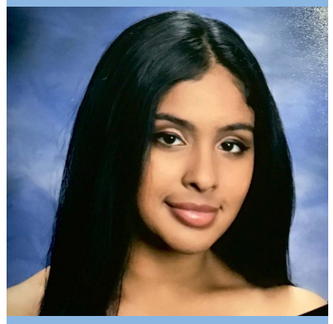

Computer Engineering
Freshman, UCLA

Low Complexity Algorithms for Transmission of Short Blocks over the BSC with Sparse Feedback

FACULTY ADVISOR

Richard Wesel

DAILY LAB SUPERVISOR

Amaael Antonini

DEPARTMENT

Electrical and Computer Engineering

ABSTRACT

Practically speaking, most communications channels are imperfect; noise will interfere with the communications and corrupt transmitted data. In order to combat this, many communications systems utilize feedback- the practice of relaying information regarding received data back to the transmitter- in order to efficiently transmit and decode messages. Research in this field, arguably set in motion by Michael Horstein in 1963, studies this phenomena and ways to mitigate interference. This research builds off an existing algorithm created by Amaael Antonini and Rita Gimelshein, which uses causal encoding over the the BSC (Binary Symmetric Channel), a channel through which binary messages can be transmitted with an equal crossover probability of zeros and ones. It modifies the algorithm to utilize sparse feedback instead of bitwise feedback- sending feedback after a specially determined number of bits have been sent through the channel, rather than after every bit, aiming to increase efficiency without loss in performance.

Low Complexity Algorithms for Transmission of Short Blocks over the BSC with Sparse Feedback

FAST TRACK TO SUCESS

Esha Thota, Sraavya Pradeep
PI: Richard Wesel, DLS: Amaael Antonini

CSL

UCLA Samueli School of Engineering
SUMMER UNDERGRADUATE RESEARCH PROGRAM

INTRODUCTION

Most communications channels are imperfect; noise will interfere and corrupt transmitted data. To combat this, communications systems relay information (regarding data sent to a receiver) back to the transmitter.

Encoder → Channel → Decoder

The current method uses causal encoding, which simultaneously transmits and verifies bits.

OBJECTIVE

New research modifies the algorithm to utilize sparse feedback: sending feedback after a determined number of bits have gone to the receiver, instead of every bit, to increase efficiency without loss in performance.

MATERIALS

- Matlab
- CLion Software
- GMP Library
- CLion

PARTITIONING

After systematic transmission, we must determine how many partitions we should use for the number of bits being transmitted. We do this by: log2((1-p)^k) Where p is the error probability of the channel, and k is the number of bits to be transmitted.

RESULTS

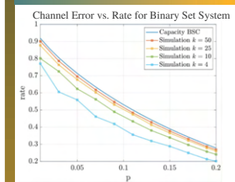

Figure 1. Regular Feedback System, ref. A. Antonini & R. Gimelshein

Regular Feedback System
The graph displays the error probability *p* of the channel against the performance rate (rate at which messages are transmitted & decoded) As the transmitted bits *k* increase, we approach performance closer to channel capacity.

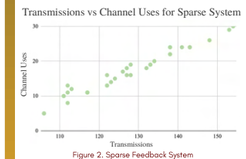

Figure 2. Sparse Feedback System

Sparse Feedback System
The graph displays the transmissions vs channel uses of the Sparse Feedback system. We see that as we increase the transmissions, the channel usage will increase. (Plot shown for block size 2, partition count 4)

SPARSE SYSTEM

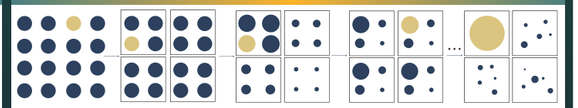

16-bit system; all messages have equal probability of being true. Receiver's belief state of each is 1/16. The true message in yellow.

Partition all messages into four sets with equal probability (S0, S1, S2, S3). Transmitter sends data about theta being in a set.

After some communication betweeen the transmitter & receiver, the probability of S0 has gone up, and other sets have gone down.

Rearrange messages within sets so probabilities of each set is close to equal. We then continue the process from steps 2 & 3.

After much repetition, the true message reaches a probability such that it is the only message contained in a set. We enter confirmation phase.

METHODS

Updating Probabilities.

Using **GMP library** for arbitrary precision + **Matlab** functionality. Modify the current algorithm to update & merge probabilities of multiple sets. First, recalculate multiple-way probabilities using **Bayes' Rule of Conditional Probability**, which is:

$$p(B \mid A) = \frac{p(A \mid B)\, p(B)}{p(A)}$$

Must use the error probability *p* and its complement *q*, aka (1-*p*), to calculate probability of the transmitted message.

Merging Probabilities.

We must store all messages with their probabilities in an ordered fashion, so we can later sort through them & partition appropriately. To do this, we place the message structs into an ordered linked list, ordering them by **decreasing probability**.

Regrouping The Sets.

Reorganize messages into determined number of sets with equal (or close to equal)probability. Use partition (see: sparse system) to organize groups by filling up each probability "bucket" (partition) to a value within tolerance of the **target probability**. Once message reaches a probability that exceeds a bucket's tolerance, we halve number of partitions.

CONCLUSION

Regular Feedback System

Binary Set system- splits all messages into one of two sets. Uses a version of ACK/NACK (Acknowledgement/Negative Acknowledgement) feedback to determine probability of theta.

- Pros: Simpler logic means less processing time/overhead
- Cons: Channel use is less efficient, bitwise transmission and decoding

Sparse Feedback System

Multiple Set system- finds the ideal number of partitions based on # of k bits. Splits probabilities into the "buckets". Uses more complicated logic to determine probability of theta from a message of multiple bits.

- Pros: Channel use decrease within certain range of tolerance, improved performance
- Cons: Limited range of improvement, overhead affected by extra processing

ACKNOWLEDGEMENTS

We would like to thank the National Science Foundation, UCLA Summer Undergraduate Research Program, and UCLA's Fast Track to Success for providing the resources for this publication. We would also like to thank Professor Richard Wesel, and Amaael Antonini for their guidance and support.

REFERENCES

Antonini, Rita G. and Richard Wesel. Causal (Progressive) Encoding over Binary Symmetric Channels with Noiseless Feedback, D1-S3-T1.2, ISIT 2021.

Brendan Towell

Electrical Engineering
Junior, UCLA

Ava Asmani

Electrical Engineering
Freshman, UCLA

High Rate Tail Biting List Decoder using a Dual Trellis

FACULTY ADVISOR

Richard Wesel

DAILY LAB SUPERVISOR

Beryl Sui

DEPARTMENT

Electrical and Computer Engineering

ABSTRACT

Encoders and decoders in communications systems are critical for the accurate and efficient transmission of information over noisy channels. Our research is focused on encoders and decoders for tail-biting convolutional codes used in conjunction with cyclic redundancy check (CRC) codes. We implement encoders and decoders that correct errors in the received message when possible. Often, when an error cannot be corrected, the CRC informs the decoder that the selected codeword is unreliable. In our research, we extend the work of Liang et al., who demonstrated that the use of distance spectrum optimal cyclic redundancy checks (DSO CRCs), along with list decoding, offered significant improvements in signal to noise ratio (SNR) with minimal additional computational cost for low rate convolutional codes of the form 1/n, which have n output bits for every 1 input bit. Our research applies this approach to high rate convolutional codes of the form (n – 1)/n, which have n output bits for every n – 1 input bits. Specifically, we implemented the decoder for a rate-3/4 tail-biting convolutional encoder, and used the dual trellis approach proposed by Yamada et al. for efficient decoding, along with the tree-trellis list decoding algorithm proposed by Roder and Hamzaoui. By implementing this system in C++, we have the ability to simulate its performance at low frame error rates and compare it to both the random coding union bound and the performance of a standard maximum likelihood decoder.

UCLA Samueli School of Engineering
SUMMER UNDERGRADUATE
RESEARCH PROGRAM

High Rate Tail-Biting List Decoder using a Dual Trellis

Ava Asmani, Brendan Towell, Wenhui Sui[1], Richard Wesel[2]
Communications Systems Laboratory, Department of Electrical and Computer Engineering
University of California, Los Angeles
[1]Daily Lab Supervisor, [2]Principal Investigator

Fast Track to SUCCESS summer scholars program — Electrical Engineering Department

Introduction

- Transmitting data across noisy channels using high rate convolutional codes and standard maximum likelihood decoding on the encoder-based trellis incurs high decoding costs. To improve efficiency, we implement the dual trellis proposed in Yamada et al. [1], which is based on the parity check matrix of the original code, and improves efficiency for high rate decoding by reducing the number of comparisons performed at each state in the trellis.
- To improve robustness, we built off the work of Liang et al. [5], who demonstrated that for low rate convolutional codes (of the form 1/n), using distance spectrum optimal cyclic redundancy checks (DSO CRCs), in conjunction with serial list decoding, provided significant improvements to signal to noise ratio (SNR) at a fairly low cost.
- Our work extends this approach to high rate codes (of the form (n-1)/n), to identify if such an approach is viable for high rate codes as well.

Materials

We implemented the dual trellis list Viterbi algorithm with DSO CRCs in C++, and plotted the results in Matlab.

Methods

- We started by building the maximum likelihood high rate tail-biting decoder, then incorporated the dual trellis, and finally implemented list decoding.
- Fig. 1 on the right outlines the process of evaluating the system.
- For each SNR, we ran trials until we reached 200 frame errors, so our FER would have a statistically significant number of errors.

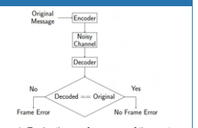

Figure 1: Evaluating performance of the system

Convolutional Codes

- Convolutional codes use memory elements in the encoding process to add redundancy to the encoded signal, which can be used to correct errors in the received message.
- Since the outputs are a function of the memory elements and inputs, this can be viewed as a state machine, which we can arrange on a trellis to account for multiple input blocks. For brevity, only one state transition is shown in Fig. 2.

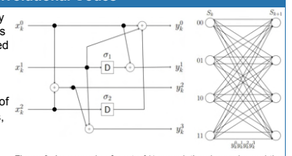

Figure 2: An example of a rate-3/4 convolutional encoder and the corresponding trellis. Each adder is modulo 2, so each value will remain a binary 1 or 0. This encoder has two memory elements, denoted by sigmas.

Dual Trellis

- For standard maximum likelihood decoding, we want to find the message closest to the received message by comparing all possible paths through the trellis, however, directly enumerating them all is computationally intractable.
- The Viterbi algorithm efficiently finds this sequence by only storing the locally optimal path at each state, upper bounding the number of paths to keep track of at the number of states.

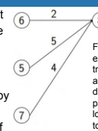

Figure 3: In this small example of one state transition, the Viterbi algorithm would discard the lower paths, since they are locally worse than the top path.

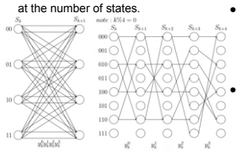

Figure 4: Standard (left) vs Dual Trellis (right)

- While highly efficient relative to the naive approach, the Viterbi algorithm on the standard trellis still struggles with high rate codes due to the high number of comparisons needed at each state.
- Using the dual trellis, which is based on the parity check matrix of the code, reduces the number of comparisons needed at each state, improving efficiency despite the larger number of states and state transitions.

List Decoding

- Adding DSO CRCs provides a further layer of redundancy to rule out invalid decoded messages.
- If a decoded message fails the CRC check, serial list decoding computes the next most likely path by using the paths that were more likely, but failed the CRC.
- The locally second best path will either be one divergence from one of the locally best paths, or a path corresponding to a different starting state, since more than one divergence will always add additional weight compared to one divergence on its own.
- This can be efficiently implemented by using a red-black binary search tree, as described by Röder and Hamzaoui [5].
- To cap decoding complexity, we fix the list size, which is the maximum number of messages that can be checked.

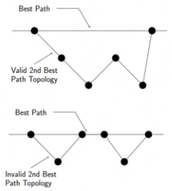

Figure 5: Valid and Invalid Next Best Path Topologies

Results

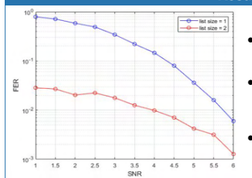

Figure 6: Frame error rate for list sizes of one and two, using the optimal rate-3/4 code with six memory elements, and a blocklength of 30 bits.

- As seen in Fig. 6, increasing list size offers significant improvements in FER for a given SNR.
- Use of the dual trellis reduced decoding complexity by 75% compared to the standard trellis for a rate-3/4 system with two memory elements.
- Larger list sizes produce less frame errors in the decoded message at the cost of increased decoding complexity.

Conclusion, Future Works, and Limitations

- The improvement to FER provided by the list decoding algorithm, with minor increases in decoding complexity, indicates that the method of using S-LVA with DSO CRC for low rate codes presented in Liang et al. [5] generalizes well to high rate codes.
- We're still working on the software implementation, so this poster only includes data for small list sizes. When fully implemented, we plan to test longer list sizes, as well as varying blocklengths and code rates.
- A high rate tail-biting list decoder using a dual trellis accurately and efficiently decodes transmitted data. However, information theory provides theoretical limits on the performance of any communication system, regardless of decoding complexity.

References

[1] Yamada, T. et al. "A New Maximum Likelihood Decoding of High Rate Convolutional Codes using a Trellis".
[2] Seshadri, N. and Sundberg, C.-E.W. "List Viterbi Decoding Algorithms with Applications".
[3] Yang, H. et al. "CRC-Aided List Decoding of Convolutional Codes in the Short Blocklength Regime".
[4] Röder, M. and Hamzaoui, R. "Fast Tree-Trellis List Viterbi Decoding".
[5] Liang, E. et al. "List-Decoded Tail-Biting Convolutional Codes with Distance-Spectrum Optimal CRCS for 5G".

Acknowledgements

We would like to thank Dean Wesel for his guidance and leadership throughout the research process. We are grateful to the National Science Foundation for funding, through the Summer Undergraduate Research Program and the UCLA Electrical and Computer Engineering Department. Finally, we would like to thank Beryl Sui, Hengjie Yang, Linfang Wang, and Ethan Liang for their assistance with the technical aspects of our project.

Lizeth Vera

Computer Science
Freshman, UCLA

Development of SpectraPlot Application for Broadband Spectral Line Survey

FACULTY ADVISOR

R. Mitchell Spearrin

DAILY LAB SUPERVISOR

Chuyu Wei

DEPARTMENT

Aerospace and Mechanical Engineering

ABSTRACT

Laser spectroscopy has been utilized to advance studies and efficiency in various fields such as energy, environment, and aerospace by providing quantitative, species-specific measurements of molecular temperature, pressure, and composition. For accurate measurements of those quantities, measured spectral data are often compared with standard calibrated databases. SpectraPlot is a web-based application that allows its users to simulate spectra and obtain calculations by sourcing from various databases including HITRAN, NIST, AD, and HITEMP. These databases have their own respective libraries of data regarding a large range of gaseous species at different conditions. The objective of this project is to create a relational database server with various spectroscopic databases and to develop application capabilities for broadband spectral simulations and line surveys. MySql was utilized as an efficient tool to manage databases with interconnected data tales and various different data types. In MySql, the server was configured, data was then uploaded as tables into their respective database within the server. When connected to the database server, the Python IDE was used to fetch data remotely and perform spectral simulations and surveys. Fetching data from the relational database is shown to be roughly four times faster (twenty times after connecting to the server), than reading data directly from local text files. Broadband line surveys were then conducted using data fetched from the server and linestrengths of different molecules within the wavenumber range of interest were plotted to provide visualization of results. Along with the line surveys, a hardware search on lasers was performed within the same wavenumber range of interest. The present work will help researchers target specific spectral regions of various species.

UCLA Samueli School of Engineering

Samueli Research Scholars
UCLA Samueli School of Engineering

Development of SpectraPlot Application for Broadband Spectral Line Survey

Lizeth Vera, Chuyu Wei || PI: Professor R. Mitchell Spearrin
Laser Spectroscopy and Reacting Flows Laboratory
Department of Aerospace and Mechanical Engineering, University of California–Los Angeles

UCLA Samueli School of Engineering
SUMMER UNDERGRADUATE RESEARCH PROGRAM

Introduction

- Laser Spectroscopy studies how light is scattered or absorbed by a sample matter.
  - This allows one to study the structure of gaseous species' atoms and molecules.
- This form of studying sample matter has been used to advance studies and efficiency in various fields such as energy, environment, and aerospace by providing quantitative, species-specific measurements of molecular temperature, pressure, and composition.
- In order to acquire accurate measurements regarding sample matter, measured spectral data are compared with standard calibrated databases.

Objective

- SpectraPlot is a web-based application that allows its users to simulate spectra and obtain calculations by sourcing from various databases.
- These databases have their own respective libraries of data regarding a large range of gaseous species at different conditions.
- The objective of this project is to create a relational database server with various spectroscopic databases and to develop application capabilities for broadband spectral simulations and line surveys.

Materials and Methods

- **Software Used**
  - Relational Database Server (RDS) Software MySQL
    - MySql was utilized as an efficient tool to manage databases with interconnected data tables and various different data types
  - Python IDE Spyder
    - Used to fetch data remotely from servers and perform spectral simulations and surveys

- **Configure Server and Databases**
  - Set up local server with the necessary settings and security access
  - Create databases within server pertaining to the databases we are outsourcing information from
  - Within each database, assign a table to every species contained in the database
  - The tables should hold various information regarding the species at different conditions
- **Building Functionalities**
  - Link the databases in MySQL to Python IDE
  - Use a cursor in Spyder to access information held in server connected to
  - The cursor can execute MySQL commands to then fetch specific data from the database tables
  - Append information to an array if it fits our objectives
  - Plot all values within our arrays as data points on a stem plot graph

Results

MySQL Relational Schema

Figure 1: HITRAN , NIST, etc. databases hold tables of species' data with their primary key being *wavenumber*. The HARDWARE table has nuStartCm and nuEndCm columns which act as composite keys corresponding to the foreign key, *wavenumber*, in the species' tables.

Compared Fetch Times

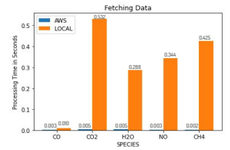

Figure 2: Compared the time taken to fetch data from various species' tables in Spyder using a connection to AWS and reading directly from the local text files

Broadband Line Survey

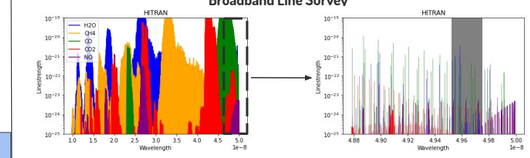

Figure 3: The linestrengths of 5 species from the HITRAN database were graphed within the wavenumber range of 2000-10000

Figure 4: The range interest was focused in to 2000-2050, giving a closer look at how they interfere with one another. The shaded region is the wavenumber range of a laser compatible with the range of interest

Conclusion

- Relational database is created to manage various spectral database
- Fetching data from the relational database is shown to be about 4-200 times faster compared to reading the databases from local files, depending on table size
- Broadband line surveys were conducted using data fetched from the server and linestrengths of different molecules within the wavenumber range of interest which were plotted to provide visualization of the simulation results
- A hardware search on lasers was performed within the same wavenumber range of interest to help users pick optical hardwares

References and Acknowledgements

- Big thank you to the Laser Spectroscopy and Gas Dynamics Laboratory at UCLA
  - Goldenstein, C.S., Miller, V.A., Spearrin, R.M. and Strand, C.L., 2017. SpectraPlot. com: Integrated spectroscopic modeling of atomic and molecular gases. *Journal of Quantitative Spectroscopy and Radiative Transfer*, *200*, pp.249-257

Kathleen Villasenor

Bioengineering
Sophomore, UCLA

Stabilized Self-Assembly of Polyelectrolyte Coacervate Droplets

FACULTY ADVISOR

Samanvaya Srivastava

DAILY LAB SUPERVISOR

Advait Holkar

DEPARTMENT

Chemical and Biomolecular Engineering

ABSTRACT

The controllable nature of coacervate polyelectrolyte complexes holds immense potential as an encapsulation and protection mechanism for proteins, drugs, and hereditary material in the human body. Two oppositely charged polyelectrolytes interact to make a complex in an aqueous solution and at high salt concentrations, these complexes take the form of coacervate liquid-phase droplets. The droplets tend to coalesce and sink to the bottom of the solution forming a polymer dense macro-phase. To increase the level of interaction of biological molecules with the complexes, the droplets must be stabilized and micro-phase separated in solution. Previously, weak polyelectrolyte complexes have been stabilized through the use of a graft polymer that interacts with the polyelectrolytes to give the complex an overall neutral charge. This experiment tested the same experimental design using strong polyelectrolytes, taking a closer look at the mechanisms behind complexation such as the effect of increasing salt concentration, varying the charge ratio of polyelectrolytes, shortening the polyelectrolyte chain length, and adding a graft polymer. To do so, the study employed PSS-Na, and PDADMAC, two oppositely charged polyelectrolytes. Salt was utilized to alter the level of electrostatic attraction to either promote or discourage precipitate complexation of the polyelectrolytes. The addition of a graft polymer with neutral offshoots was found to interact with the polyelectrolytes and disperse the complexes throughout the solution. The shortening of the polyelectrolyte chain weakened electrostatic interactions and lowered the degree of complexation, while charge ratio variation resulted in minimal changes to complexation tendencies. With an increased degree of control over polyelectrolyte complexation, the optimal concentration of polyelectrolytes, salt, and graft polymer was combined to yield a stabilized solution of polyelectrolyte complex coacervate droplets. This study demonstrates a method for stabilizing strong polyelectrolyte complex coacervates, and the success of the aforementioned experimental approach makes it viable for future stabilization attempts with precipitate and polyelectrolyte-protein complexes.

UCLA Samueli School of Engineering

Samueli Research Scholars

Stabilized Self-Assembly of Polyelectrolyte Coacervate Droplets

Kathleen Villasenor, Advait Holkar, Dr. Samanvaya Srivastava

UCLA Samueli School of Engineering SUMMER UNDERGRADUATE RESEARCH PROGRAM

Introduction:

The controllable nature of polyelectrolyte complexation holds immense potential as an encapsulation and delivery mechanism for proteins, drugs, and biological molecules. The following study takes a closer look at the mechanisms behind polyelectrolyte complexation such as the effect of increasing salt concentration, varying charge ratio, and adding a graft polymer.

Objective:

The goal of the following research is to investigate the optimal conditions for evenly dispersed coacervate polyelectrolyte complexes in order to stabilize the droplets in solution.

Future Applications: enable the creation of protein-polymer microparticles for the protection and storage of proteins.

Key Terms:

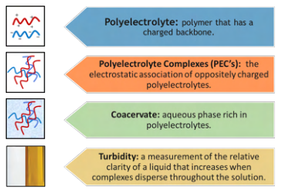

Materials:

1.PSS-Na: negatively charged strong polyelectrolyte

2. PDADMAC: positively charged strong polyelectrolyte

3. Salt: Potassium Bromide

4. Graft Polymer: a polymer with a charged backbone and neutral offshoots.

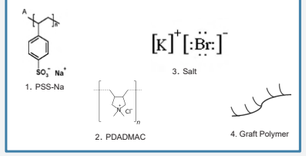

Experimental Design:

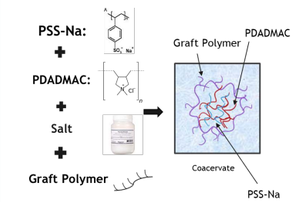

Tuning Polyelectrolyte Morphology:

1 The Variance of Charge Ratio

- Experimentation with different ratios of positively charged PDADMAC to negatively charged PSS-Na.

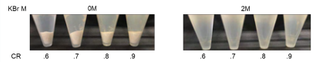

2 The Addition of Salt

- The addition of salt screens electrostatic interactions lowering the degree of complexation and inducing a solid to liquid phase transition in PECs.

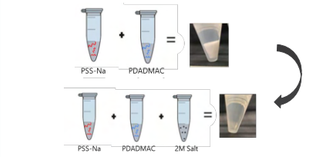

Lack of distinguishable difference with changes of charge ratio suggests that the charge offset has no observable effect on degree of complexation.

3 The Addition of Graft Polymer

- Glenium (GLE) was utilized as graft polymer to surround polyelectrolytes to give complex an overall neutral charge.

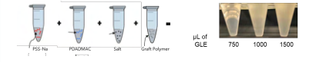

- Addition of GLE elevates solution turbidity indicating an increase in dispersion and stability of PECs

Finding the Optimal Salt Concentration:

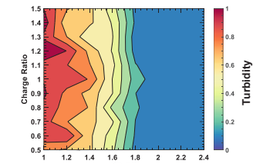

Experimental Conditions: 240 K PDADMAC, 70K PSS, varying KBR, H2O.

- 1.8M KBr is the added salt conc. at which most coacervate PEC's are present without precipitation (indicated by Turbidity > 0).

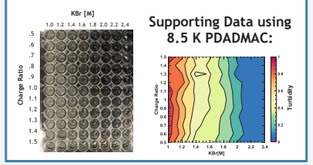

Stabilizing the Coacervates:

Experimental Conditions: 8.5 K PDADMAC, 70K PSS, 1.8 KBR, GLE.

The samples remain stable and uniformly dispersed for over 48 hours, indicating that the complexes are stabilized in solution.

Conclusion:

Our experiments characterize the driving factors of polyelectrolyte complexation and demonstrate a method for stabilizing strong polyelectrolyte complex coacervates in an aqueous solution.

Acknowledgements: I would like to thank the Srivastava Lab and the Samueli Summer Undergraduate Research Program for providing funding and guidance throughout this research endeavor.

Works Cited:

Li, Lu et al. "Effects Of Non-Electrostatic Intermolecular Interactions On The Phase Behavior Of Ph-Sensitive Polyelectrolyte Complexes". *Macromolecules*, 2020.

Sophie Wells

Civil Engineering
Freshman, UCLA

Can Satellites Actually Measure the Turbidity of the Water in Southern California

FACULTY ADVISOR

Jennifer Jay

DAILY LAB SUPERVISORS

Marisol Cira and Ileana Callejas

DEPARTMENT

Civil and Environmental Engineering

ABSTRACT

Turbidity is the measurement of how much light passes through a liquid. Turbidity is important to study as particles in turbid water can act as vectors to bacteria. In this study, images taken from the Sentinel-2 satellite measured the turbidity of beaches around Los Angeles. First, we compared satellite-derived turbidity from the Nechad algorithm to in situ turbidity samples, then turbidity was compared to Fecal Indicator Bacteria. This experiment was split up into three parts: first, the total suspended solids (TSS) test, measuring how many particles are in a sample. Second, the fecal indicator bacteria (FIB) test, measuring the probability of how much bacteria is in 100mL of the sample. Lastly, Google Earth Engine (GEE), a cloud-based platform for planetary-scale geospatial analysis, calculated turbidity from the Sentinel-2 satellite. After collecting water samples from Los Angeles beaches for in situ TSS and FIB tests, the correlation was found to be low (R2=0.2), suggesting that the clarity of the water does not translate to how much bacteria was in the sample. Yet, there was a correlation between in-lab TSS and the Turbidity from Sentinel-2 (R2=0.8), indicating that Sentinel-2 accurately measured turbidity. In the future, research should be done to compare TSS from different algorithms, satellites, and different beaches. This would have a major impact on society as satellites would be able to detect whether water is safe to recreate in.

UCLA Samueli School of Engineering

Can Satellites Actually Measure the Turbidity of the Water in Southern California

Sophie Wells, Yuwei Kong, Marisol Cira, Ileana Callejas, Professor Jennifer Jay
Department of Civil and Environmental Engineering, University of California -- Los Angeles

Samueli Research Scholars

UCLA Samueli School of Engineering
SUMMER UNDERGRADUATE RESEARCH PROGRAM

Abstract

Turbidity is the measurement of how much light passes through a liquid. Turbidity is important to study as particles in turbid water can act as vectors to bacteria. In this study, images taken from the Sentinel-2 satellite measured the turbidity of beaches around Los Angeles. First, we compared satellite-derived turbidity from the Nechad algorithm to in situ turbidity samples, then turbidity was compared to Fecal Indicator Bacteria. This experiment was split up into three parts: first, the total suspended solids (TSS) test, measuring how many particles are in a sample. Second, the fecal indicator bacteria (FIB) test, measuring the probability of how much bacteria is in 100mL of the sample. Lastly, Google Earth Engine (GEE), a cloud-based platform for planetary-scale geospatial analysis, calculated turbidity from the Sentinel-2 satellite.

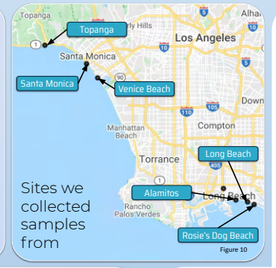

Figure 10

Materials/Methods

This experiment was split up into three parts:

Part 1 - Total Suspended Solid (TSS)

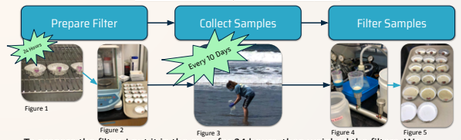

Figure 1 Figure 2 Figure 3 Figure 4 Figure 5

To prepare the filter, I put it in the oven for 24 hours, then weighed the filters. We collected water samples from LA beaches on August 22nd, 2021 (when the Sentinel-2 satellite passed over). Then after filtering the beach samples, I weighed the filters again. To get the total suspended solid (mg/L), I did the equation (Fig. 6) then took the average of the answer to get the average total suspended solid per site.

$$\frac{weight\ after\ (g) - weight\ before\ (g)}{volume\ added} = 0.000001$$

Figure 6

Part 2 - Fecal Indicator Bacteria (FIB)

After collecting beach samples, my lab partner diluted the water sample, added IDEXX Quanti-Tray® bacteria indicator, then dried out the samples. After taking it out of the oven, we counted the number of big and small yellow squares to calculate the probability of coliforms in the water. Then, we put the trays under the UV light and counted the number of big and small illuminated squares to calculate the probability of *E. Coli* in the sample.

Figure 7 Figure 8

Part 3 - Google Earth Engine (GEE)

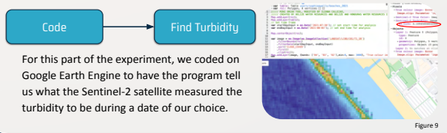

For this part of the experiment, we coded on Google Earth Engine to have the program tell us what the Sentinel-2 satellite measured the turbidity to be during a date of our choice.

Figure 9

Results

Part 1 - Total Suspended Solid (TSS)

We noticed that after averaging each one of the tss data for each filter, we got the data seen in Figure 11. (the * are control filters that we filtered distilled water so we know we are filtering properly) We decided to only take into account the data I collected on July 22nd, 2021.

Date Collected	Site	TSS Average (mg/L)
7/22/21	SM1	
7/22/21	SM2	14.3333
7/22/21	SM3	
7/22/21	VB1	
7/22/21	VB2	10.6667
7/22/21	VB3	
7/22/21	AB1	
7/22/21	AB2	27.1111
7/22/21	AB3	
7/22/21	LB1	
7/22/21	LB2	87.6667
7/22/21	LB3	
7/22/21	DB1	
7/22/21	DB2	44.3333
7/22/21	DB3	
7/22/21	*1	0
7/22/21	*2	

Figure 11

Key:
VB = Venice Beach
SM = Santa Monica Beach
DB = Rosies Dog Beach
AB = Alamedos Beach
LB = Long Beach City Beach
* = Control (Distilled Water)

Date	Site	(MPN/100mL)*Dilution
7/22/2021	SM	74
7/22/2021	VB	657
7/22/2021	LB	327
7/22/2021	DB	75
7/22/2021	AB	7270

Figure 12 - TC

Date	Site	(MPN/100mL)*Dilution
7/22/2021	SM	10
7/22/2021	VB	10
7/22/2021	LB	52
7/22/2021	DB	109
7/22/2021	AB	30

Figure 13 - EC

Date	Site	(MPN/100mL)*Dilution
7/22/2021	SM	0
7/22/2021	VB	0
7/22/2021	LB	0
7/22/2021	DB	41
7/22/2021	AB	146

Figure 14 - ENT

Part 3 - Google Earth Engine

Also known as the ORCAA tool, I simply pressed a black point seen on Figure 10, and as Figure 9 shows, it gave me the turbidity circled in red.

Site	Date	ORCAA Turb (NTU)
SM	7/22/21	2.744664345
VB	7/22/21	3.850354287
AB	7/22/21	4.139171672
LB	7/22/21	6.369673523
DB	7/22/21	4.14109737

Figure 15

Part 4 - Final Data

We noticed that there was a correlation (R^2=.8) meaning that the satellite can accurately measure that the water was not clear (Fig. 16). However, after correlating the TSS with the FIB (Fig 17-19), there wasn't a correlation. This means that murky water doesn't necessarily mean a lot of bacteria in it. So satellites can measure turbidity but not the bacteria.

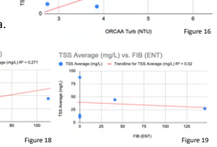

Figure 16

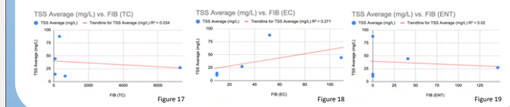

Figure 17 Figure 18 Figure 19

Conclusion

After collecting water samples from Los Angeles beaches for in situ TSS and FIB tests, the correlation was found to be low (R2=0.2), suggesting that the clarity of the water does not translate to how much bacteria was in the sample. Yet, there was a correlation between in-lab TSS and the Turbidity from Sentinel-2 (R2=0.8), indicating that Sentinel-2 accurately measured turbidity. In the future, research should be done to compare TSS from different algorithms, satellites, and different beaches. This would have a major impact on society as satellites would be able to detect whether water is safe to recreate in.

Acknowledgement

I would like to thank the Summer Undergraduate Research Program, my professor Jennifer Jay, my daily lab supervisor Ileana Callejas, and my lab partner Yuwei Kong for their help and support on my research.

References

Callejas, Ileana A., Christine M. Lee, Deepak R. Mishra, Stacey L. Felgate, Claire Evans, Abel Carrias, Andria Rosado, Robert Griffin, Emil A. Cherrington, Mariam Ayad, Megha Rudresh, Benjamin P. Page, and Jennifer A. Jay. "Effect of COVID-19 Anthropause on Water Clarity in the Belize Coastal Lagoon." *Frontiers*. Frontiers, 12 Apr. 2021. Web. 08 July 2021.

"Notes from the Field - On the Ground in Belize to Improve How Satellites "See" Water Quality from Space." *NASA*. NASA. Web. 08 July 2021.

Steele, Jim. "Study of How COVID Tourism Decline Affects Belize's Coastal Waters Earns NASA Grant." *The University of Alabama in Huntsville*. The University of Alabama in Huntsville, 24 Sept. 2020. Web. 08 July 2021.

Written by Brian Spaen, Writer for Green Matters. "Belize's Barrier Reef Is No Longer Endangered." *World Economic Forum*. Web. 08 July 2021.

Tyler Xu

Electrical Engineering
Freshman, UCLA

A Personalized Approach to Federated Learning

FACULTY ADVISOR

Suhas Diggavi

DAILY LAB SUPERVISOR

Kaan Özkara

DEPARTMENT

Electrical and Computer Engineering

ABSTRACT

Federated learning, a machine learning technique, has been gaining popularity as a method of protecting user data privacy for modern-day devices while still providing a great user experience by only sending model updates to the server instead of exchanging sensitive data. However, utilizing a singular global model is extremely restricting as the data is exceedingly diverse, which limits the global model from maximizing performance for each individual client. This heterogeneously distributed data across multiple clients is the primary motivation in utilizing personalized versions of federated learning. In this research, we implement algorithms that use personalized federated learning techniques such as clustering clients and utilizing temporary models for communication. Various hyperparameters - batch size, local communication rounds, number of clients - are adjusted to maximize the algorithm's accuracy levels. The algorithms are implemented using PyTorch (a machine learning library developed by Facebook's AI Research Lab) and both trained and tested using the CIFAR-10 image dataset. Using random heterogeneously distributed data, the algorithms converge to higher accuracy levels through these personalization techniques when compared to traditional federated learning utilizing a singular global model. Personalized federated learning is a key component within future machine learning applications - such as connecting autonomous vehicles - as it combines the effectiveness of traditional machine learning with crucial cloud security and data privacy protection.

UCLA Samueli School of Engineering

SUMMER UNDERGRADUATE RESEARCH PROGRAM

A PERSONALIZED APPROACH TO FEDERATED LEARNING

Tyler Xu, Kaan Özkara[DLS], Suhas Diggavi[PI]
Information Theory and Systems Laboratory (Licos)
Department of Electrical and Computer Engineering, University of California – Los Angeles

Research Experiences for Undergraduates National Science Foundation

FAST TRACK TO SUCCESS UCLA Electrical and Computer Engineering

Introduction

Problem

Federated learning struggles with non-IID (non-idependent and identically distributed) diverse datasets due to its reliance upon a singular global model for multiple clients (devices). This traditional strategy is limited, as one global model cannot maximize the testing accuracy for different sets of data.

Approach

Implement personalized federated learning algorithms.
Personalized techniques (client clustering and utilizing temporary models) will result in algorithms converging to higher accuracy levels.

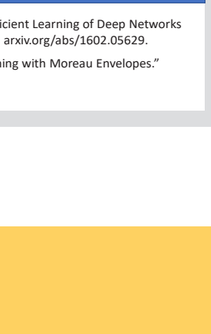

Materials and Methods

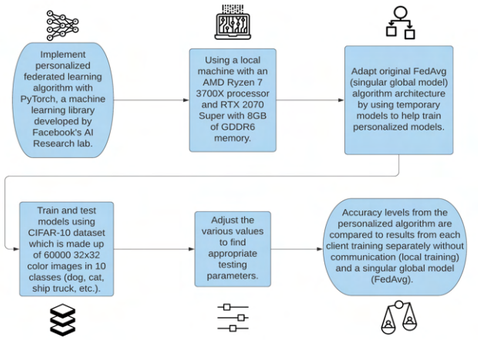

Results and Discussion

Setting batch size to 50, local epochs to 20, and number of clients to 6, the hyperparameters of regularization (reg) and learning rate levels are adjusted to achieve the optimized accuracy for the personalized (pFedMe) federated learning algorithm.

FedAvg Individual Client Model (IID)	FedAvg Global Model (non-IID)	pFedMe Personal Model (non-IID)
73%	49%	79%

Learning rate of 0.01 and regularization of 20 converges to the highest testing accuracy rate of 79% for the personalized algorithm.
A lower regularization is too slow to converge, while a high regularization will diverge.

	Reg 30	Reg 20	Reg 15	Reg 10	Reg 5
Learning Rate 0.01	76%	79%	78%	77%	74%
Learning Rate 0.05	71%	75%	74%	72%	70%

Conclusions

Personalized federated learning algorithms allow for models to outperform traditional federated learning algorithms when using non-IID data. Future implementation of other personalized algorithms such as FedFomo will further showcase the advantages of personalization techniques.

These techniques are key components within future machine learning applications (autonomous vehicles, traffic predictions, etc.) as they increase the performance of machine learning models on heterogenous datasets while eliminating data security risks within the cloud.

References

McMahan, H. Brendan, et al. "Communication-Efficient Learning of Deep Networks from Decentralized Data." ArXiv.org, 28 Feb. 2017, arxiv.org/abs/1602.05629.

Dinh, Canh T., et al. "Personalized Federated Learning with Moreau Envelopes." ArXiv.org, 3 Mar. 2021, arxiv.org/abs/2006.08848.

Acknowledgements

I would like to thank Kaan Özkara and Suhas Diggavi for their guidance and resources throughout this project. I would also like to thank NSF (REU) for their funding and the UCLA Summer Undergraduate Research Program (SURP) for this research opportunity.

Lime Yao

Computer Engineering
Freshman, UCLA

Courtney Gibbons

Electrical Engineering
Freshman, UCLA

Verifying Conditions for Magnetic Alignment in Canine Urination and Defecation with Citizen Science Dataset

FACULTY ADVISOR

Clarice Aiello

DAILY LAB SUPERVISOR

João Carlos Ribeiro-Silva

DEPARTMENT

Electrical and Computer Engineering

ABSTRACT

Numerous species of animals are known to have magnetoreception, or the ability to detect the Earth's magnetic field, for orientation and navigation. However, more research is needed to confirm the underlying mechanics of magnetoreception in animals. Compelling evidence has suggested that dogs align to the Earth's magnetic field during excremental activity if the nearby magnetic field declination, or the difference between true north and magnetic north, is stagnant. Nonetheless, this phenomenon needs a robust source of experimental data before it can be established. We are compiling a large image dataset of urinating and defecating dogs with citizen science and automating the analysis of geomagnetic metadata embedded within these images. We hope to verify whether canine alignment in urination and defecation depends on magnetic field declination. Initial results from a low sample size indicate dogs face random directions even when the percent change magnetic field declination is less than 1%. However, the project will require more image submissions from across the world to yield more refined results. If dogs demonstrate magnetoreception in the course of this project, their potential role as experimental subjects will be pivotal in developing future magnetoreception research.

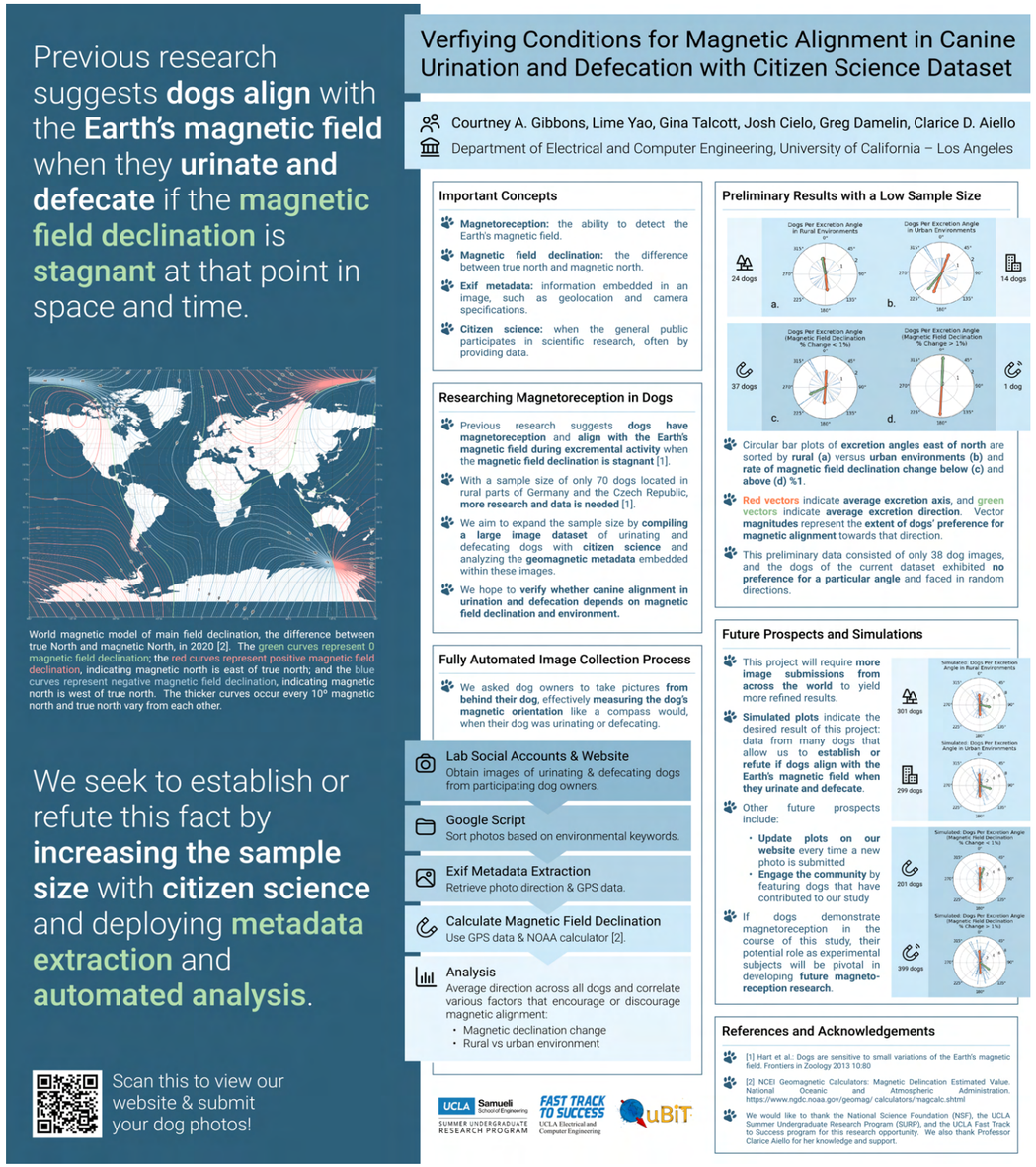

Justin Yao

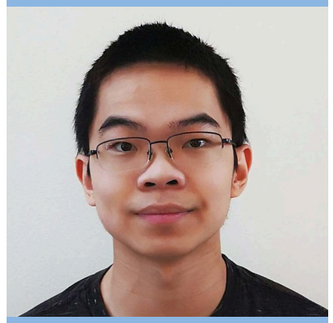

Electrical Engineering
Freshman, UCLA

Isabella Jordan

Electrical Engineering
Freshman, UCLA

Quantifying the Kerr Rotation Angle from the Magneto-Optic Kerr Effect of CoFeB and GdFeCo Films

FACULTY ADVISOR

Kang Wang

DAILY LAB SUPERVISOR

Bingqian Dai

DEPARTMENT

Electrical and Computer Engineering

ABSTRACT

We explored the magneto-optic Kerr effect (MOKE), which refers to the changes in light reflected from a magnetized surface. In MOKE, the incident circular polarized light becomes elliptically polarized and its axis of polarization rotates after reflection. These changes are termed Kerr ellipticity and Kerr rotation angle, respectively. Our objective is to achieve milli-radian Kerr rotation angle readout resolution on ferro/ferrimagnetic materials, such as CoFeB and GdFeCo, with a MOKE setup at near-normal incidence. By modulating the incident light with a photoelastic modulator (PEM-100), magnetizing the sample by placing it between two solenoids, and extracting voltage signals from a photo-detector with a lock-in amplifier (SR830) and multimeter (Keithley 2000), a magnetic hysteresis loop relating applied magnetic field strength and Kerr rotation angle was generated using MATLAB. The CoFeB sample was a wedge, meaning its thickness changed linearly from 0.4 to 1.4 nm. For this CoFeB wedge, we observed many hysteresis loops along the wedge to find both quantitative Kerr rotation angle and perpendicular magnetic anisotropy at various thicknesses. The GdFeCo film was of uniform thickness, but of a nonuniform makeup as it was a composition gradient from one side being Gd-rich and the other being FeCo-rich. For the GdFeCo film, the loops generated near the Gd-rich side neared but did not reach indication of a magnetization compensation point (where the net magnetic moment is 0). Points around the middle of the film were dominated by out-of-plane anisotropy, and the FeCo-rich side displayed predominantly in-plane anisotropy.

Quantifying the Kerr Rotation Angle from the Magneto-Optic Kerr Effect of CoFeB and GdFeCo Films

UCLA Samueli School of Engineering
SUMMER UNDERGRADUATE RESEARCH PROGRAM

Justin Yao and Isabella Jordan
Professor Wang, Bingqian Dai, Hanshen Huang
Department of Electrical and Computer Engineering

UCLA Electrical and Computer Engineering

Introduction and Background

Magneto-Optic Kerr Effect

The magneto-optic Kerr effect (MOKE) refers to the changes in light reflected from a magnetized surface.

These changes primarily involve Kerr rotation angle, Kerr ellipticity, and intensity.

Name	(a) Polar	(b) Longitudinal	(c) Transverse
Geometry	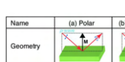		
Detection	Out-of-plane	in-plane	in-plane
Polarization Variation	Rotation Ellipticity		None
Measurement	Polarization Analysis		Intensity measurement

Figure 1: The geometries of MOKE and the changes they introduce to incident light

Previous Work and Goals

The limitations of measuring MOKE stem from the extremely small changes that the effect produces, generally below 0.1 degrees. Previous research has explored all geometries of MOKE over a wide range of magnetic materials.

Our objective is to achieve milli-radian Kerr rotation angle readout resolution on ferro/ferrimagnetic materials, such as CoFeB and GdFeCo, with a MOKE setup at near-normal incidence.

Materials and Methods

Experimental Setup

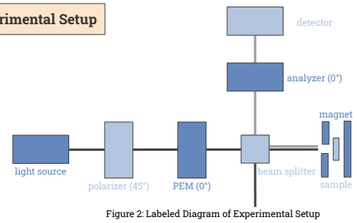

Figure 2: Labeled Diagram of Experimental Setup

Data Collection

1. **Adjust the Sample Position** — The CoFeB wedge sample has linearly changing thickness (0.4-1.4 nm) along its length, and the GdFeCo is a composition gradient along its length. Adjusting where the beam shines on the sample produces a different result.
2. **Align the Laser and Equipment** — Angle the sample in the magnet so that the laser reflects to the beam splitter at its brightest. Line up the analyzer and detector with the reflected beam until the lock-in amp reads a steady voltage
3. **Run the Matlab Program** — Run the Matlab program that causes a current sweep from a max to min value at a designated step. A text file containing all the pertinent measurements will be saved.
4. **Graph the Data** — Using a graphing software, graph Kerr rotation angle (of which the formula is given below) vs magnetic field.

$$\theta_k = \frac{\sqrt{2}}{4J_2}\frac{V_{2f}}{V_{DC}}$$

θ_k = Kerr rotation angle
V_{2f} = PEM 2nd harmonic
V_{DC} = DC signal
J_2 = Bessel function coeff.

References

https://www.researchgate.net/figure/Illustration-of-the-polar-magneto-optical-Kerr-effect-MOKE-Linearly-polarized-light_fig1_318002760
https://www.hindsinstruments.com/techniques/moke/

Results

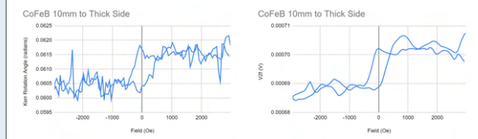

Figure 3: Magnetic hysteresis loops for the CoFeB wedge sample at 10mm to the thick side from the center. Left displays Kerr rotation angle, right displays V_{2f} for comparison

Figure 3 showcases the out-of-plane anisotropy of the CoFeB wedge sample, as there are two states of Kerr rotation angle corresponding to the two magnetization states. It is worth noting there is noise present in both graphs. In the Kerr rotation angle calculation, the ratio V_{2f}/V_{DC} is meant to eliminate drift or noise from the V_{2f} signal, but the V_{DC} signal itself has noise.

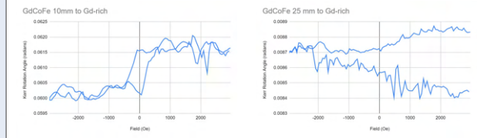

Figure 4: Magnetic hysteresis loops for the GdFeCo composition gradient sample, with one side being Gd-rich and another being CoFe-rich. Length measurements are taken from the center.

The GdFeCo sample had some unexpected results along its length. Figure 4 showcases the most prominent of these oddities, where out of plane anisotropy that is extremely similar to the CoFeB is displayed 10 mm towards the Gd-rich side instead of on the CoFe-rich side. Similarly, the magnetization compensation point, which should be in the middle of the sample, did not show, but 25mm towards the Gd-rich side, which is nearing the edge of the sample, a magnetic hysteresis loop bearing some resemblance to what would normally indicate a magnetization compensation point shows.

Conclusions and Future Prospects

Generating the CoFeB sample's hysteresis loops was more demonstrative as it showcased perpendicular magnetic anisotropy and verified the functionality of our setup. However, the GdCoFe sample and the data collected was far more unexpected. We attribute the irregular behavior to the sample, and suspect that the Gd was at no point dominant over the CoFe, and in the future we would certainly like to examine a GdCoFe sample with a centered magnetization compensation point

Ultimately, the data presented here possesses a signal to noise ratio doesn't quite meet the standard we had hoped for. We have a proposed solution that unfortunately the timescale of this project did not allow for, which was to doubly modulate the light with an optical chopper, then add a lock-in amplifier to read V_{DC} with significantly less noise.

Acknowledgements

We would like to thank the National Science Foundation for funding this research project and UCLA ECE Fast Track for the organization of this experience. Finally, we would like to thank Professor Kang Wang, Bingqian Dai, Hanshen Huang and the Device Research Laboratory for giving us this opportunity and their patience, mentorship, and support.

Ivy Zhang

Electrical Engineering
Freshman, UCLA

Tiffany Tsou

Electrical Engineering
Freshman, UCLA

Solving Large-Scale Non-metric Multidimensional Scaling Problems Using ADMM Optimization

FACULTY ADVISOR

Lieven Vandenberghe

DAILY LAB SUPERVISOR

Xin Jiang

DEPARTMENT

Electrical and Computer Engineering

ABSTRACT

Analysis of the relative orderings of the differences between model predictions as opposed to a quantitative method is often required in cases such as customers expressing their preferences instead of giving numerical scores. The purpose of this research project is to use an algorithm based on the alternating direction method of multipliers (ADMM) to solve large-scale non-metric multidimensional scaling (NMDS) problems. The NMDS problem seeks to optimize the Gram matrix of the calculated position vectors by minimizing violations of the inequality constraints that express the ordering relations of their pairwise distances. ADMM is a method for large-scale optimization which splits variable x into two parts and performs alternating optimizations over each part. The problem is coded using Python and Matlab, allowing us to see what fraction of the ordering of the original distances is preserved. We are working with randomly generated datasets. We are also working with more interesting data, including Swiss Roll and S curve data generated using Python, and real-world data such as sets of related images. For our initial results, which did not include any code for ADMM, the fraction of the ordering of distances preserved was quite high, indicating that the relative ordering of the original distances was preserved overall.

UCLA Samueli School of Engineering

Solving Large Scale Non-metric Multidimensional Scaling Problems Using ADMM Optimization

Tiffany Tsou and Ivy Zhang
Professor Lieven Vandenberghe, Xin Jiang, Taylor Chung

Samueli Research Scholars

UCLA Samueli School of Engineering
SUMMER UNDERGRADUATE RESEARCH PROGRAM

INTRODUCTION + OBJECTIVE

The goal of this research project is to use an algorithm based on the alternating direction method of multipliers (ADMM), to solve large-scale non-metric multidimensional scaling (NMDS) problems with randomly generated datasets and more interesting and real-world datasets such as the Swiss roll, S curve, and related images. Our hypothesis is that the calculated Gram matrix will preserve the ordering of the original distances between points in our initial dataset.

PRINCIPLES

NMDS: attempts to preserve the original distances between inputs in a dataset.
ADMM: a method for large-scale optimization which performs alternating optimizations over two vector variables x and y.
Convex optimization: a convex objective function is subject to inequality constraints that are summarized by a slack variable that we seek to minimize.

Figures: S curve and Swiss roll.

Source: https://www.semanticscholar.org/paper/Nonlinear-Manifold-Learning-6-.-454-Summary-Ihler/62bc7f7507f8f3e7c9c4ac62215d31b06e45da98/figure/0

MATERIALS

Python: Optimization package cvxpy
Matlab: Optimization package CVX
Datasets: Random datasets of size 50, Swiss roll dataset, S curve dataset, images

METHODS

1. Generate datasets with random data points, Swiss roll, S curve, images.
2. Code optimization problem along with ADMM solution into Python and then into Matlab.
3. Analyze results in Python and Matlab.
4. Make necessary adjustments to code and repeat.

$$\begin{aligned} \min_{K,\xi_{ijkl}} \quad & \sum_{(i,j,k,l)\in\mathcal{S}} \xi_{ijkl} + \lambda \operatorname{Trace}(K) \\ \text{subject to} \quad & k_{kk} - 2k_{kl} + k_{ll} - k_{ii} + 2k_{ij} - k_{jj} \geq 1 - \xi_{ijkl} \\ & \sum_{ab} k_{ab} = 0, \quad K \succeq 0. \qquad \text{(GNMDS)} \end{aligned}$$

This is the optimization problem with inequality constraints represented as linear equations of Gram matrix K which define a unique K which can solve the problem and have specifications that disallow translations, rotations, and scalings of K.
Source: Agarwal et al.

$$\begin{aligned} \text{minimize} \quad & \sum_{k=1}^{m} \max\{0, u_k\} + \lambda \mathbf{1}^T x + g(x) + h(y) \\ \text{subject to} \quad & \begin{bmatrix} I & 0 \\ 0 & I \end{bmatrix} \begin{bmatrix} x \\ u \end{bmatrix} + \begin{bmatrix} -I \\ -A \end{bmatrix} y = \begin{bmatrix} 0 \\ \mathbf{1} \end{bmatrix}. \end{aligned}$$

This is the optimization problem in an ADMM-ready form, which consists of first optimization over x and u, then optimization over y, and lastly the dual update. Source: Boyd et al.

RESULTS

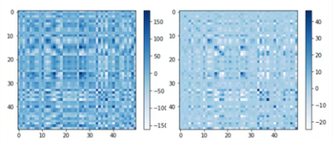

Figure: Shows the original Gram matrix calculated from the original distances matrix (left) and the calculated Gram matrix obtained by solving the non-metric multidimensional scaling problem (right).

Figure: Shows the values of the slack variable (error); ordering of distances is overall preserved.

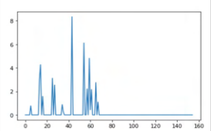

REFERENCES

Agarwal, S., Wills, J., Cayton, L., Lanckriet, G., Kriegman, D., & Belongie, S. (2007, March). Generalized non-metric multidimensional scaling. In Artificial Intelligence and Statistics (pp. 11-18). PMLR.
Boyd, S., Parikh, N., & Chu, E. (2011). Distributed optimization and statistical learning via the alternating direction method of multipliers. Now Publishers Inc.

ACKNOWLEDGEMENTS

We would like to thank the Summer Undergraduate Research Program for providing the guidance and resources to succeed with this project, Professor Lieven Vandenberghe, Xin Jiang, and Taylor Chung for providing their knowledge and resources, and NSF for funding this project.

Jolin Zhang

Computer Engineering
Freshman, UCLA

Trung Vong

Computer Science
Sophomore, East Los Angeles College

Rudy Orre

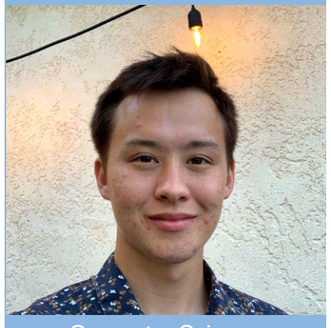

Computer Science
Sophomore, El Camino College

Reinforcement Learning in an Imperfect Information Game

FACULTY ADVISOR

Gregory Pottie

DAILY LAB SUPERVISORS

Sunay Bhat, Jeffrey Jiang

DEPARTMENT

Electrical and Computer Engineering

ABSTRACT

Reinforcement learning (RL) has been a growing subset of machine learning with increasing success and promise - but it has just begun to be used in complex, multiplayer environments and games. An agent learns in a complex environment through trial and error, beginning from fully random trials and finishing with sophisticated actions. We apply RL to the imperfect information game known as Liar's Dice, which presents a challenging mix of two-player dynamics and partial information to explore. The game forces players to call bluffs and doubt opponents while reading others' potential actions. Implementing reinforcement learning to imperfect information games allows us to find successful strategies and models in dynamic Markov Decision Process (MDP) environments that require sequential decision making. Utilizing both Python and MATLAB, we employed the popular Q-learning method of RL to train agents that begin with random actions or to use a combination of fixed strategies against others. An agent employing Q-learning improved its win rate from 50% to only 65% within 1,000,000 episodes against a simple agent. On the other hand, an agent that made decisions based on various fixed strategies available increased its win rate from 11% to 77.7% with 100,000 episodes. Those varying speeds demonstrate the difficulty of learning and the variability of Q-learning in a game with partial information. In future work, we may compare counterfactual regret minimization and more state-of-the-art RL algorithms, which would expand our understanding of various methods of a partially observed, dynamic environment such as Liar's Dice. By studying this game, we hope to one day broaden our results to the education space, a similar Markov process where individuals also make decisions sequentially. Using intervention tools such as quizzes and lectures, the interactions between students and instructors may be refined to improve student learning outcomes.

UCLA Samueli School of Engineering
SUMMER UNDERGRADUATE RESEARCH PROGRAM
FAST TRACK TO SUCCESS
UCLA Electrical and Computer Engineering

Reinforcement Learning in an Imperfect Information Game

Rudy Orre, Jolin A. Zhang, Trung N. Vong, Dr. Gregory J. Pottie, Sunay Bhat, Jeffrey Jiang
Department of Electrical and Computer Engineering, UCLA

Introduction

- As an imperfect information game, players in Liar's Dice are not omniscient.
- To find optimal strategies and models in dynamic Markov Decision Process (MDP) environments that require sequential decision making, we coded and tested out various agents to find key aspects.
- We applied reinforcement learning (RL), particularly Q-learning, to assist us with producing results regarding the most effective methods.

Key Terms

- *Q-learning* is an off-policy RL algorithm, and it learns from outside the policy taking random actions.
- *SARSA* is State-Action-Reward-State-Action on-policy RL algorithm and it updates the policy based on taken actions.

Game Rules

Within the scope of our work, Liar's Dice is a two-player game, where each player rolls 5 dice and has visual access solely to their own hand.

The first player begins bidding and announces any face value (max of 6) and the number of dice (max of 10). The other player has two choices: they may make a higher bid with a larger face or quantity, or they may call "liar," whereupon all dice are revealed to examine the bid. The winner is determined by the validity of the latest bid.

Objectives

We aim to employ reinforcement learning methods, particularly Q-learning and SARSA algorithms, to attempt to outperform fixed strategies and, ultimately, beat a human player.

Methods

Project Diagram

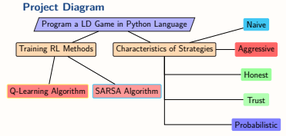

- Set up a sequential environment where an agent's current actions influences its future moves across different episodes.
- Generate a series of game strategies as a baseline.
- Establish two reinforcement learning algorithm methods, tabular and meta-RL, to learn to play against other bots.

Tools

Baseline Bots (Fixed Strategies Agents)

1. Naive: Makes a valid random bid.
2. Honest: Calls the smallest honest bet in its hand.
3. Aggressive: Calls the highest honest bet in its hand.
4. Trusting: Makes a bid based on the opponent's call or calls the lowest bid in its hand.
5. Probabilistic: Calculates the probability of calls and makes a move based on the results.

A Reinforcement Learning Bot

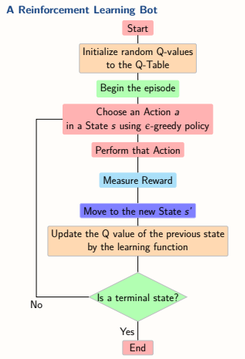

The *Q-learning* equation:

$$\mathbf{Q}(s,a) = \mathbf{Q}(s,a) + \alpha[R + \gamma max_a \mathbf{Q}(s',a) - \mathbf{Q}(s,a)] \quad (1)$$

The *SARSA-learning* equation:

$$\mathbf{Q}(s,a) = \mathbf{Q}(s,a) + \alpha[R + \gamma \mathbf{Q}(s',a') - \mathbf{Q}(s,a)] \quad (2)$$

Results and Analysis

Part 1: Examined Fixed Bots' Performance

	NaiveAg	HonestAg	ProbAg	MixedAg
Human	90%	80%	60%	55%

Figure 1: By playing 25 games, we may evaluate the strengths and weaknesses of each bot. A human can beat the naive and honest agents easily after 3 to 4 games. Since we programmed the various agents with a particular functionality, we are able to quickly distinguish the strategy that the bot employs. The mixed agent, an advanced version of trust, honest, aggressive, and probabilistic agent combined, is more effective against humans.

Part 2: RL Bots' Performance

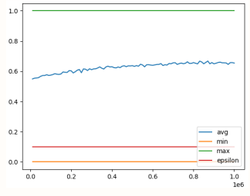

Figure 2: Q-learning agent begins with random actions and learns effective strategies against the naive agent over 1 million episodes of the game with constant epsilon $\epsilon = 0.1$. As this algorithm is a direct tabular Q-learning approach with more than 2 million Q-values, its learning curve is flat with a low slope value.

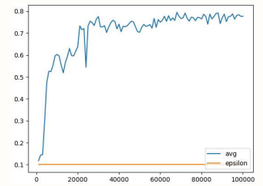

Figure 3: Within 100000 episodes, the meta/combination agent quickly learns the optimal strategy to utilize in a game with $\epsilon = 0.1$.

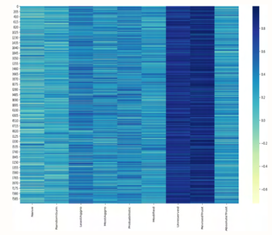

Figure 4: Q-table visualization of the most effective strategy that the meta agent learns to choose. It is trained to determine that the naive agent is a poor selection, while the probabilistic and trust agents are optimal choices. Lighter colors display lower Q-values, whereas deeper colors represent higher values and the most successful strategies.

Conclusion

The agent employing Q-learning generates a better performance by learning to choose an optimal action compared to other fixed strategies. However, this study indicates that the true Q-learning model is slow and requires innumerable training episodes - at least 2 million - to learn effectively.
In future work, we plan to explore counterfactual regret minimization and the ReBeL Facebook algorithm to reverse the downsides of our model and ultimately apply reinforcement learning to other dynamic environments that require sequential decision making, such as education.

References

[1] Brown, N., Bakhtin, A. (Dec 03, 2020). ReBeL: A general game-playing AI bot that excels at poker and more. https://ai.facebook.com/blog/rebel-a-general-game-playing-ai-bot-that-excels-at-poker-and-more/

[2] Sutton. Richard, Barto. Andrew G, Reinforcement Learning An Introduction, *The MIT Press*.

[3] http://www.en.wikipedia.org/wiki/Liar_Dice

Acknowledgements

We would like to thank the National Science Foundation for funding our research project through the UCLA Summer Undergraduate Research Program. We especially thank Dr. Greg Pottie, who has given us incredible guidance since the first day and our daily lab supervisors, Sunay Bhat and Jeffrey Jiang for their support and resources.

David Zheng

Electrical Engineering
Freshman, UCLA

Serina Mummert

Physics
Sophomore, Citrus College

Flexible Prined Circuit Boards for Panofsky Quadrupole Electron Beam Guiding

FACULTY ADVISOR

Rob Candler

DAILY LAB SUPERVISOR

Benjamin Pound

DEPARTMENT

Electrical and Computer Engineering

ABSTRACT

Electron beam therapy (EBT) utilizes electrons to kill cancer cells with up to 60% less radiation affecting surrounding healthy tissue compared to photon-based radiation therapies. EBT typically uses cm-scale beams; this project focuses on using Panofsky quadrupoles to guide sub-millimeter beams in a flexible and changeable trajectory so that beam placement, and therefore treatment outcomes, are improved. Flexible Printed Circuit Boards (PCBs) were designed in a Panofsky quadrupole-like geometry, which consists of parallel copper traces that generate a quadrupolar magnetic field. The flexible material of the PCB allows for manipulation of electron beams in hard-to-reach areas for deeper tissue treatment. Joule heating of the PCBs was simulated in COMSOL Multiphysics, and the limiting current density extracted. The limiting current density was used in magnetostatic simulations to find the magnetic characteristics of these devices. Particle tracing simulations were then performed to investigate efficiency of guiding electrons at different curvatures of the flex-PCB. Flex PCBs were fabricated for testing and the thermal response of the PCBs was experimentally measured using a FLIR OnePro thermal camera.

UCLA Samueli School of Engineering

Flexible Printed Circuit Boards for Panofsky Quadrupole Electron Beam Guiding

Serina Mummert, David Zheng, Benjamin Pound, Professor Rob Candler
Department of Electrical and Computer Engineering, University of California -- Los Angeles

NSF UCLA Samueli School of Engineering SUMMER UNDERGRADUATE RESEARCH PROGRAM

Introduction

Flexible printed circuit boards were designed, simulated, and tested for potential use in **Electron Beam Therapy** (EBT) treatments.

EBT is a cancer treatment currently administered to patients around the world. It is highly effective and valued for its ability to treat tumors without causing excessive damage to surrounding healthy tissue. This makes EBT ideal for surface tumors, but treatment can improve with greater precision and control of electron beam placement.

Objectives

- Design smaller, cheaper, and easier to manufacture quadrupoles using Printed Circuit Board (PCB) technology.
- Test characteristics of these PCB quadrupoles to determine if they are feasible for use in real applications using simulations.
- Check if the quadrupoles still work even if they are bent.
- Measure thermal response with manufactured PCB designs.

Principles

Electrons are influenced by magnetic fields. This behavior is demonstrated in this research project using flexible printed circuit board (Flex-PCB) technology to induce magnetic fields via electric current. Flex-PCBs used as **Panofsky quadrupoles** guide electrons, focusing them in one axial direction.

A configuration of magnets as shown in Fig. 1 create a magnetic field focusing beams of charged particles.

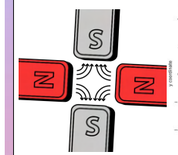

Figure 1: A quadrupole created by four permanent magnets with magnetic field direction.

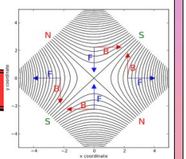

Figure 2: Magnetic force diagram of quadrupole configuration. Forces focus in vertical direction, and push away from the center in the horizontal direction.

Quadrupoles can be created using either permanent or electromagnets. Electromagnets are generally preferred as they are more easily controlled, allowing adjustment of the amount of current going through to achieve a desired magnetic field strength.

Quadrupole fields linearly vary with the distance from the beam axis. The field gradient of the quadrupole describes how fast the field strength changes with respect to distance from the center.
A higher value for this parameter means that particles feel a stronger force towards/away from the center.

Materials and Methods

01 CREATE A PCB DESIGN

- Determine magnetic properties of design using FEMM.
- Use Python to simulate electrons passing through multiple quadrupoles.
- Create Gerber files to send to the PCB factory for fabrication.

SIMULATE IN COMSOL MULTIPHYSICS 02

- Joule heating of PCBs was simulated and current density limits extracted.
- The limiting current density was used in magnetostatic simulations to find the magnetic characteristics of these devices.
- Particle tracing simulations were then performed to investigate efficiency of guiding electrons at different curvatures of the flex-PCB.

03 TESTING OUR DESIGNS

- PCBs were bought and tested with various amounts of current.
- Thermal response was recorded using FLIR OnePro thermal cameras.
- The results were compared to expected results from simulations.

Simulational Data

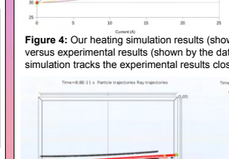

Figure 3: A cross sectional magnetic FEMM simulation of a flex-PCB Panofsky device with current running out of the page. The field lines are similar to that of an actual quadrupole.

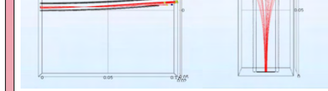

Figure 4: Our heating simulation results (shown by the colored lines) versus experimental results (shown by the data points). The simulation tracks the experimental results closely.

Figure 5: Particle tracing with electrons traveling at 10 MeV. (Left) View from the side. The electrons are following the bent quadrupole (with a 1 meter radius of curvature), and the electrons are focusing at around the 0.03 meter mark. (Right) View from the top. The simulation clearly shows that the electrons are defocusing, as predicted.

Test Results

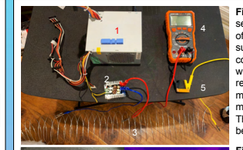

Figure 6: The test setup used consists of a 12V power supply (1), a buck converter (2), steel wire as a variable resistor, (3) and a multimeter to measure current (4). The quadrupole being tested is at (5).

Figure 7: (Left) A picture of the quadrupole under test, with alligator clips to provide current. (Right): A picture of the same quadrupole but imaged with a thermal camera. The PCB is getting slightly warm in the picture.

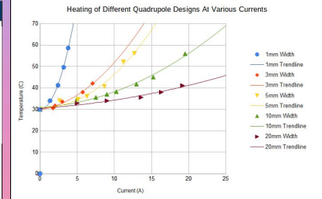

Figure 8: A plot of the temperature of the quadrupoles versus the amount of current passing through them. The temperature increases quadratically with respect to the current as predicted by Joule's Law of Heating. Due to outgassing, only a temperature increase of 10 degrees is allowed. The data shows that pulsed power is necessary for our PCB quadrupoles to reach the required field strength, otherwise overheating would occur with DC currents.

Conclusions and Applications

Flexible Printed Circuit Boards are viable for use in Panofsky quadrupole electron guiding, but they require pulsed power. Research can further explore the limitations of different designs and their use for Electron Beam Therapy application.

The next step with this research would be to conduct real life tests with electron beams to determine how well the quadrupole directs beams. We could also determine how the quadrupole performs when bent at various angles. A suitable power supply for driving the quadrupole would also need to be designed in order to provide the pulsed power.

In the future, better designs using thicker copper or using superconductors could be created to mitigate heating issues and allow for continuous operation without overheating. A separate cooling system using heat pipes to dissipate heat could also be used.

References

D. C. Meeker, Finite Element Method Magnetics, Version 4.2

Magnetic field of an idealized quadrupole with forces.svg. (2021, June 1). *Wikimedia Commons, the free media repository*.

Magnetic quadrupole moment.svg. (2020, September 27). Wikimedia Commons, the free media repository.

Acknowledgements

We appreciate the **National Science Foundation** for funding this research and thank the **UCLA SURP** for arranging this opportunity. We give special thanks to **Rob Candler** and **Benjamin Pound** for allowing us to assist with their great work.

SURP is an umbrella program that administers and scaffolds summer undergraduate research opportunities within UCLA Samueli Engineering. SURP participating sub-programs include National Science Foundation (NSF) Research Experience for Undergraduates (REU) Sites, Samueli Research Scholars (SRS) Program, Faculty-funded grants, and Electrical and Computer Engineering Fast Track Program.

William Herrera, the director of SURP, is also director of UCLA Samueli Engineering's Undergraduate Research and Internship Program (URP/UIP) during the academic year. URP/UIP is committed to helping you find research/internship opportunities. Our Peer Advisors are trained to help you with any questions and concerns you may have, and appointments are available on our website.

For any questions about these resources, please reach out to us at urp@seas.ucla.edu and uip@seas.ucla.edu, or scan the QR code on the next page to get to our website.

We also encourage you to follow us on social media to stay updated on future professional development event and opportunities.

seasoasa.ucla.edu/undergraduate-research-program/

Samueli Engineering Undergraduate Research and Internship Program

UCLA Samueli Undergraduate Internship Program

UCLA Engineering Internship and Research Program

samueliurpuip

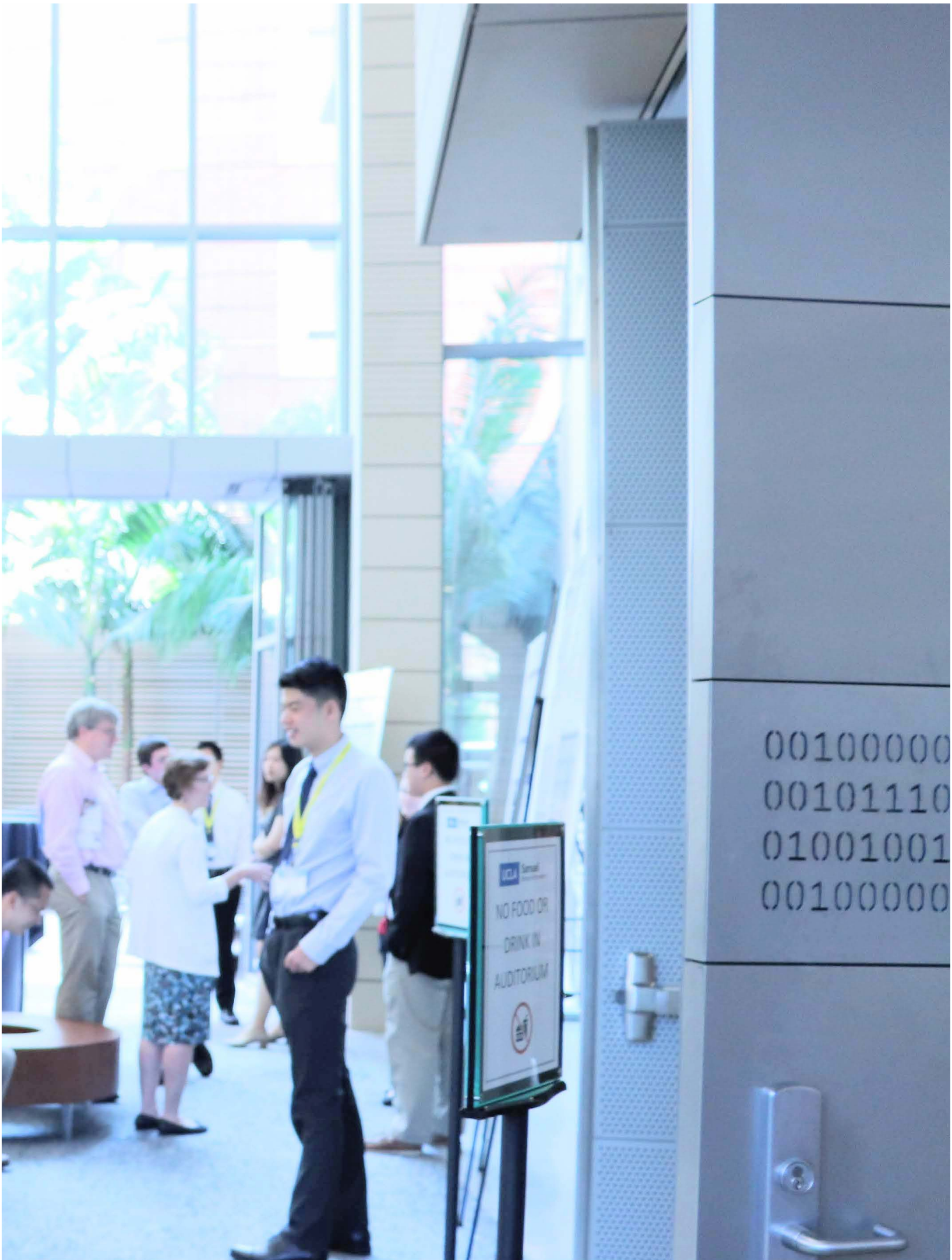
00100000
00101110
01001001
00100000
NO FOOD OR
DRINK IN
AUDITORIUM